SOME STUDIES OF SOME RARE EARTH HALIDES AND RELATED COMPOUNDS

BODLEIAN LIBRARY OXFORD
DEPOSITED
THESIS
16 XI 67

A Thesis for

The Degree of Doctor of Philosophy

at

The University of Oxford

Submitted by

R. G. Shore

of

Brasenose College

Trinity Term 1967

ACKNOWLEDGEMENTS.

The author wishes to thank:-

Professor B. Bleaney F.R.S. for providing research facilities at the Clarendon Laboratory.

Dr. G. Garton for his helpful supervision during the period of the research.

Mr. D. Saxton and the other glass-blowers for constructing so much silica apparatus,

and also the following for assistance or helpful discussion:-

Dr. D. Hukin, Dr. T. Cooke, Dr. T. Thorpe, Messrs. M. Wells M. Davies, J. Stoy, G. Gwynn and Mrs. C. Peagram.

This work was supported by the U.S.A.F. Cambridge Research Centre, through its European Office.

CONTENTS

			Page
Chapter 1		Introduction.	1
Chapter 2		Preparation of Rare Earth Chlorides and Bromides.	8
	2.1	Preparation of Rare Earth Chlorides	8
	2.2	Preparation of Rare Earth Bromides	12
	2.3	Discussion	12
Chapter 3		Growth of Crystals by the Bridgman-Stockbarger Method	13
	3.1	Introduction	13
	3.2	Design of Furnace and Control Equipment	16
	3.3	Setting up and using the Furnaces	19
	3.4	Results and Discussion	20
Chapter 4		Some Phase Systems containing Rare Earth Halides	25
	4.1	Introduction	25
	4.2	Experimental Methods	25
		(a) Preparation of the Mixtures	27
		(b) X-Ray Powder Diffraction	28
		(c) Differential Thermal Analysis	28

4.3 Results and Discussion 33
(a) Systems containing Pr^{4+}, Tb^{4+}, U^{4+} 34
(b) Systems containing Rare Earth Chlorides only 47
(c) Systems containing Rare Earth Chlorides and Alkali Metal Chlorides 52
(d) The Systems $CsCl/CeCl_3/Cl_2$ and $CsCl/ZrCl_4$ 53
4.4 Summary 55

Chapter 5 Physical Measurements on some Rare Earth Halides 57
5.1 (a) Introduction 57
(b) The YCl_3 Structure 58
(c) The $LaCl_3$ Structure 60
5.2 Preparation of Samples 60
(a) Introduction 60
(b) Preparation of Samples for Specific Heat Experiments 61
(c) Preparation of Samples for A.C. Susceptibility and D.C. Magnetic Moment Measurements 61
(d) Preparation of Samples for Resonance Experiments 63
(e) Preparation of Samples for Optical Spectroscopy 64

5.3 Some Physical Measurements 66
(a) Introduction 66
(b) Measurement of the A.C. Susceptibility of $DyCl_3$ and $HoCl_3$ 67
(c) Measurements of the Specific Heat of $DyCl_3$, $HoCl_3$ and $ErCl_3$ 71
(d) Discussion 74

Chapter 6 X-Ray Diffraction Studies of some Rare Earth Compounds 75
6.1 Crystal Structure of $TbCl_3$ and β-$DyCl_3$ 75
(a) Introduction 75
(b) Structure Determination 76
(c)Description of Structure 86
6.2 Determination of the Yttrium Positions in Li_3YCl_6 89
(a) Introduction 89
(b) Determination of Unit Cell Size and Symmetry 89
(c) Determination of the Yttrium Positions 90
6.3 The Crystal Structure of $GdBr_3$ 93
(a) Introduction 93
(b) Determination of Structure 93
(c) Description of Structure 95

6.4 Determination of the Cerium Positions in $CeCl_3.7H_2O$ 97
(a) Introduction 97
(b) Determination of the Cerium Positions 97

Chapter 7 X-Ray Diffraction Studies of some Group III B Compounds 102
7.1 Introduction 102
7.2 Gallium Hypophosphite Complexes 103
7.3 Indium Oxyhalides 104
7.4 Indium Tri-cyanide, Yttrium Tri-cyanide and Indium Tri-thiocyanate 106
7.5 Barium Chloride Fluoride 120
7.6 Summary 121

Chapter 8 Materials based on the Mineral Elpasolite 122

Chapter 9 Discussion 143

References 153

Abstract i

INTRODUCTION.

In the last decade the introduction of large scale ion-exchange methods of separation has made pure rare earths readily available. This has stimulated an expansion of physical research on the properties of individual rare earths, which has led in its turn to an increased demand for their compounds in forms suitable for various types of physical measurements. In this, as in other fields of solid-state research, a close collaboration between physicists and chemists is essential for its rapid development. This thesis is concerned principally with the chemical aspects of some cooperative work on rare earth halides and related compounds. It forms part of a broadly-based programme of research into the optical, magnetic and thermal properties of solid rare earth compounds, which is being conducted in this laboratory.

Many rare earth ions have large magnetic moments arising from unpaired electron spins in the 4f orbitals. There is considerable interest in magnetic dipole-dipole

and exchange interactions between these ions when they are closely spaced in a magnetically concentrated material. Information about these interactions is provided by measuring the variation of magnetic susceptibility and specific heat with temperature. More information about interaction between isolated pairs of magnetic ions or about the effects of crystal field on the properties of magnetically isolated single ions is obtained from such measurements as electron spin resonance, nuclear magnetic resonance, optical absorption and fluorescence spectroscopy. In all cases except the measurement of specific heat, it is necessary to work with single crystals, preferably of compounds with simple structures, if a complete understanding of the various effects is to be achieved.

In the early days of physical research on rare earths, compounds which could be grown easily as large single crystals from aqueous solution and which were non-hygroscopic were widely used (e.g. rare earth ethyl sulphates, hexa-antipyrene iodides, double nitrates).

Later, crystals such as synthetic garnets $Ln_3Al_5O_{12}$ and other mixed oxides which could be grown moderately easily from a fluxed-melt received much attention.

Although easy to obtain, most of the above crystals have rather complex structures, as do the rare-earth sesqui-oxides. The anhydrous trihalides have relatively simple structures and the chlorides are easily prepared in a pure state. Unfortunately they are extremely hygroscopic and for this reason they are never likely to provide materials of technological importance, unlike oxide and possibly fluoride compounds of the rare earths. Nevertheless, anhydrous rare earth chlorides have the advantage for fundamental research that they constitute a series of rare earth compounds of known structure in which it is possible to study in detail magnetic interactions and crystal field effects with some hope of understanding the results.

Some physical measurements have already been made on rare earth trichloride crystals. Dieke (41) has measured some optical absorption spectra. In this laboratory, using material prepared by the author during his work for Part II of the Honours degree in chemistry the electron spin resonance spectra of Ce, Pr, Nd, Sm, Gd, Dy, Er and Yb in $LaCl_3$, YCl_3 and Lu Cl_3 have been studied (1,2) and the magnetic susceptibilities of powder specimens of the trichlorides have been measured at low temperatures (3). This work has now been extended

to include the optical absorption and nuclear magnetic resonance spectra, and the specific heats of the rare earth trichlorides.

The need for large, good-quality, single crystals in order to carry out this type of work gave the original impetus to the author's research. To this end, conditions for the preparation of pure rare earth trichlorides and their growth into large crystals by the Bridgman-Stockburger method have been studied, leading to the establishment of a reliable preparative method.

Many possible experiments on rare earth ions call for the solid solution of one rare earth compound in another, usually a dilute solution of a paramagnetic species in a diamagnetic host lattice but sometimes more concentrated solutions. Since the rare earth trichlorides crystallize in three different structure types as the atomic number increases, and since at least two, $DyCl_3$ and $TbCl_3$, are known to be dimorphic, it is essential to know the extent of mutual solubility between chlorides of different structures and the limits of existence of the various phases as a function of composition and temperature. There appears to be no previous work on phase equilibrium in binary systems

of rare earth trichlorides. Accordingly, the partial phase diagrams of several typical systems have been constructed from differential thermal analysis and X-ray diffraction measurements.

There is a possibility that compounds between rare earth and other metal chlorides may have simple crystal structures and symmetrical rare earth site symmetry. Some results, mainly from Russian workers, have been published on systems of alkali metal/rare earth chlorides. As there was no data on lithium chloride/rare earth chloride systems, some of these were examined with a view to obtaining new chloride compounds suitable for physical examination. Congruently-melting compounds of the type Li_3LnCl_6 have been prepared and grown as single crystals. The crystal structure of a typical member of the series, Li_3YCl_6, has been partially elucidated.

A highly-symmetrical, preferably cubic, crystal field for rare earth ions is not often found but would be advantageous for testing certain theoretical predictions. Following the work of Hukin (4) on cubic crystals of complex rare earth fluorides such as Cs_2KYF_6, which have the elpasolite type of structure, it appeared that

chloro-analogues might be permitted to exist by the known ionic radii relationships. Cs_2KYCl_6 has been prepared, and does have the cubic elpasolite structure, in which the rare earth ion must be octahedrally coordinated.

When the author started his work on rare earth chlorides, the crystal structure of the low temperature (orthorhombic) form of terbium trichloride was unknown. An X-ray diffraction analysis of the structure was therefore undertaken but refinement was not carried to the limit because a full description of the structure was published by other workers in the meantime. The author's results agree exactly with the published data. Another gap in knowledge of the rare earth chlorides was the structure or indeed the mere existence of a low temperature modification of dysprosium chloride. Its existence had been suspected from abnormal heat of solution measurements (5). Further evidence came from the author's own work on differential thermal analysis of materials containing $DyCl_3$ and from erratic results of physical measurements at low temperatures. By cooling $DyCl_3$ under pressure through its suspected transition temperature, the low temperature form was obtained in sufficient quantity to show from its X-ray powder pattern that it has the same crystal structure as low temperature $TbCl_3$.

Difficulties in handling all these hygroscopic chlorides led to a study of methods for shaping, mounting and orienting the specimens.

The properties of rare earth ions in unusual oxidation states are of great interest since they permit comparison of isoelectronic ions of different charge (e.g. Eu^{2+},Gd^{3+},Tb^{4+}). Methods of stabilizing some tetravalent ions by incorporation in complex fluorides were investigated. The system NaF/TbF_4 has been examined for the first time and new information has been obtained on the system NaF/PrF_4. Due to the thermal instability of the tetravalent rare earth fluoride compounds it appears unlikely that any of them can easily be grown into single crystals large enough for most physical measurements. Only magnetic susceptibility measurements on the powders were attempted.

X-ray data for yttrium cyanide and for some new compounds of Group IIIB elements, prepared by co-workers in the Inorganic Chemistry Laboratory, Oxford, are presented in the final chapter.

CHAPTER 2. 2.1.

PREPARATION OF ANHYDROUS LANTHANON CHLORIDES AND BROMIDES.

Supposedly anhydrous lanthanon chlorides have recently become commercially available, but these materials contain traces of carbon, and water, which render any crystals grown from them opaque. This commercial material is suitable for the study of phase systems but must be distilled with great care before it can be used to grow single crystals of good optical quality.

Lanthanon Chlorides.

Lanthanon chlorides are generally obtained in the form of the hexahydrates, $LnCl_3.6H_2O$, which crystallize from aqueous solution. These hydrated salts cannot be dehydrated by simple ignition, since a large fraction is converted to the oxyhalide by hydrolysis:-

$$LnCl_3 + H_2O \longrightarrow LnOCl + 2HCl.$$

Anhydrous lanthanon chlorides have been prepared by heating a mixture of the oxide with ammonium chloride, by passing carbon tetrachloride vapour over the heated oxide, and by dehydration of the hydrates in the presence of thionyl chloride, hydrogen chloride, or ammonium

chloride to suppress hydrolysis (6 & 7). The last method is the one used in this laboratory and gives good results. Final purification of the anhydrous trihalides from traces of oxyhalide can be effected by distillation under vacuum (8).

A solution of the chloride was prepared by dissolving the oxide (15 grms.) in hot, moderately concentrated hydrochloric acid, or by dissolving the hydrated chloride (3o gms) in deionised water. Ammonium chloride (30 gms) was added to this solution, which was evaporated to a boiling-point of 132°C. The resulting paste was allowed to cool into a solid mass, which was broken up and loaded into a Pyrex dehydration-tube (Fig. 2.1A), where it was kept in place with a silica wool plug. The tube was placed in a furnace and connected to a cold trap and a vacuum line (Pressure $\frac{1}{10}$mm of mercury). The temperature of the furnace was raised to 400°C over a period of $2\frac{1}{2}$ days, and left at 400°C for 12 hours before being allowed to cool to room temperature. The system was filled with dry helium, and the tube was removed from the vacuum line. The tube was then cracked open between the sublimate of ammonium chloride and the residue of anhydrous lanthanon trichloride. The lanthanon

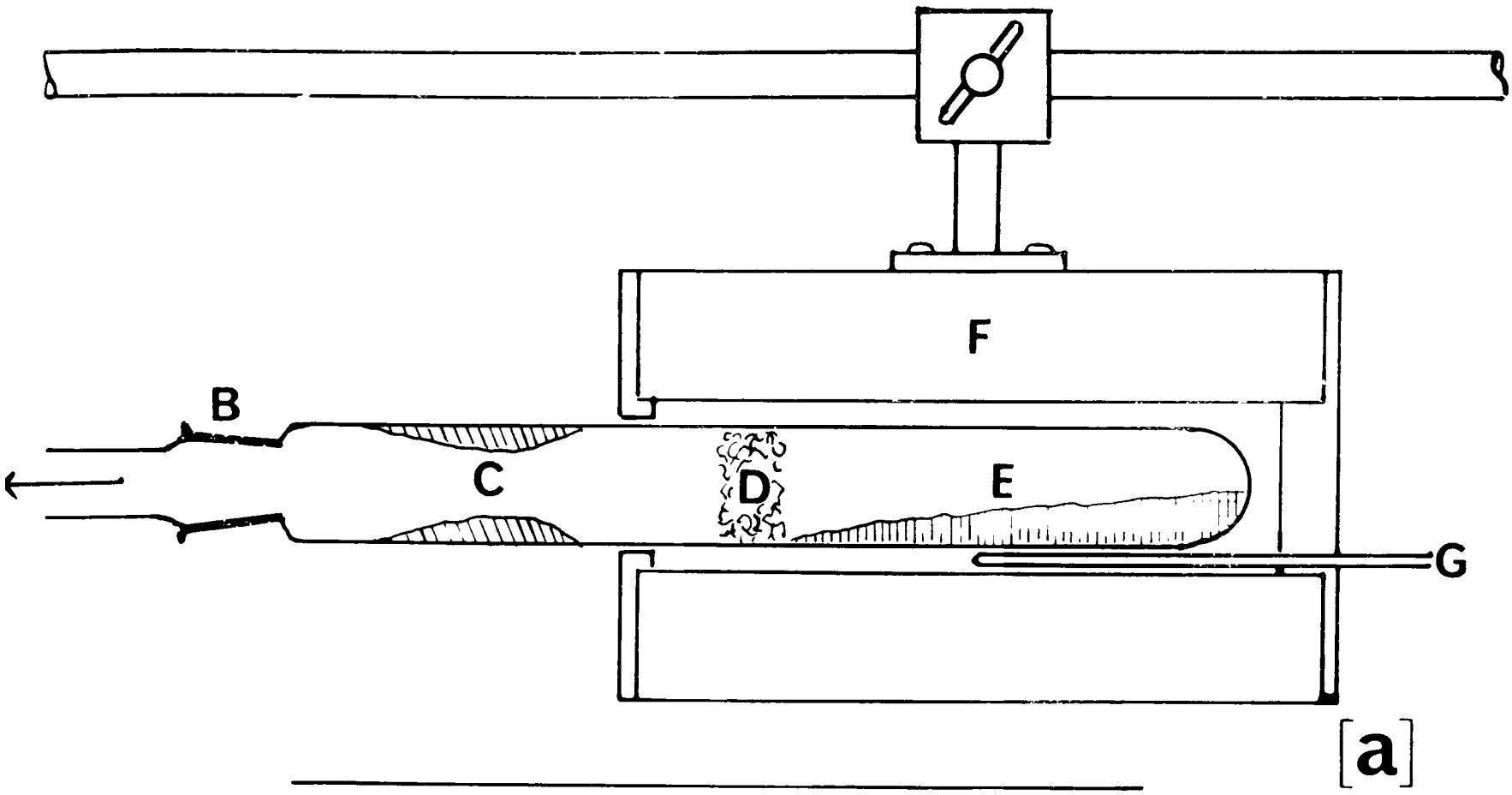
Key to Fig. 2.1.

(a)

A To Pump via Cold Trap
B B 34 Joint
C $LaCl_4$ Condensate
D Silica Wool.
E Anhydrous Lanthanon Chloride
F Furnace
G Thermocouple

(b)

H 1 Foot in Length.
I 6" in Length.
J 1½" width.
K 1" width.
L 5" length.
M 1 cm. narrowing to wiggly
N B 24. Socket
O Constriction 3-5 mm across



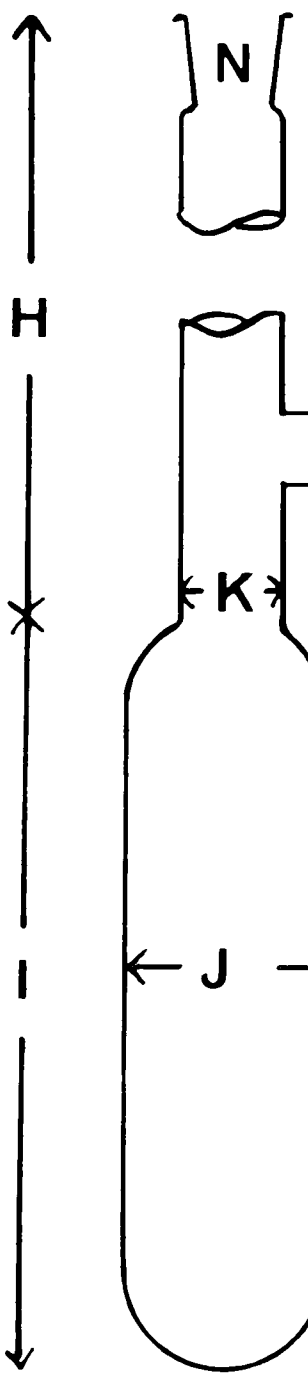


FIG. 2.1

trichloride was then transferred rapidly to a silica distillation vessel (Fig. 2.1.b. and Fig.2.2.) which was immediately connected to a high vacuum line by a ball and socket joint (Fig. 2.2.), and pumped down to less than 5 microns pressure. The lanthanon trichloride was then distilled at 900°C, and condensed in the neck of the distillation vessel. This step was generally complete in less than 12 hours.

The furnace was then removed, and the distillation vessel was rotated to a horizontal position with the side-arm hanging vertically. By means of a gas-oxygen blowtorch the distillate was melted down into the crucible (Fig.2.2.c.) which was then sealed off under vacuum, and separated from the distillation tube. Sometimes, in the case of the higher-melting lanthanon trichlorides, one third of an atmosphere of dry helium was admitted to the system to reduce sublimation during the melting down operation and assist transfer of heat.

Any distillate that appeared in the neck of the flask before the furnace tempefature had reached 700°C was moved up the distillation vessel by local heating with a gas-oxygen blowtorch. The lanthanon trichloride should not be heated too vigorously while melting-down, because

Key to Fig. 2.2.

A Universal Joint.

B B24 Joint

C Crucible

D Lanthanon Halide Sublimate.

E Thermocouple

F Furnace

G Silica Wool.

H Molten Impure Lanthanon Halide.

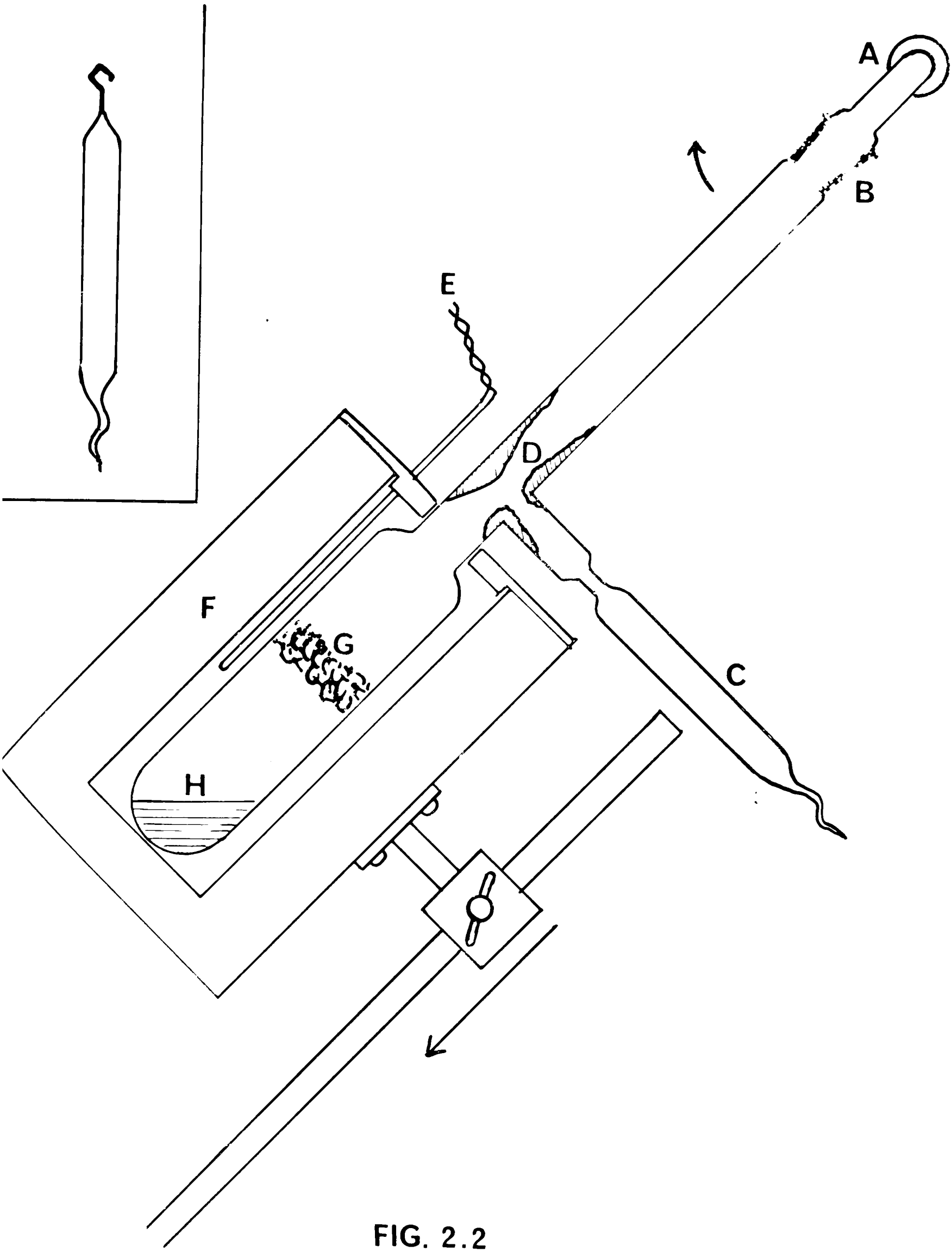


FIG. 2.2

it reacts with the silica, forming some oxychloride.

The starting materials were of high purity (99.9% or better in terms of other rare-earths). Only glass or bone spatulas were used, to avoid contaminating the product with metallic impurities. All glassware and evaporating dishes were boiled with dilute hydrofluoric acid before use, to remove impurities. The only impurity to be expected in the product was oxychloride, which is separated by distillation, since it is involatile below 1000°C. Small amounts of oxychloride may however be formed while melting-down. A pure product, when melted, is clear, free of any solid material, and does not wet the silica crucible (the meniscus is strongly convex).

The tube furnaces used for the distillation and dehydration procedures were made by winding Nichrome wire on threaded alumina tubes. These were held by asbestos end-plates in sections of asbestos-cement drainpipe, and insulated with asbestos wool.
A ¾ Kw. motor-driven Variac was used with the dehydration furnace, and a 2 Kw Variac was used with the distillation furnace. Temperatures were measured with chromel-alumel thermocouples feeding into millivoltmeter pyramaters.
The calibration was checked periodically with a potentiometer.

2.2. Lanthanon Bromides.

Lanthanon Oxide was dissolved in hydrobromic acid, and a fourfold molar quantity of ammonium bromide was added. The dehydration and distillation processes were carried out exactly as described for the preparation of lanthanon trichloride. Yields of the anhydrous bromides were lower than those of the chlorides due to much hydrolysis even in the presence of ammonium bromide.

2.3. Discussion.

The method for preparing anhydrons lanthanon chlorides and bromides which has been described above has been used in this laboratory for some years, and with excellent and consistent results. After distillation there is only a very small quantity of oxygen as impurity in the anhydrous halide. Crystals which showed no specks of oxychloride and were optically clear were grown from such material (Chapter 3).

CHAPTER 3.

THE GROWTH OF SINGLE CRYSTALS BY THE BRIDGMAN-STOCKBARGER METHOD.

3.1. Introduction.

Maximum information can be obtained only from those physical measurements which are made on single crystals, since many properties depend on the direction of measurement relative to the crystal axes. The largest crystals used in the present work are about 5 mm cube. Therefore, the majority of crystal-growing runs were made using 1 cm. diameter crucibles, from which it was possible to obtain sufficiently large pieces of single crystal for most requirements. Measurements of the Raman Spectrum of $CeCl_3$ and possibly other lanthanon trichlorides have been planned. Cylinders about 2 cms. across and 10 cms. long are required, and $CeCl_3$ has been grown in 2 cm. diameter crucibles.

The growth of crystals of the lanthanon trichlorides presents some problems. Due to the hygroscopic nature of the anhydrous material, all contact with the air must be avoided. This is best effected by sealing the material in a silica crucible. There is also a large contraction

of the material on freezing, and a similar contraction on cooling to room temperature. This contraction tends to crack the crystal, particularly if the melt wets the silica as it does if any oxychloride is present, but a slow rate of growth from the melt and slow cooling reduces this tendency. Certain trichlorides, especially $GdCl_3$, supercool. This often results in the growth of a polycrystalline sample.

Previous work has indicated that the Bridgman-Stockbarger method is capable of producing good single crystals of lanthanon trichloride (6 and 9). In the Bridgman-Stockbarger method of crystal growth, a crucible containing the molten material is lowered through a sharp temperature gradient, the temperature of the lower half of the furnace being ideally just below the melting-point of the material. The top zone of the furnace is ideally just above the melting point of the material.

The principle of the method is simple. The crucible has a sharp point, which gradually widens out into the main body of the tube. For these experiments the tip was also bent (Fig. 2.2. insert). As the temperature of the tip reaches the melting-point of the substance, crystallization will commence, generally at several points, and each crystallite will be differently oriented. Each crystallite

has a preferred direction of growth, and eventually a crystallite will grow completely across the narrow tip, and growth will continue as a single crystal. The bends in the tip aid the isolation of one crystal front. When the whole of the crucible has passed into the lower zone and crystallized, the crystal is then cooled to room temperature.

It has been reported that, for lanthanon trichloride, the lowering and annealing rates should both be slow. Williams (9) finds that lowering at a rate of 1mm/hr., and cooling at a rate of 40°C/hr. should be used.

The success of the Bridgman-Stockbarger method depends upon a sharp temperature gradient, which must be sharp enough to minimise supercooling, yet small enough so that, when the crystal has started to grow, there will not be a steep thermal gradient along the crystal, which may cause the crystal to crack. These requirements are conflicting, and after some experimentation it was found that consistently good results were obtained if the temperature of the top half of the furnace was 30-35°C above the melting-point of the material, and the lower half of the furnace was 30-40°C below the melting-point.

3.2. FURNACE AND CONTROL EQUIPMENT.

The furnace and control equipment had to provide maximum flexibility and control of conditions inside the furnace. Opinions vary as to whether it is preferable to control the temperature of the furnace or to use a well-insulated furnace with a voltage-regulator in the supply-line. Those who hold the second view maintain that temperature controllers introduce an undesirable ripple in the temperature of the growth-zone, and that the system will tolerate slow but fairly large variations better than rapid but small fluctuations. The best solution is probably to use a stepless temperature controller based on saturable core reactors or silicon-controlled rectifiers, but these items are expensive.

Two Smith's Proportional Controllers were available in the laboratory. These have a 20 second proportioning cycle, and switch a power supply on and off for different fractions of a cycle, depending on the amount by which the actual temperature deviates from a set temperature. Although the thermal capacity of the furnaces is large, switching the whole of the power on and off would clearly introduce fairly large oscillations of the temperature with a 20-second period. In order to overcome this problem,

the controllers were used to switch only a small fraction (about 5%) of the total power required to maintain a particular temperature.

The furnace, Fig.3.1., was made of two concentric threaded alumina tubes, 20" long and wound with 20 gauge nichrome wire, the inner winding having a centre tap. The outer winding supplied most of the power, and by adjusting the resistance R (100w maximum) Fig. 3.2., which was in series with the lower half of the inner winding, the temperature gradient could be adjusted. The use of two windings increased furnace life. Two chromel-alumel thermocouples were placed in the annular space between the windings, being respectively 1" above and below the centre tap. The space between the windings was filled with alumina powder for good thermal contact, and the space between the windings and the outer case was insulated with asbestos wool.

The upper thermocouple was connected to the proportional controller and was used to control the temperature of the whole furnace. The controller actuated a heavy-duty electronic relay, ((A.E.I. Type EA4H) which shorted out a low resistance in parallel with the relay (Fig.3.2) and in series with the outer winding. In this

Key to Fig. 3. 1.

O Inner Winding Terminals
P Nickel Rod
Q Outer Winding Terminals
R Asbestos Terminal Cover
S Air Holes
T Crucible
U Top Thermocouple
V Bottom Thermocouple
W Outer Winding
X Inner Winding
Y Silica Window
Z Outer Asbestos Cover

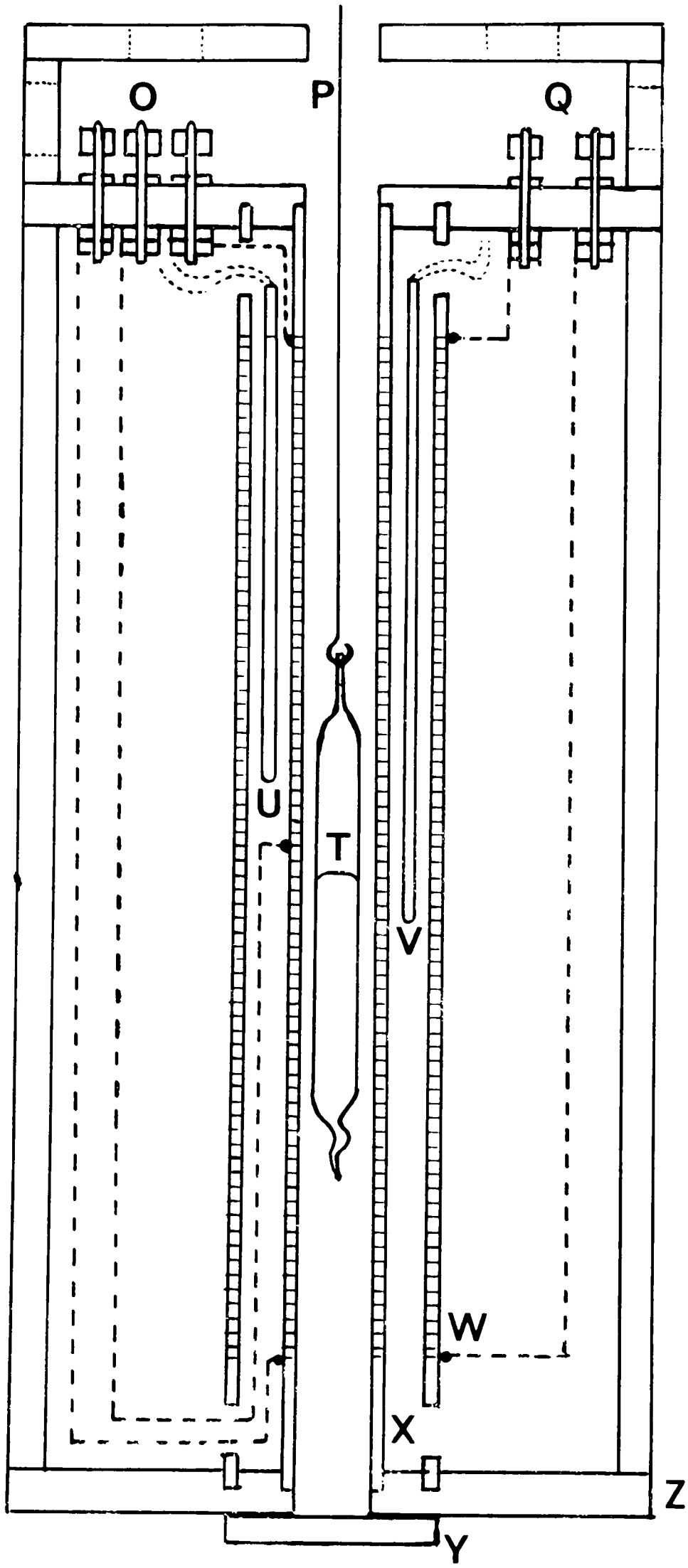


FIG. 3.1

Key to Figure 3.2.

M Motor to Drive Variac Q

N Motor to Lower Crucible

C Microswitches

P Inner Winding Variac

Q Outer Winding Variac

R Resistance (about 10w)

S Mercury Switch (Later replaced by electronic relay)

T Variable Resistance (0-100w)

U Top Half of Inner Winding.

V Lower Half of Inner Winding

W Outer Winding

X Upper Thermocouple

Y Controller Microswitch

Z Relay (Later replaced by electronic relay)

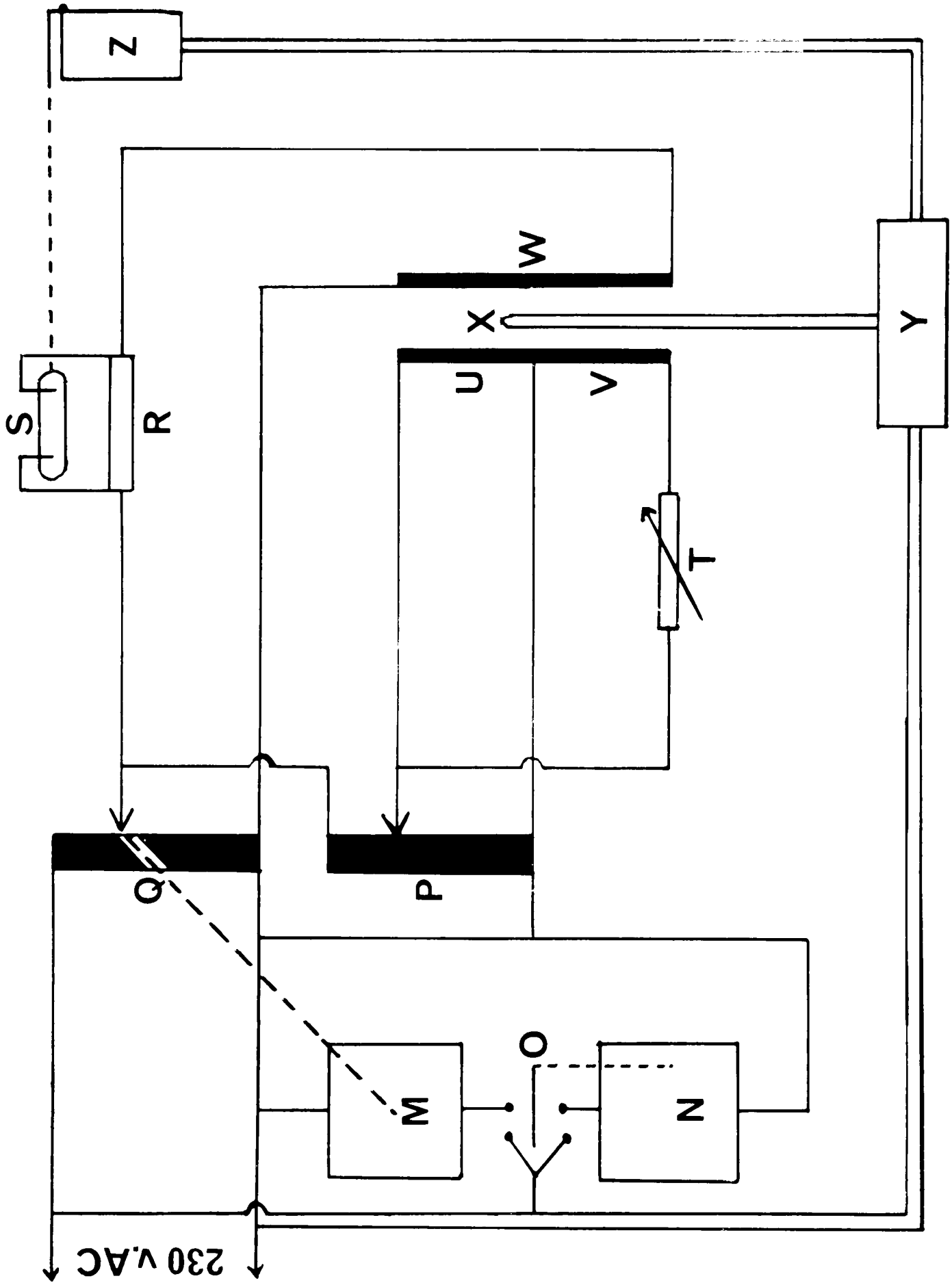


FIG. 3.2

way small variations in temperature of the upper thermocouple were counteracted by varying the average power dissipated in the outer winding. The small fluctuations in temperature of the outer winding, caused by switching the resistance in and out of the circuit, were not transmitted to the inside of the furnace, as shown by a monitor thermocouple inserted in the central tube.

The temperature of the lower thermocouple was read on an indicating pyrometer.

The mechanism for lowering the crucible is shown in Fig. 3.3. Rates of lowering of between 20 and 0.2 mm/hr were obtainable by using different gear trains and a standard 1 rev/hr. geared motor unit. When the crucible had been lowered far enough, the plate, which could be adjusted vertically on the lead screw, actuated a microswitch which switched off the lowering motor and switched on the motor-driven Variac to lower the temperature. The Variac was driven by a 1 rev/day motor, which, by changing the gear-train, could lower the temperature of the furnace at rates between 40°C/hr and 10°C/hr. A cam on the Variac spindle switched off the motor when the Variac supplied zero volts. A block diagram of the electrical circuits is given in Fig. 3.2.

Key to Fig. 3. 3.

A.

P Spur gears.

Q Slow-speed Motor.

R Slot in rod S in which screw T fits.

U Plate and locking nut.

V Screw Thread (2 mm. pitch)

W Microswitch.

X Clutch block.

Y Hook for crucible support rod.

B.

A Fixed Block.

B Threaded Hole for screw.

C Clutch Blocks.

D. Plungers.

E Tension Spring.

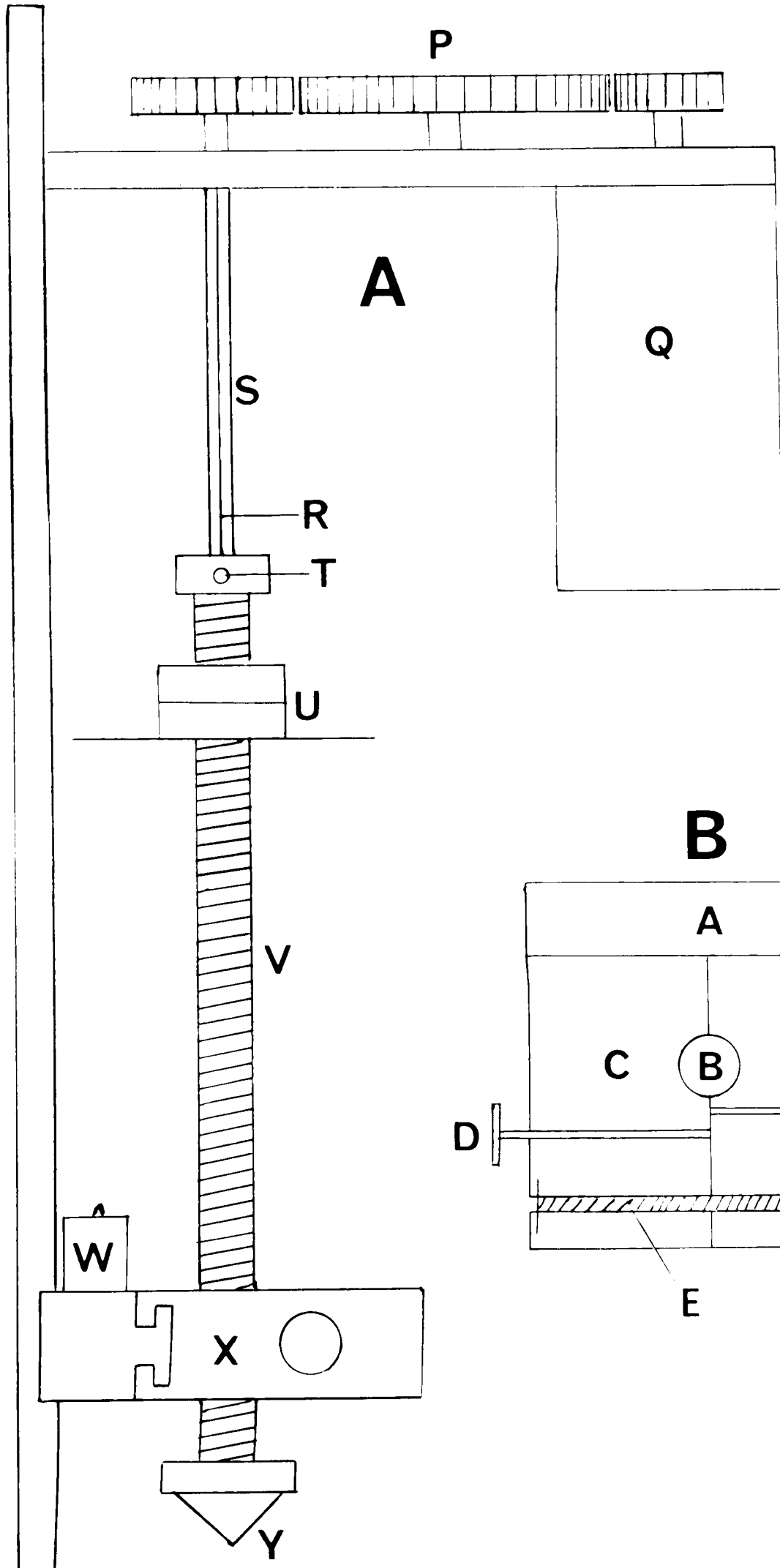


Fig 3.3

Three furnaces were constructed, two to take 1 cm. diameter crucibles, and one to take 2 cm diameter crucibles. The furnaces could be mounted, two at a time, on a Dexion framework, and could be used independently, since all the electric circuits were duplicated.

3.2. METHOD OF SETTING-UP AND USING THE FURNACES.

When the proportioning band of the controller was set to fine limits for most accurate temperature control, the voltages across the windings had to be set accurately, otherwise large fluctuations in mains voltages would have caused the temperature of the furnace to drift outside the proportionning band. Therefore, it was necessary to use the following procedure when setting up the furnace for a run.

From the melting-point of the substance concerned, say $t^{o}C$, the temperatures required in the top and bottom zones of the furnace were selected. Generally they were $t+30^{o}C$ and $t-40^{o}C$ respectively. Then, having set the proportioning band of the controller to its widest extent ($\pm$ $50^{o}C$) the controller set point was set at $t+30^{o}C$. The furnace was then warmed up to $t-150^{o}C$ (approximately) using the outer winding only. The inner winding was then used to raise the temperature of the top half of the furnace

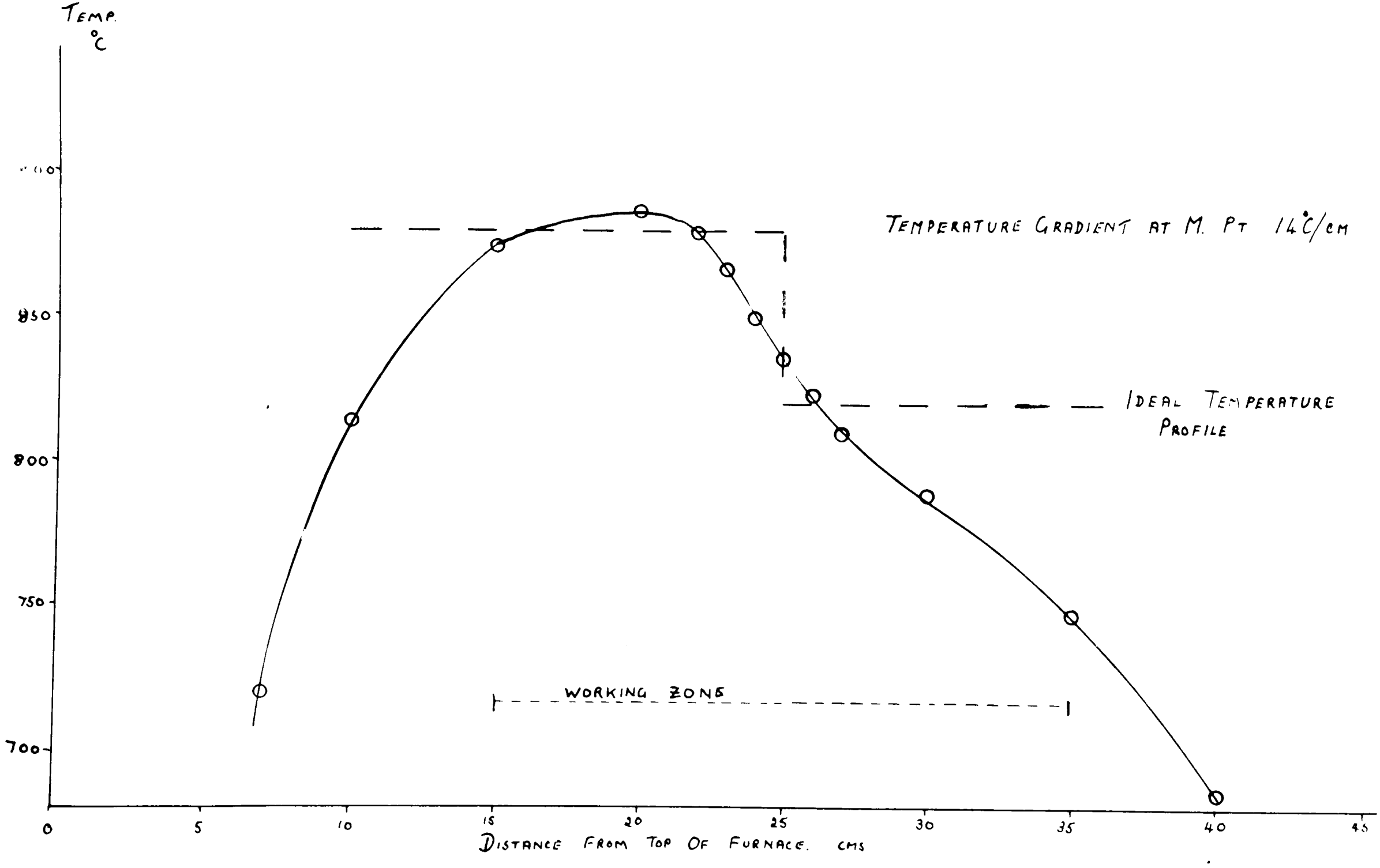
to the required temperature. The temperature of the bottom half of the furnace was then brought to t-40°C using the variable resistance R. When the temperature of the top half of the furnace was within 15°C of the required temperature the proportioning bandwidth was reduced to ± 5°C. The furnace was then ready for use.

The lowering mechanism was adjusted to give the required amount of travel to the crucible, which was suspended from the hook by a nickel rod. The contents of the crucible were then melted very carefully from the top with a gas-oxygen torch, and the crucible was then transferred to the furnace. All the bubbles were removed from the tip and sides of the crucible by very careful tapping against the side of the furnace. After an interval of 1 hour to allow the temperature of the furnace to restabilise, the lowering motor was switched on, and from that point the crucible was lowered through the temperature gradient and cooled to room temperature without further attention.

3.4. RESULTS AND DISCUSSION.

The design of the furnace is simple yet practical. Although the temperature gradient in the furnace is not very sharp, (Fig. 3.4), good and consistent results were obtained using this arrangement. The temperature profile

Fig. 3.4


TEMP. °C
850
800
750
700
0
5
10
15
20
25
30
35
40
45
DISTANCE FROM TOP OF FURNACE. CMS
TEMPERATURE GRADIENT AT M. PT 14°C/CM
IDEAL TEMPERATURE PROFILE
WORKING ZONE

could have been improved by inserting a silver tube in the lower half of the furnace, and it is possible to produce a furnace with a nearly ideal temperature profile by using a large number of independent windings, but these refinements were not found to be necessary in this work.

A large number of different crystals was grown in these furnaces. The melting-points and physical characteristics varied greatly (Table 3.1) A complete failure was experienced only in the case of $TbCl_3$. This failure was due to a phase-change, occuring at 530°C, which will be discussed later (Chapters 4 and 6). In addition to the crystals tabulated in Table 3.1. many crystals were grown which contained deliberate impurities in small amounts (.01%-10%), generally using $LaCl_3$ as the host lattice. In addition $HoCl_3$ was grown containing 5% and 10% of $ErCl_3$, and $GdCl_3$ was grown containing in one case 5% $NdCl_3$ and in another case 2% of $DyCl_3$. Pure and "doped" silver halides and sodium chloride were also grown.

Lanthanon halides which crystallize with the hexagonal $LaCl_3$ structure are in general the most difficult to grow, only about half the samples growing a good single crystal on the first pass through the furnace, even when using the slowest growth rates. The crystals tended to grow with the hexad axis along the length of the crucible,

and they were generally striated parallel to this axis. These crystals also tended to be twinned, the crystal twins differing in their orientation by up to 5^{o}. However, twinning did not seriously affect the majority of the experiments for which the crystals were subsequently used.

Some points with regard to the growth of $GdCl_3$ are interesting. $GdCl_3$ is the last of the lanthanon chlorides to crystallize with the $LaCl_3$ structure. It is able to accommodate the larger ions of the preceding lanthanons which form chlorides of the same structure type. On the other hand, $GdCl_3$ will not take in more than 30% $DyCl_3$ before the structure type changes, although Dy^{3+} is only 3% smaller than Gd^{3+}

Crystals of $GdCl_3$ containing 5% Nd and Dy were grown, using the slowest possible rates and, as expected, the crystal doped with Nd was of a better quality than that doped with Dy. Untwinned pieces of the latter crystal measured only 2 mm cube. However, these pieces were large enough for the optical experiments for which they were required.

It is also of interest to note that a crystal containing approximately equal amounts of $CeCl_3$ and $PrCl_3$

was grown. The quality was not at all good, but there was no sign of segregation in the crystal. A differential thermal analysis run showed that the crystal melted sharply.

Chlorides of the monoclinic YCl_3 structure-type grew readily as single crystals, even at the fastest growth rates. The crystals always cracked along the (001) cleavage plane into lamellae 2-5 mm thick, but specimens large enough for the present work were easily obtained.

Crystals of Li_3YCl_6 doped with both 5% and 10% of both $ErCl_3$ and $DyCl_3$ were grown up to 5 mm^3, but very slow cooling had to be used in order to prevent cracking, due to a large contraction on cooling. Several methods of preparing the stoichiometric mixtures were tried, but the best appeared to be to fuse stoichiometric quantities of the anhydrous chlorides.

Pure crystals of Cs_2KYCl_6 could only be grown by zone-refining the fused chlorides. Up to ten passes were used, the last pass was at a rate of 1cm/hr, and crystals of up to 5 mm^3 were obtained.

It is of interest to note that "mixed halide" crystals were always cloudy unless they were zone-refined, even though

the starting materials were purified either by distillation or zone-refining. The reason for this is not known.

TABLE 3.1.

M.Pt.°C.	Substance	Structure Type.	Comment.
434	AgBr	Cubic NaCl	$\frac{1}{3}$ atmosphere of bromine gas
455	AgCl	" "	
801	NaCl	" "	
852	$LaCl_3$	Hex. $LaCl_3$	Also grown containing impurities up to 5%
802	$CeCl_3$	" "	
789	$CeCl_3/PrCl_3$	" "	
760	$NdCl_3$	" "	
588	$TbCl_3$	Orthrh.$PuBr_3/YCl_3$	Only grown as twinned needles 1mm x 1mm x 3mm
654	$DyCl_3$	Monoclinic YCl_3	
892	$LuCl_3$	" "	
700	YCl_3	" "	
783	$LaBr_3$	Hexagonal $LaCl_3$	
765	$GdBr_3$	----	Difficult to grow into large clear crystals.
498	Li_3YCl_6	Hexagonal	Grown Pure & Doped.
830	Cs_2KYCl_6	Cubic	Material must be zone refined for pure crystals.

CHAPTER 4.

SOME PHASE SYSTEMS CONTAINING RARE-EARTH HALIDES.

4.1. INTRODUCTION.

The properties of lanthanon ions in different crystal lattices are currently the subject of research in many laboratories through the world. To date, most of this work has been concentrated on previously known compounds of the lanthanons and on compounds of simple crystal structures which contain substitutional lanthanon ions. The need for good single crystals of these materials and the methods used to prepare some of them have been discussed in the previous chapter. To ensure a supply of suitable materials for future research it is necessary, (a) to examine the possibility of preparing new lanthanon compounds and (b) to obtain more physico-chemical information on compounds already being studied.

(a) This thesis is largely concerned with a study of lanthanon trichlorides, both pure and in various admixtures with one another. As discussed later (Chapter V) lanthanon trichlorides crystallize in three different types of structures, depending on the ionic radius of the lanthanon. From the point of view of planning experiments on mixed

lanthanon chlorides, it is clearly important to know the extent of mutual solubility in the solid state, particularly between chlorides of two different structure-types. For this reason, several binary systems of lanthanon chlorides have been investigated. Two, possibly three, lanthanon chlorides are known to be dimorphic (5), and the relationship between composition and structure of several mixed lanthanon chlorides has also been examined.

(b) Compounds of lanthanon chlorides and alkali metal chlorides have been reported (10 and 11). Some of these systems have been investigated in more detail, and a completely new investigation of the lithium chloride-yttrium chloride system has been undertaken, with the discovery of a new series of rare-earth compounds of general formula Li_3LnCl_6.

Systems containing tetravalent lanthanons have been examined briefly. The only pure tetravalent lanthanon compound that has been obtained as single crystals is cerium dioxide. Such compounds as CeF_4 and TbF_4 have been obtained as powders (12). As there is considerable interest in the properties of tetravalent lanthanon ions, especially Tb^{4+}, which is isoelectronic with Gd^{3+}, attempts have been made to stabilise the tetravalent ions sufficiently to

enable single crystals to be grown. This has not been successful, but considerable information about binary systems of alkali fluoride and lanthanon tetrafluorides has been acquired.

The methods used to determine the phase diagrams fall into two parts. A preliminary investigation of the phase system was accomplished by the X-ray powder diffraction, disappearing-phase, method, whereby the formulae of the compounds formed could be determined. The X-ray powder diffraction patterns were indexed where possible to give information on the unit cell size and symmetry. The phase diagram was then determined using differential thermal analysis (D.T.A.) The basis of this method will be described in the next section.

4.2. EXPERIMENTAL METHODS.

4.2a. Preparation of mixtures. The starting-point for all investigations was the anhydrous chloride of the metal. Rare-earth chlorides were prepared as described in Chapter 2. Alkali metal chlorides were dehydrated by fusion under vacuum, ($\sim$ 10 microns pressure). The chlorides were weighed out in the correct proportions in stoppered bottles, all transfer of material taking place in a dry-box. The

chlorides were mixed, and fused under ½ atmosphere of dry helium gas, and the samples stored in a drybox until needed.

4.2b. X-ray powder diffraction method. The X-ray powder diffraction pattern of a substance is solely characteristic of that substance, and can be used to identify that substance when alone or in a mixture. The limits of compound formation and the phases present in a mixture were determined by this method. The presence of high temperature crystallographic forms was determined using quenching techniques, since a high temperature camera was not available.

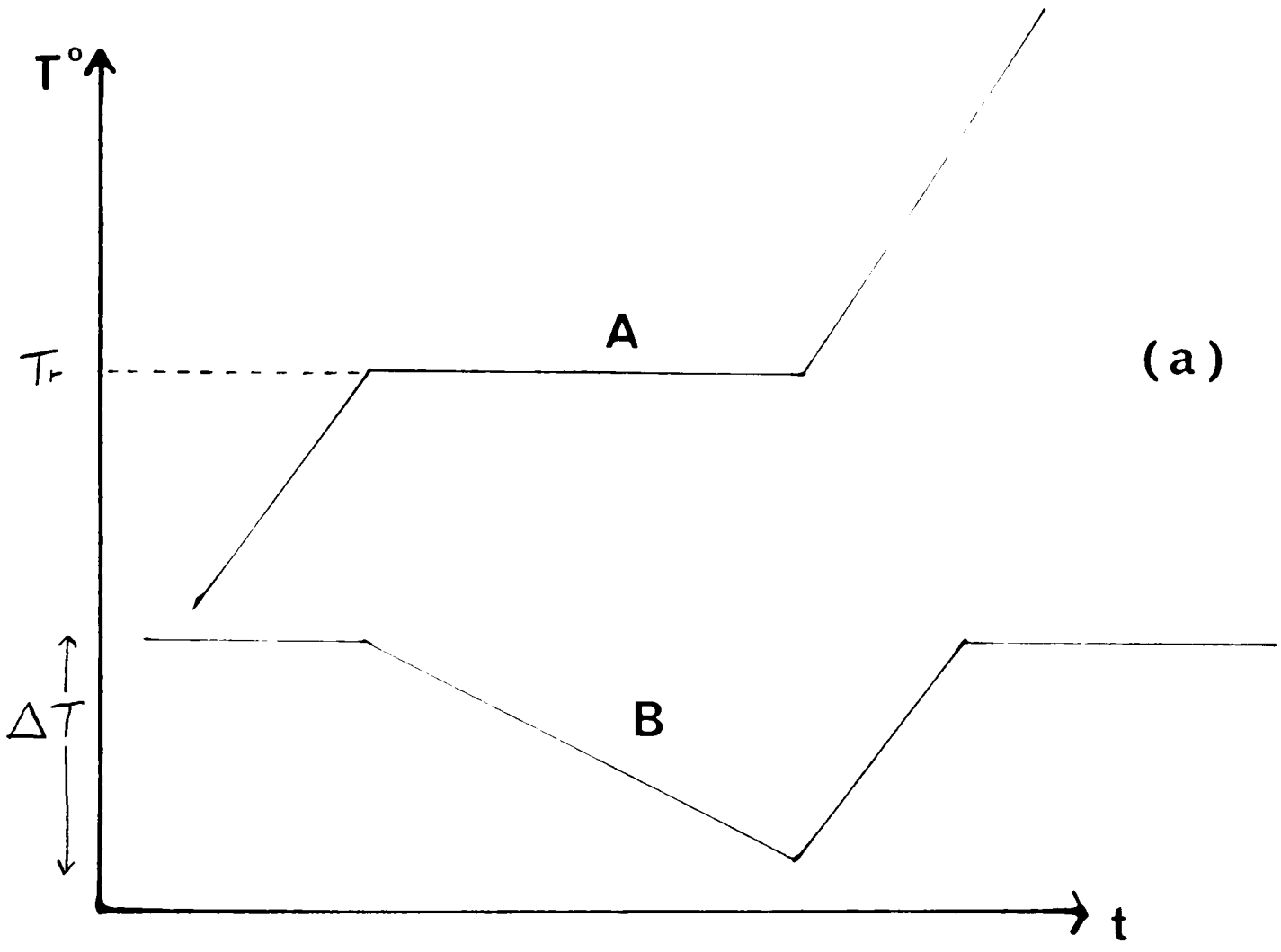
4.2c. Differential thermal analysis. An extensive coverage of the history and development of D.T.A., the various techniques and apparatus and also the available literature is given by Smothers and Chiang (13). Although the method was first developed for use in the identification of clays and minerals, it can also be used to study phase systems.

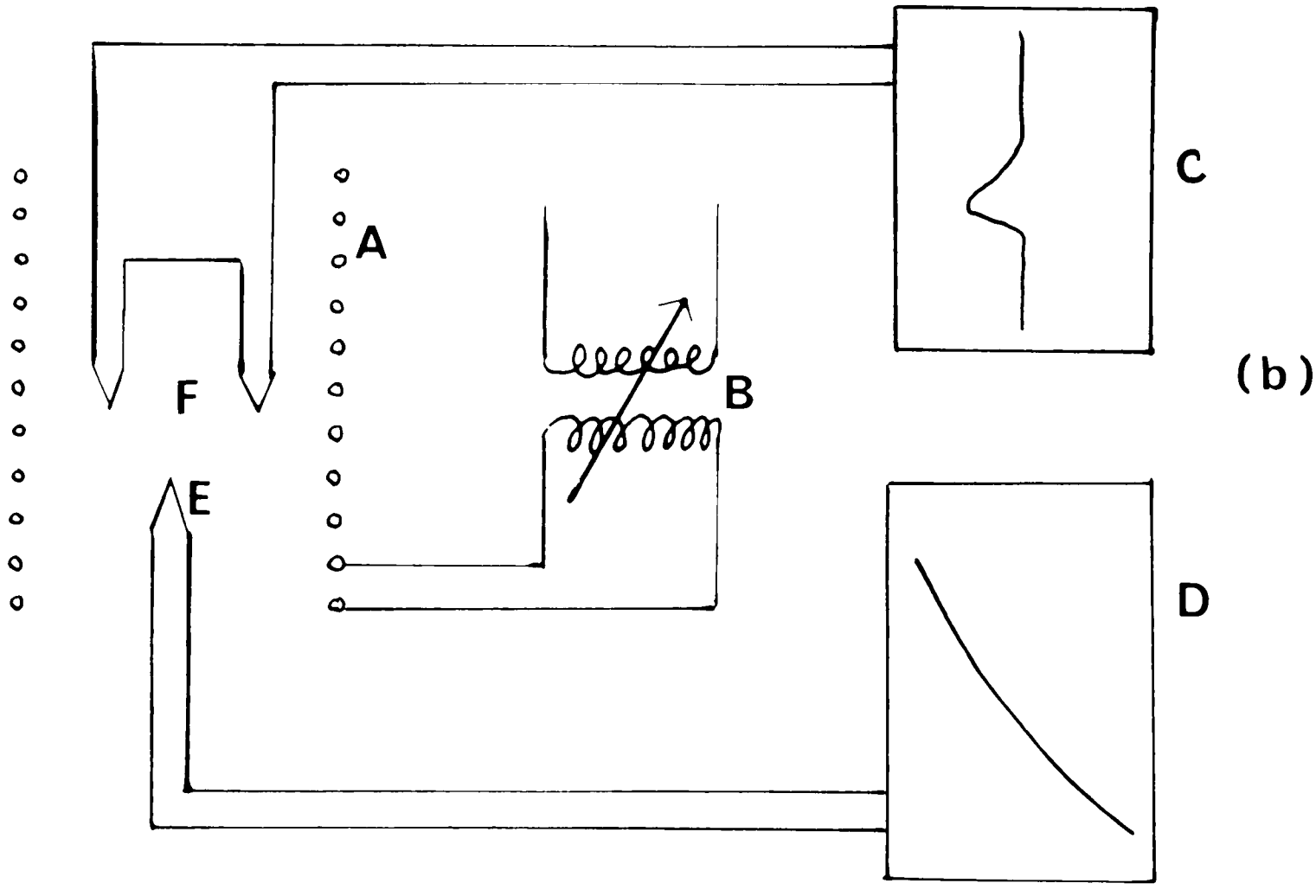
The basis of the method is as follows. When a chemical reaction or a change of phase occurs, heat is either liberated or absorbed. If a substance is heated at a constant rate and a change occurs, the temperature of the centre of the sample, when plotted against time, gives a curve of the type shown in Fig. 4. 1 (a) A, Tr being the temperature

Key to Fg. 4. 1.

(b)

A Furnace Windings
B Variac
C Differential Recorder
D Temperature Recorder
E Temperature Recording Thermocouple
F Differential Thermocouples.





F I G 4.1

of the onset of the transformation. This is the basis of the method of thermal analysis. However, if the temperature of the centre of the sample is compared with the temperature of an inert sample subject to the same conditions, and the differential temperature plotted either against time or the temperature of the sample a curve similar to that shown in Fig. 4.1. (a) B. is obtained. The temperature of the onset of the change is the temperature at which the graph leaves the baseline. A block diagram of the thermocouple arrangement is shown in Fig. 4. 1 (b).

The fundamental advantages of D.T.A. are twofold. The differential signal from the thermocouple can be amplified, producing a greater sensitivity than thermal analysis, provided that noise and A.C. pick-up can be avoided. A peak is also easier to detect on a recorder trace than an arrest or a change in slope. These two factors increase the resolution of the method, allowing much smaller quantities of material to be used than in thermal analysis. This last is an important consideration when dealing with some lanthanon halides.

A small sample size has additional advantages. Thermal gradient effects in what is, after all, a dynamic system,

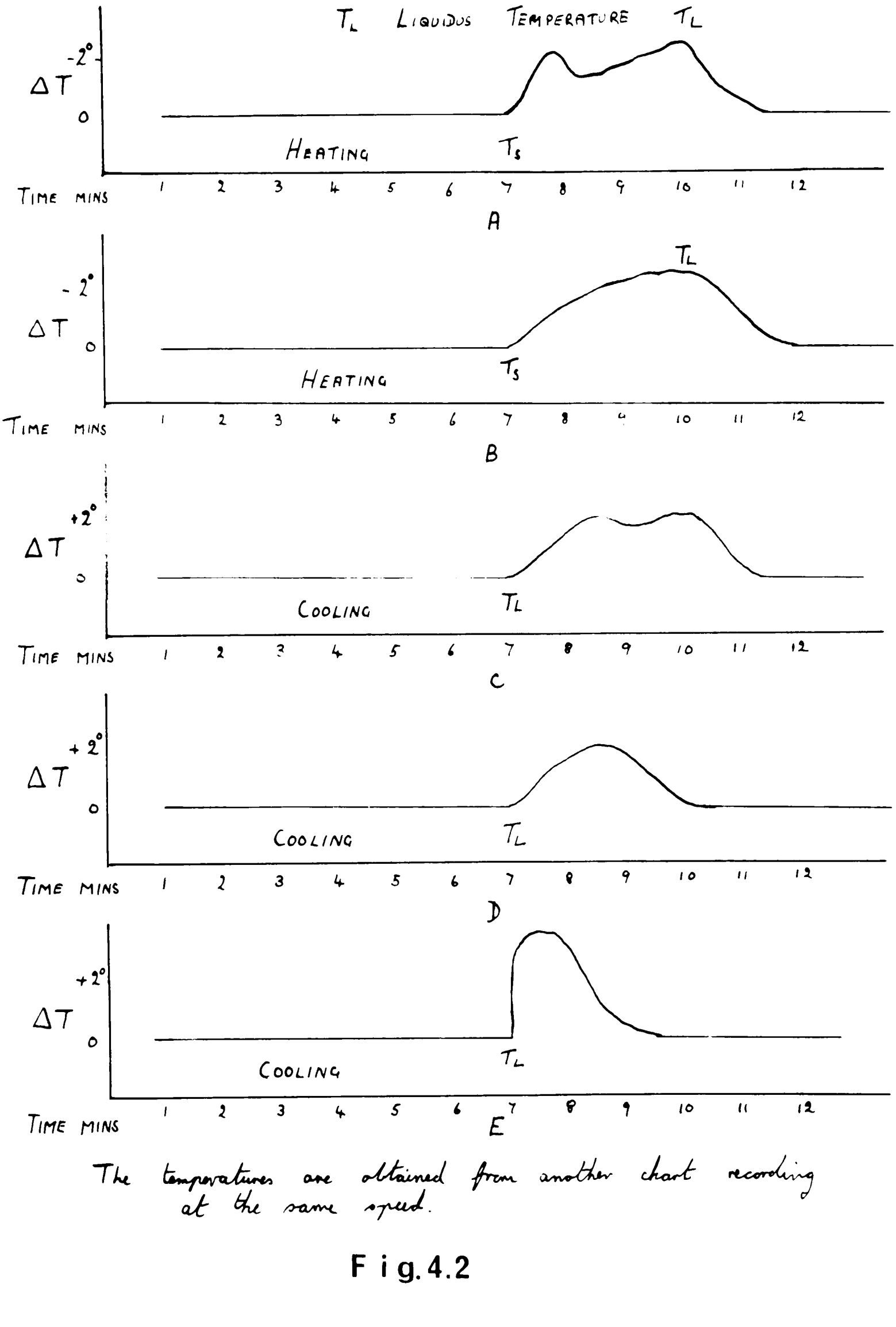
are minimised. This is especially important where solid state changes are concerned, since Stirring a sample is not possible. Also effects due to any inhomogeneities in the sample are minimised. Another major advantage of the D.T.A. method lies in the determination of liquidus points. Thermal analysis curves will only show an inflexion, which is often missed if the heating or cooling rate is not constant.

D.T.A. curves show a variety of effects. Often a solidus-liquidus transition is shown by two peaks (Fig.4.2.A). These two peaks are sometimes not resolved (4.2.B) In both cases the liquidus temperature, T_L , is taken as the temperature at which the trace starts to return to baseline. The liquidus temperature can be checked by allowing the system to cool through the liquidus temperature, when a curve similar to 4.2.C. or 4.2.D. can be obtained. Sometimes supercooling occurs, when an extremely sharp deviation from the baseline is seen (Fig.4.2.E)

The differential thermal analysis apparatus was designed and built by Mr. T. Cooke in the laboratory (14) and is described in detail elsewhere. A diagram of the reaction-chamber is shown in Fig. 4.3. The sample is contained in a silica cup, made from 7MM I.D. quartz tubing,

T_S SOLIDUS TEMPERATURE

T_L LIQUIDUS TEMPERATURE



The temperatures are obtained from another chart recording at the same speed.

Fig.4.2

tubing, which rests on the end of a chromel-alumel thermocouple. A second thermocouple supports the reference sample in a similar cup. The third thermocouple, which has a thermostatically controlled cold junction, measures the temperature in the chamber. The reaction chamber is connected to a vacuum line with rubber tubing. The chamber could be filled with helium gas which had been dried by passing it through activated charcoal at liquid nitrogen temperatures. The reaction chamber is small enough to go into a dry-box, so that samples can be loaded in an inert and moisture-free atmosphere.

The thermocouples were made from "Thermocoax" thermocouple wire. The thermocouple wires were insulated with MgO, and the whole was sheathed in stainless steel. The total thermocouple thickness was 1 mm. Use of this type of thermocouple reduced both A.C. "pick-up" from the furnace, and also thermocouple wear, due to corrosive gases being emitted when a slightly damp sample was heated.

Two recorders were used, one to record the differential temperature, and one to record the temperature of the chamber. Both recorders were Wests "Rustrak" potentiometric recorders, recording twice per second on pressure-sensitive paper. Each recorder could be offset from + 7mV to -20 mV, with the

Key to Fig. 4. 3.

A Silica Tube.
B Sample Cup.
C Graphite Felt
D Stainless Steel Plate
E Stainless Steel Rod
F Thermocoax Thermocouple Wire
G "O"-rings
H To Vacuum Line
J Thermocoax Socket
K Vacuum Seal

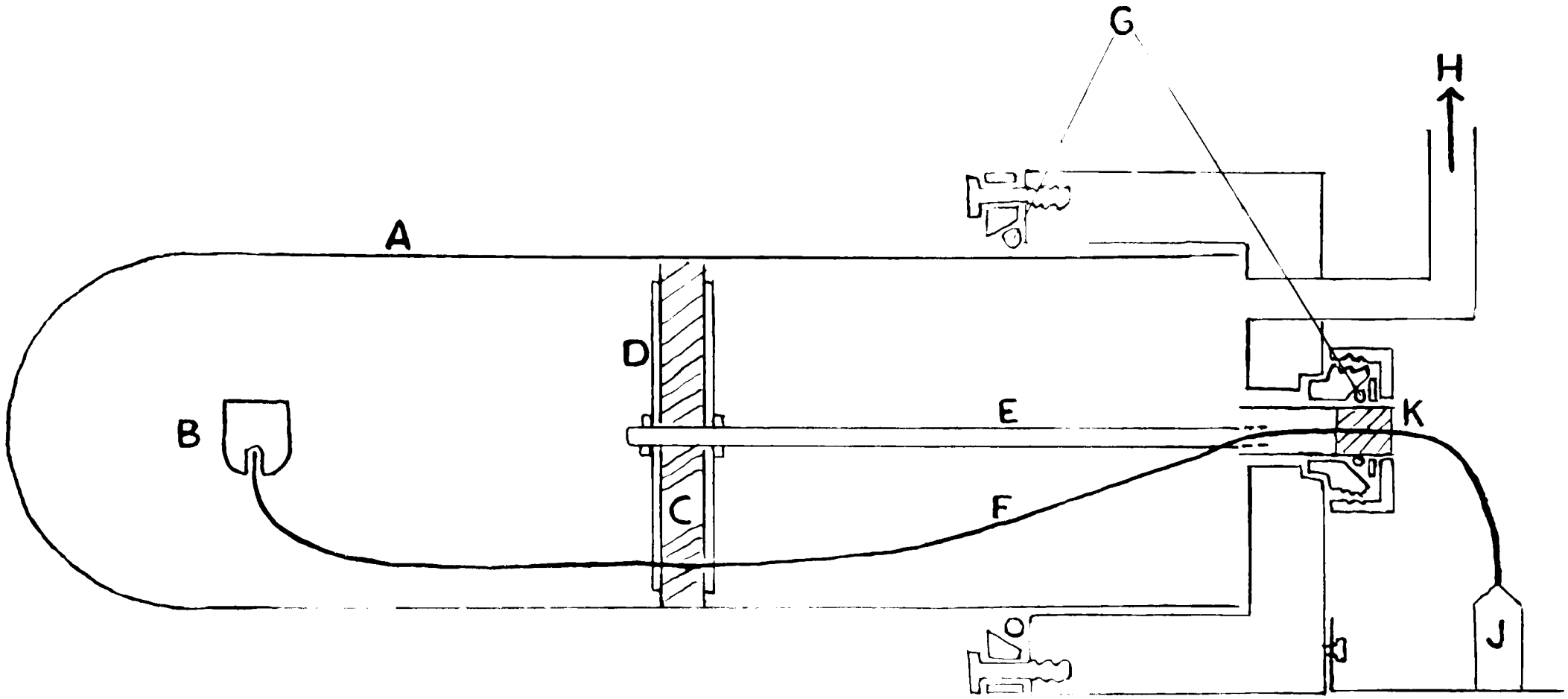


FIG 4.3

sensitivity adjustable from 600 μV to 200mV full-scale. In practice the differential recorder was set at full gain, the temperature recorder at 4mV full scale, corresponding to about 100°C. The input to the temperature recorder was measured with a potentiometer for calibration purposes.

The following operating procedure was adopted after several trials. The sample cup was cleaned with aqua regia and dried. The sample and reference sample of alumina were loaded in a drybox. The chamber was then sealed, removed from the dry-box and placed on the vacuum line, and pumped out to 10 microns while the furnace temperature was 200°C. Dry helium at atmospheric pressure was then admitted to the sample chamber. The Variac which was attached to the furnace was then set manually to give the required rate of increase of temperature in the range of temperature to be studied. The normal rate of heating was 10°C/min. If the Variac setting were altered in the course of a run, a change of baseline occurred which made the charts difficult to interpret.

The apparatus was calibrated using cesium chloride as a standard. The following temperatures were used;

(a) Inversion temperature 445°C.

(b) Melting Point 646°C.

The heating-rate in both cases was about 10°C/min. The melting-points of all the pure components of a phase-system were checked, and found to be correct to within 5°C, the accuracy of the apparatus. The following temperatures were obtained from the D.T.A. curves.

1) A solid-state transition point or the melting-point of a substance was taken where the first deviation from baseline occurred.

2) The solidus temperature was taken as the point at which the baseline first deviated.

3) Liquidus temperatures were the most difficult to determine accurately. Two methods were used
(a) The point at which the curve started to return to baseline, while heating the sample and
(b) the temperature of first deviation from baseline on cooling. If there was more than 5°C discrepancy between the points, the results were judged to be unreliable.

4.3. Results and Discussion.

The types of binary system that were studied fall into several groups, and each will be treated separately.

4.3(a). The systems NaF/PrF_4, NaF/TbF_4 and NaF/UF_4.

TbF_4 has been made (12) but does not order magnetically at liquid helium temperatures (3). PrF_4 is not known, but the system NaF/PrF_4 has been said to form three compounds, $NaPrF_5$, Na_2PrF_6 and Na_4PrF_8 (15). Zachariasen (16) has studied the system NaF/UF_4, and found the compounds $NaUF_5$, Na_2UF_6 and Na_3UF_7. Until this work no attempt has been made to prepare analogous compounds of terbium.

All the terbium and praseodymium compounds were prepared by fusion of stoichiometric mixtures of the anhydrous chlorides, followed by fluorination or hydrofluorination of the finely ground product in a nickel boat at 350°C. The uranium compounds were prepared by fusion of the anhydrous fluorides.

The compounds formed were identified by their X-ray powder diffraction patterns (Table 1). Analysis of the Terbium (iV) compounds was difficult, due to their low solubility. The method described by Asprey and Keenan (15) was used but with little success.

A known weight of the compound was dissolved in .1M $Al\,Cl_3$ solution containing HCl and KI, and the iodine liberated was titrated with standard thiosulphates. The following results were obtained:-

Table 4.1

	Tb^{4+}	Pr^{4+}	U^{4+}
Ionic radius	.84Å	.90Å	.93Å
$NaF + MF_3$	$NaTbF_4$ Hexagonal a=6.008Å c=3.566Å	$NaPrF_4$ Hexagonal[6] a=6.11Å c=3.74	
$2NaF + MF_3$	$NaTbF_4 + NaF$	$NaPrF_4 + NaF$	
$3NaF + MF_3$	$NaTbF_4 + 2NaF$	$NaPrF_4 + 2NaF$	
$4NaF + MF_3$	$NaTbF_4 + 3NaF$	$NaPrF_4 + 3NaF$.	
$NaF + MF_4$	$NaTbF_5$ Rhombohedral a=8.79Å α=107.0°	$NaPrF_5$ Rhombohedral[6] a=8.86Å α=107.9°	$NaUF_5$ Rhombohedral
$2NaF + MF_4$	Na_2TbF_6 Hexagonal a=14.10Å c=9.53Å	Na_2PrF_6 Orthorhombic[6] a=5.54Å b=3.97Å c= 11.57Å	Na_2UF_6 Cubic a = 5.565Å Hexag. a = 5.94Å c= 3.74Å Ortho. a = 5.56 Å b = 4.01 Å c = 11.64 Å
$3NaF + MF_4$	Na_3TbF_7 Tetragonal a=10.66Å c=7.60 Å	Na_3PrF_7 Tetragonal a=10.82Å c=7.68 Å	Na_3UF_7 Tetragonal[7] a = 5.448 Å c = 10.896 Å or a = 10.86Å c = 7.73 Å
$4NaF + MF_4$	$Na_3TbF_7 + NaF$	$Na_3PrF_7 + NaF$	$Na_3UF_7 + NaF$

Table 4.2.

$NaTbF_4$ (CrK_α Radiation).

Reflection hkl.	Intensity.	$Sin^2\theta$ obs. x 10^4	$Sin^2\theta$ calc. x 10^4
100	M	491	485
110	M+	1459	1454
101	M+	1520	1517
200	W	1938	1939
111	W	2475	2486
201	S	2965	2971
210	W	3382	3393
002	W	4128	4128
300	M-	4358	4362
211	S	4418	4425
102	W	4624	4613
112	M	5587	5582
270	M	5811	5816
202	M-	6068	6067
310	W	6305	6301
311	M+	7331	7333
212	M	7520	7521
302	S	8492	8490
401	W-	8791	8787
320	W-	9207	9209

Table 4.3.

$NaTbF_5$ (CuK_α Radiation)

Reflection hkl Hex.	Rhomb.	Intensity.	$Sin^2\theta$ obs. x 10^4	$Sin^2\theta$ calc. x 10^4
011	010	W	103	104
201	$11\bar{1}$	W	223	222
102	110	M-	300	299
$\bar{1}31$	$\bar{1}20$	M-	341	341
220	$02\bar{2}$	W-	472	473
311) 003)	030) 221)	M-	937	938
223) 501)	$13\bar{3}$) 223)	M-	1051	1056 1050
124	130	M	1314	1313
242	$04\bar{2}$	M	1362	1362
143) 413)	$04\bar{1}$} $23\bar{2}$}	M	1412	1413 1411
314	$23\bar{1}$	S	1546	1549
044	040	M	1665	1667
432	$14\bar{3}$	M-	1716	1717
611	$23\bar{4}$	W	1761	1759
253) 523)	$05\bar{2}$) $24\bar{3}$)	S	2119	2118 2120
622	$24\bar{4}$	M	2308	2310
451	$05\bar{4}$	W	2468	2468

Table 4.3. (continued.)

Reflection hkl Hex.	Rhomb.	Intensity.	$Sin^2\theta$ obs. x 10^4	$Sin^2\theta$ calc. x 10^4
801	$33\bar{5}$	W	2588	2586
245	$15\bar{1}$	W	2723	2723
173) 713)	$\bar{1}6\bar{2}$) $34\bar{4}$)	W	2835	2832 2829
435	$25\bar{2}$	M	3083	3078
470) 740) 625) 724)	$\bar{1}6\bar{5}$) $15\bar{6}$) $35\bar{3}$) $35\bar{4}$)	M	3670	3664 3664 3669 3677
256) 526)	$16\bar{1}$) $35\bar{2}$)	M	3876	3874 3869

Table 4.4.

Na_2TbF_6 CuK_α Radiation.

Reflection hkl.	Intensity.	$Sin^2\theta$ obs. x 10^4	$Sin^2\theta$ calc. x 10^4
101	W+	107	105
200	W	156	160
111	W	197	185
201	S	221	225
002	M	262	262
102	W	303	301
300	M	356	359
301) 202)	M	419	424) 421)
220	M	482	479
003	W	587	588
302	S	611	621
312	W	780	780
321	W	813	823
213	W	871	868
223) 330)	W	1072	1067) 1077)
421	W	1192	1182
403	W	1236	1227
332) 214)	W	1331	1339) 1325)
421) 304)	W	1391	1378) 1405)

Table 4.4. (continued).

Reflection hkl.	Intensity.	$Sin^2\theta$ obs. x 10^4	$Sin^2\theta$ calc. x 10^4
314	M	1566	1565
521	S	1623	1621
205	W	1790	1794

Table 4.5.

Na_3TbF_7 CuK_α Radiation.

Reflection hkl.	Intensity.	$Sin^2\theta$ obs. x 10^4	$Sin^2\theta$ Calc. x 10^4.
200	M	212	209
210	S	261	260
002	M	413	412
202	S	619	621
320	M	680	679
222	W	827	830
113	M	1034	1031
402	W+	1255	1248
332	W	1352	1352
440) 004)	S	1658	{1672 {1647
204	W-	1854	1856
214	W	1906	1908
620	M	2721	2717
524	W	3156	3162
444	W	3327	3319
820	M	3560	3553
733	M	3948	3957
317	W	5557	5567

Table 6.

Na_3PrF_7 (CuK_α).

Reflection hkl	Intensity.	Sin^2 obs. x 10^4	Sin^2 calc. x 10^4
200	M	205	203
210	S	254	254
002	M	403	403
202	S	606	606
320	M	661	660
222	W-	808	809
113	M	1009	1008
322	M	1062	1063
402	W+	1215	1215
500	S	1278	1269
323	W	1557	1566
440) 004)	M	1618	1625) 1611)
403	M	1718	1719
423	S	1911	1922
602	S	2229	2230
523	M	2360	2379
550	M	2550	2539
731	W	3060	3045
633	M	3194	3192

Table 4.6. (continued).

Reflection Hkl.	Intensity.	Sin^2 obs. x 10^4	Sin^2 calc. x 10^4
006) 624)	M	3634	3625) 3641)
644	W	4254	4251
317	W	5338	5242

Table 4.7.

Na_3UF_7 (CuK_α Radiation).

Zachariasen.			Present Work.		
Refn. hkl.	Sin^2 Calc.x 10^4	Int.	Sin^2 obs.x 10^4	Sin^2 calc.x 10^4	Refn. hkl.
100 002	200	M	203	201 200	200 111
101	250	S	253	252	210
		W	321	300	201
102 200	400 400	M	404	403 398	220 002
202	600	S	603	603 599	311 202
103	650	DM	671	655 650	320 214
004 200	801 801	M	807	806	400
		DW	897	902 895	312 003
210 202	1001 1001	M	997	996 1008	113 331
211	1051	M	1056	1053	322
		DS	1121	1106	421
212 114	1201 1201	M	1208	1204	402
		S	1348	1358 1348	501 503
213	1451	M	1457	1461	520
220 204	1602 1602	S	1611	1612	440

Table 4.7 (contd.)

	Zachariasen.			Present Work.	
Refn. hkl.	Sin^2 Calc.x 10^4	Int.	Sin^2 obs.x.10^4	Sin^2 calc.x 10^4	Refn. hkl.
006) 300) 214)	1802 1802 1802	W	1813	1813 1812 1802	600 531 333
310) 116) 304)	2002	S	2012	2015 2010	620 642
312) 116)	2202	S	2217	2211	602

TbF_4	84%	of	calculated	amount	of	Tb^{4+}
$NaTbF_5$	36%	"	"	"	"	"
Na_2TbF_6	72%	"	"	"	"	"
Na_3TbF_7	90%	"	"	"	"	"

In all cases part of the sample remained undissolved, even after several days, but the X-ray powder diffraction patterns showed no undissolved phase to be present in detectable amounts (i.e. >5%).

Gravimetric determination of terbium, as the trifluoride or the oxide also gave inconsistent results. Samples containing uranium and praseodymium were not analysed.

The X-ray powder diffraction results are summarised in Table 1. No D.T.A. runs were made on these systems, due to the thermal instability of TbF_4 and PrF_4. All the diffraction results are as expected from previous work, except for the following two discrepancies.

Na_2TbF_6 is not isostructural with Na_2PrF_6, and their diffraction patterns are in no way similar. However, since Na_2UF_6 is polymorphic, Na_2TbF_6 and Na_2PrF_6 may be polymorphic.

The compound, $3NaF.PrF_4$ was said not to exist (15) but present work indicates that this is the phase previously thought to be $4NaF.PrF_4$; the latter being Na_3PrF_7 containing

dissolved NaF. This is in agreement with Zachariasen's observations (16) that Na_3UF_7 could dissolve considerable amounts of NaF. The compound Na_3UF_7 has a similar diffraction pattern to Na_3PrF_7 and Na_3TbF_7 (Tables 5, 6, 7). However, the pattern obtained for Na_3UF_7 cannot be indexed on the basis of the unit cell postulated by Zachariasen. The reflections can be indexed on the basis of a related unit cell, isostructural with Na_3PrF_7 and Na_3TbF_7. Single crystal diffraction would resolve this problem, but attempts to produce a single crystal have not been successful.

Estimation of the relative stabilities of the phases containing TbF_4 and NaF was impossible due to difficulties encountered in the chemical analysis. All oxidised phases decompose over a period of a month with the evolution of fluorine. The only feasible way of making single crystals of these compounds would appear to be a low temperature flux method under fluorinating conditions. As this would necessitate a major piece of research it has not been attempted.

4.3.b. Systems containing rare-earth chlorides only. No work has been published on phase systems of this type. The only information available is that $TbCl_3$, $DyCl_3$ and possibly $HoCl_3$ are dimorphic (5).

The objectives of the work were three-fold. Firstly, the limits of stability of the three rare-earth chloride structure types were investigated, i.e. the systems $TbCl_3/GdCl_3$, $TbCl_3/DyCl_3$, $TbCl_3/HoCl_3$, $TbCl_3/TmCl_3$ and $GdCl_3/DyCl_3$. The systems $CeCl_3/EuCl_3$ and $TbCl_3/EuCl_3$ were briefly investigated in order to determine whether a reaction of the type

$$M_1^{3+} + M_2^{3+} \longrightarrow M_1^{2+} + M_2^{4+}$$

occurred, to give complex chloride compounds. Lastly, the systems $LaCl_3/TbCl_3$, $LaCl_3$-$DyCl_3$ and $LaCl_3$-YCl_3 were investigated in order to determine whether any new structures types occurred, in which two different rare-earth ions of very different ionic radii occupied two different lattice sites. In addition the variation in temperature of the α(monoclinic) -β(orthorhombic) transition was also observed.

The phase-diagrams of the systems given above are shown in Figs. 4.4 to 4.11. It was not possible to separate the solidus and liquidus points on all the phase diagrams.

$TbCl_3$ and $DyCl_3$, $HoCl_3$ and $TmCl_3$ are completely miscible in the solid state, although as normally obtained they have different structures. However, this is due to the high temperature α- form of $DyCl_3$ (having the YCl_3 structure) being quenched in. It is apparent from the phase diagram

that the stable form of $DyCl_3$ below 350°C is the β-form with the $TbCl_3$ structure. The corresponding transition temperature for $HoCl_3$ is, by extrapolation approximately 160°C.

The transition temperature of pure $DyCl_3$ is very difficult to determine, and it has not been possible to prepare pure β-$DyCl_3$, although it is possible to prepare it in an impure state. The following attempts were made either to observe the transition, or to prepare pure β-$DyCl_3$.

(a) α-$DyCl_3$ was cooled at ~ 5°C/hr. and also annealed at 340°C ± 2°C for 48 hours. Any β-$DyCl_3$ which was formed could not be determined by X-ray powder diffraction (5%).

(b) $DyCl_3.6H_2O$ was slowly dehydrated under vacuum at 150°C. The product was mainly α-$DyCl_3$. A D.T.A. run on the product sometimes gave endothermic peaks at 352°C, although the results were rarely consistent. This value of 352°C compares well with the values obtained by extrapolating the phase boundaries in the $TbCl_3/DyCl_3$, $GdCl_3/DyCl_3$ and $DyCl_3$/LiCl (17) systems.

(c) If the powder were annealed at 340-350°C under 6000 psi for 3 hours, there was approximately 50% conversion to β-$DyCl_3$.

(d) Attempts were made to prepare β-$DyCl_3$ by using solvents other than water. Alcohol and acetone, while giving appreciable solution, did not give β-$DyCl_3$ as a product, even after evacuation at 100°C. Soxhlet extraction with $CHCl_3$, CCl_4, C_2Cl_4, C_2HCl_3 showed that there was no appreciable solution. Hexachloropropene dissolved appreciable quantities of $DyCl_3$, but the product after the solvent had been removed gave a powder diffraction pattern which could not be interpreted.

The possible explanations for these phenomena are as follows. The activation energy for $\alpha \rightarrow \beta$ transition may be so high that the rate of reaction at 350°C is infinitely slow. The presence of impurity ions appears to reduce the activation energy by introducing distortions in the lattice.

The effects of pressure can be explained because of the reduction in molecular volume during the $\alpha \rightarrow \beta$ transformation. The molecular volume of α-$DyCl_3$ is 124Å^3, while that of β-$DyCl_3$ being 96Å^3. The formation of α-$DyCl_3$ is therefore favoured by low pressures, and vice-versa.

The corresponding crystallographic transformation of $HoCl_3$, which should occur at ~160°C, was never observed, even using the identical experimental conditions as for $DyCl_3$. There appears to be no region of two solid phases in the

system $GdCl_3/TbCl_3$. The change from the hexagonal $GdCl_3$ structure to one of the two $TbCl_3$ structures occurs quite sharply, and the X-ray evidence shows no co-existence of two solid phases. The two-phase region, which is demanded by the laws of thermodynamics must cover a composition range of no more than 1%. For all practical purposes, therefore, $GdCl_3$ and $TbCl_3$ are miscible in infinite proportions in the solid state, albeit with a change in structure, depending on the temperature and the composition.

The phase diagram of the system $GdCl_3/DyCl_3$ shows that these two substances have considerable mutual solubility, but there is a clear indication of a region in which two solid phases coexist.

The phase diagrams of the system $TbCl_3/DyCl_3$ and $TbCl_3/HoCl3$ show infinite solid solubility, and that the temperature of the phase transition decreases from $TbCl_3$ to $HoCl_3$. The phase diagram of the system $TbCl_3/TmCl_3$ shows infinite solid solubility, but the phase transition is not detectable at a composition of more than 40% $TmCl_3$. There also appears to be a minimum in the liquidus curvw.

The phase diagrams of the systems $LaCl_3/TbCl_3$, $LaCl_3/DyCl_3$ and $LaCl_3/YbCl_3$ are very similar. The solid solubility of the large La^{3+} ion in $TbCl_3$, $DyCl_3$ and

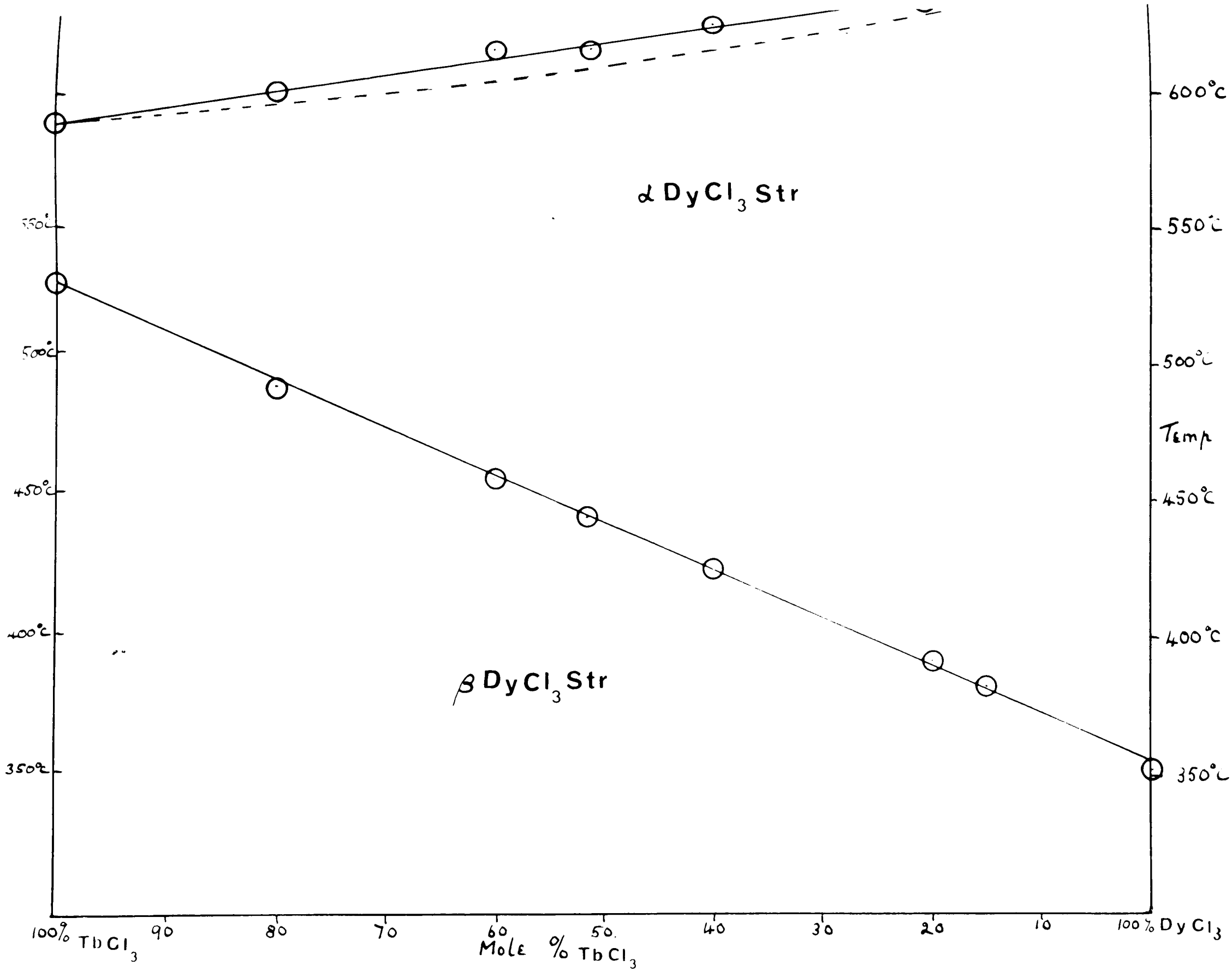

600°C
550°C
500°C
450°C
400°C
350°C
Temp
α DyCl3 Str
β DyCl3 Str
100% TbCl3
90
80
70
60
50
40
30
20
10
100% DyCl3
Mole % TbCl3

Fig 4.4

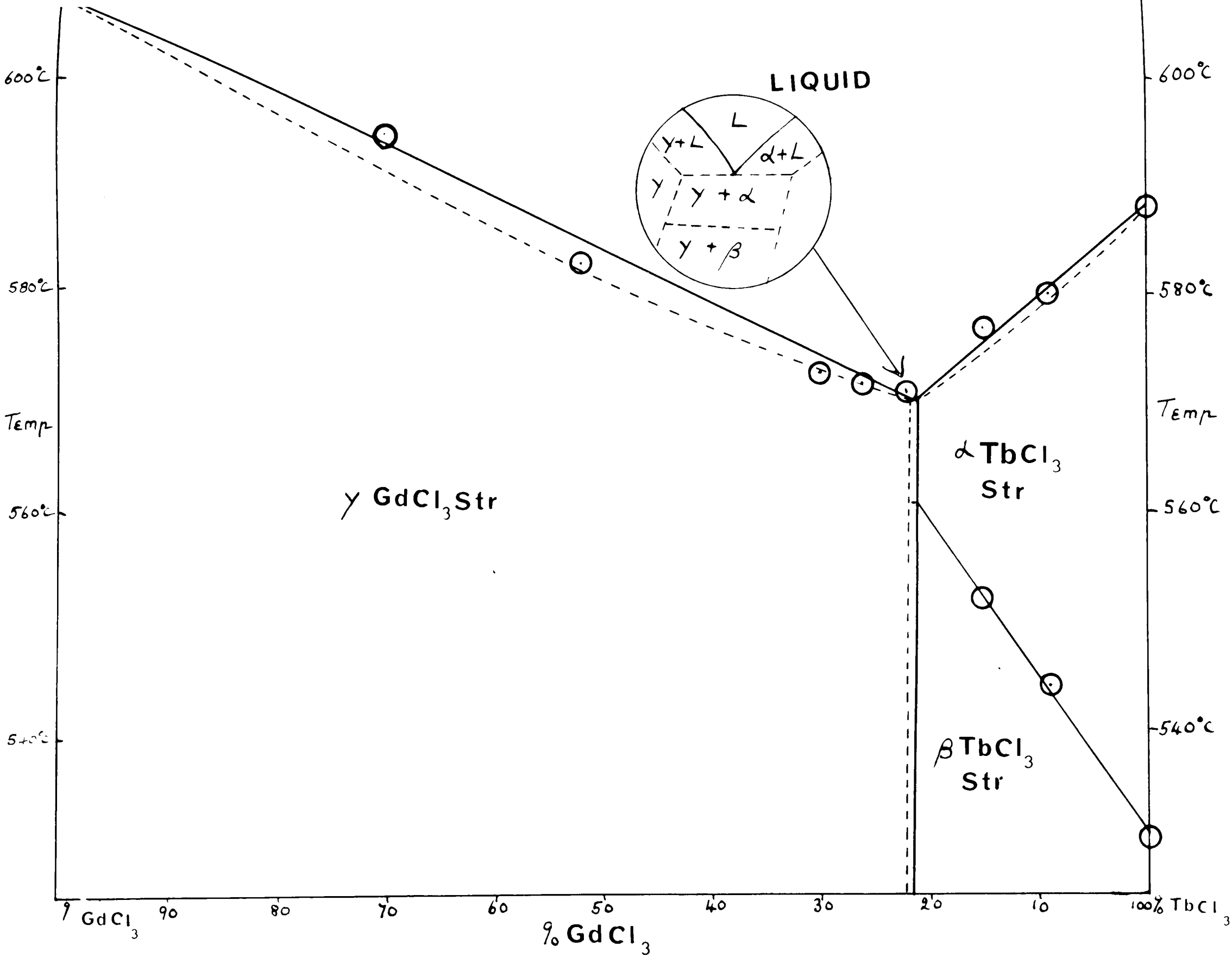

LIQUID
L
γ+L
α+L
γ
γ + α
γ + β
600°C
580°C
560°C
540°C
Temp
γ GdCl3 Str
α TbCl3 Str
β TbCl3 Str
100% GdCl3
90
80
70
60
50
40
30
20
10
100% TbCl3
% GdCl3

Fig 4.5

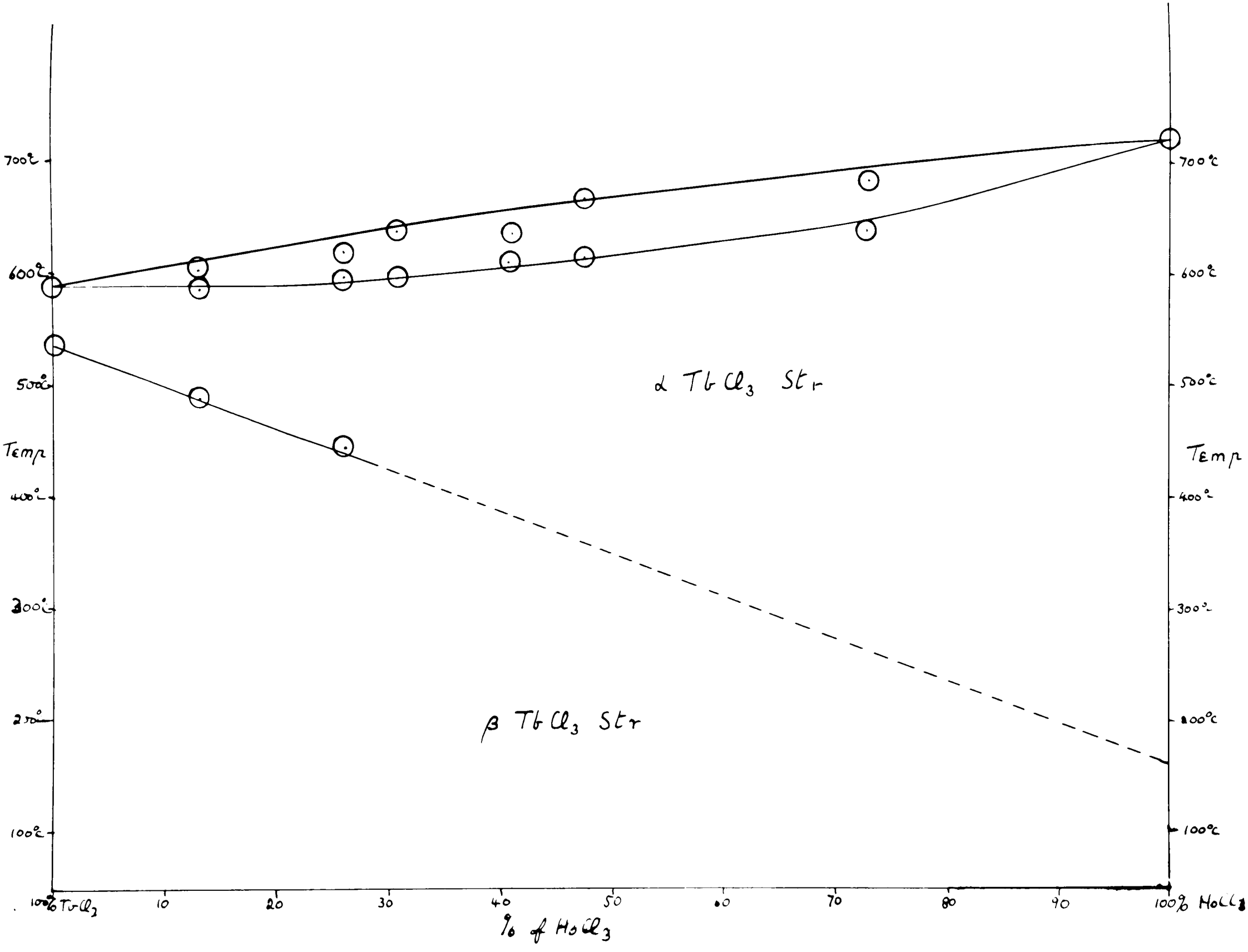

700°C
600°C
500°C
Temp
400°C
300°C
200°C
100°C
α TbCl3 Str
β TbCl3 Str
10% TbCl3
10
20
30
40
50
60
70
80
90
100% HoCl3
% of HoCl3

Fig 4.6

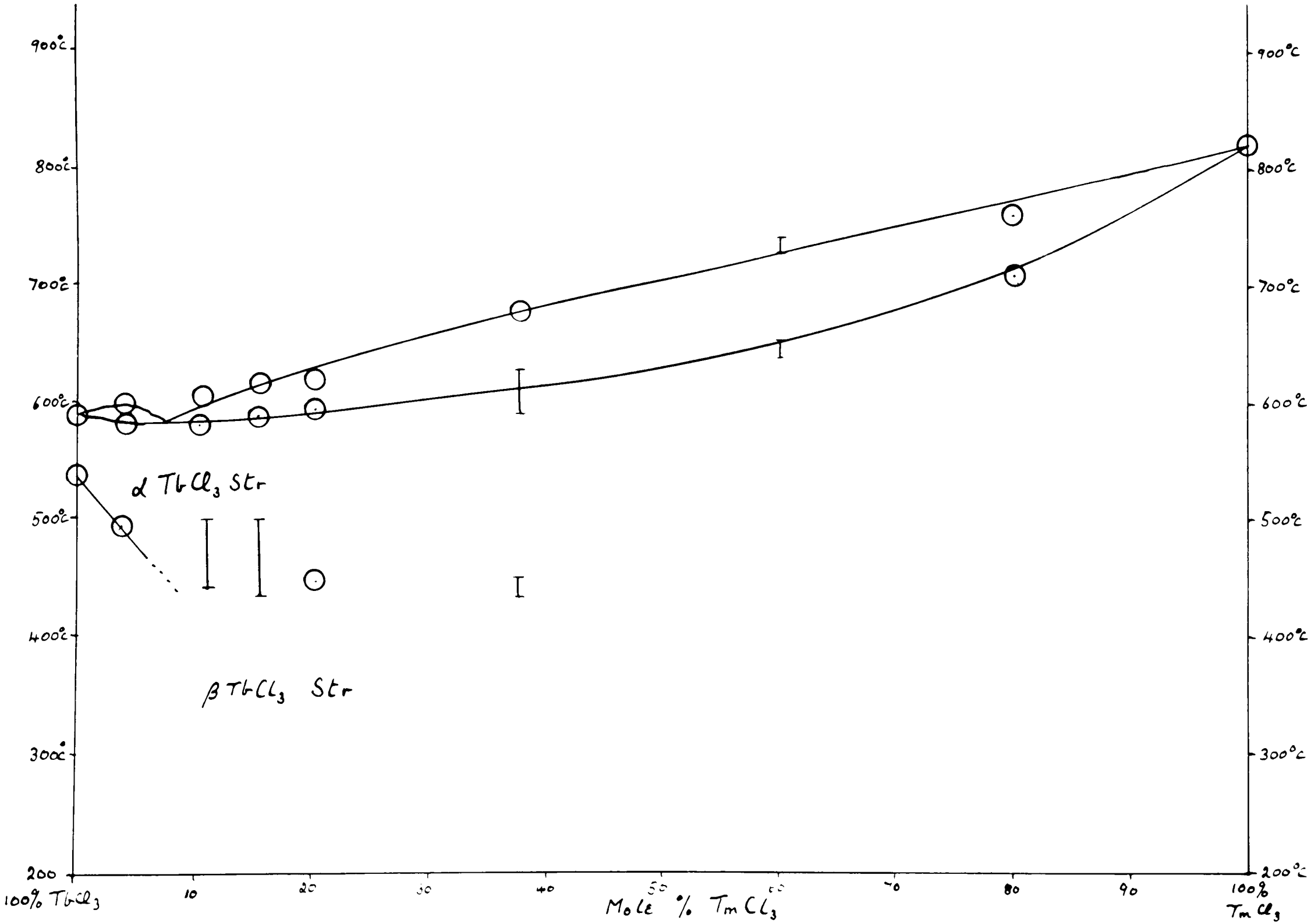

900°C
800°C
700°C
600°C
500°C
400°C
300°C
200
α TbCl3 Str
β TbCl3 Str
100% TbCl3
10
20
30
40
50
60
70
80
90
100%
TmCl3
Mole % TmCl3

Fig 4.7

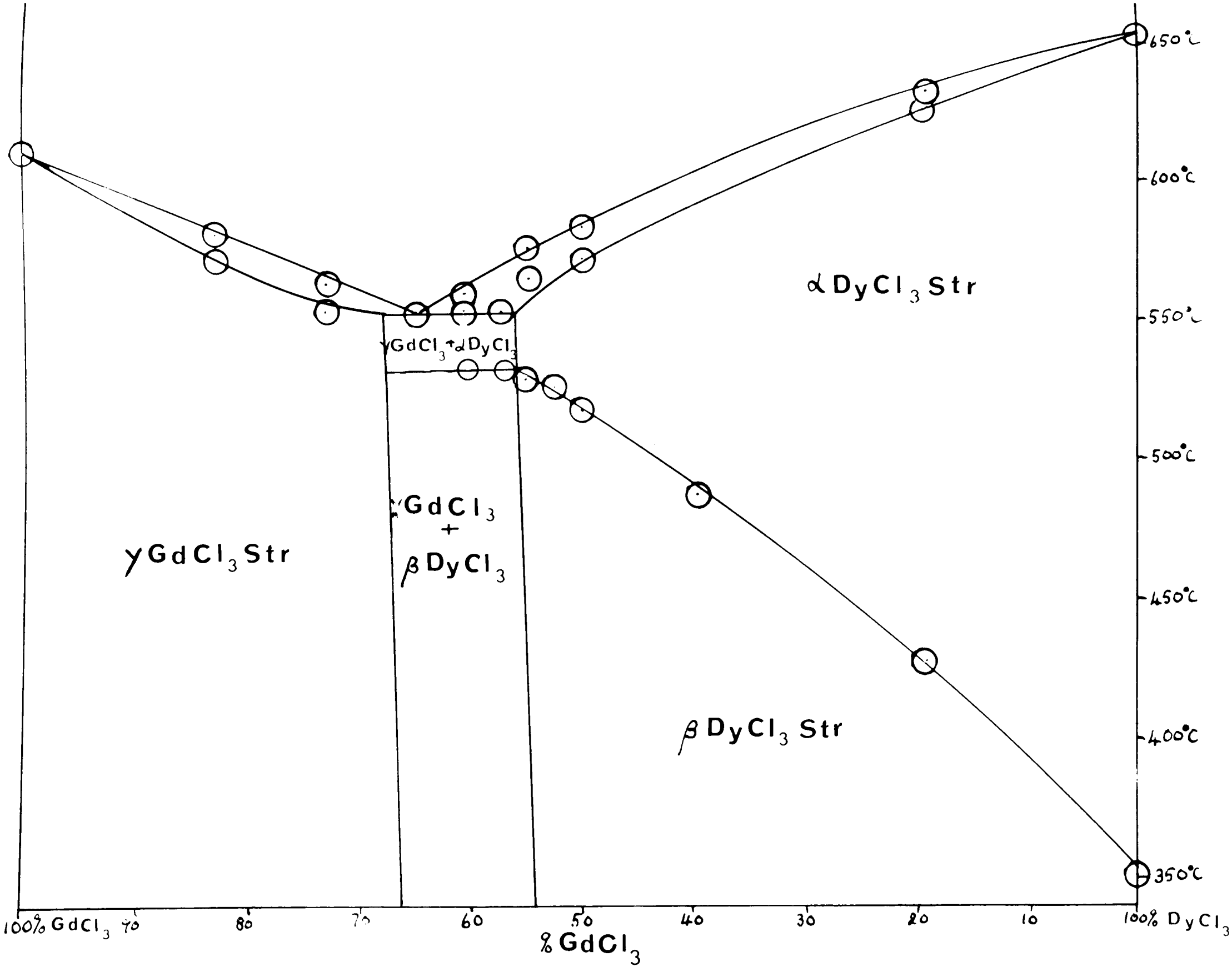

650°C
600°C
550°C
500°C
450°C
400°C
350°C
αDyCl3 Str
γGdCl3+αDyCl3
γGdCl3 Str
γGdCl3 + βDyCl3
βDyCl3 Str
100% GdCl3
80
70
60
50
40
30
20
10
100% DyCl3
% GdCl3

Fig 4.8

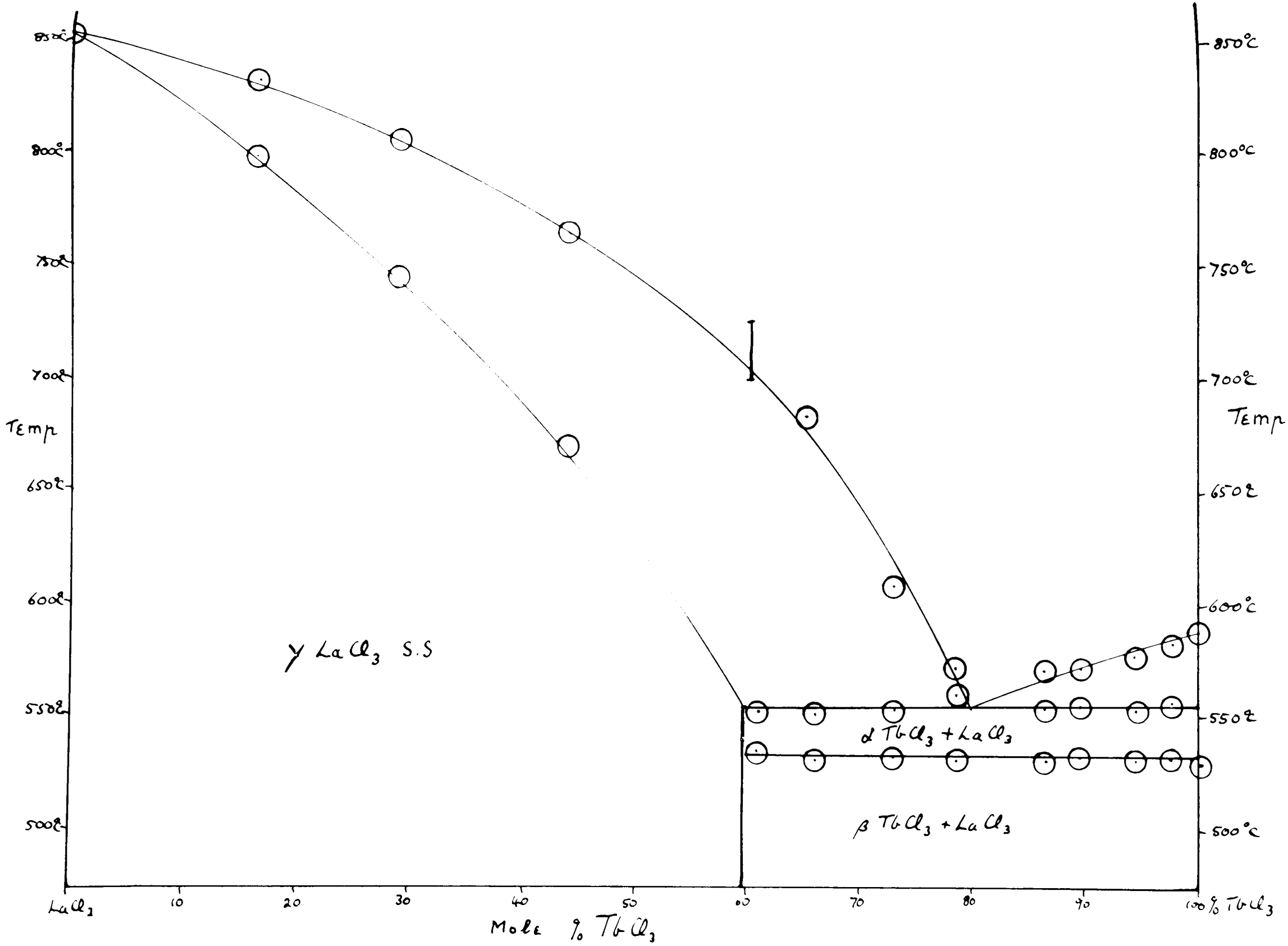

850°C
800°C
750°C
700°C
Temp
650°C
600°C
550°C
500°C
γ LaCl3 S.S
α TbCl3 + LaCl3
β TbCl3 + LaCl3
LaCl3
10
20
30
40
50
60
70
80
90
100 % TbCl3
Mole % TbCl3

Fig 4.9

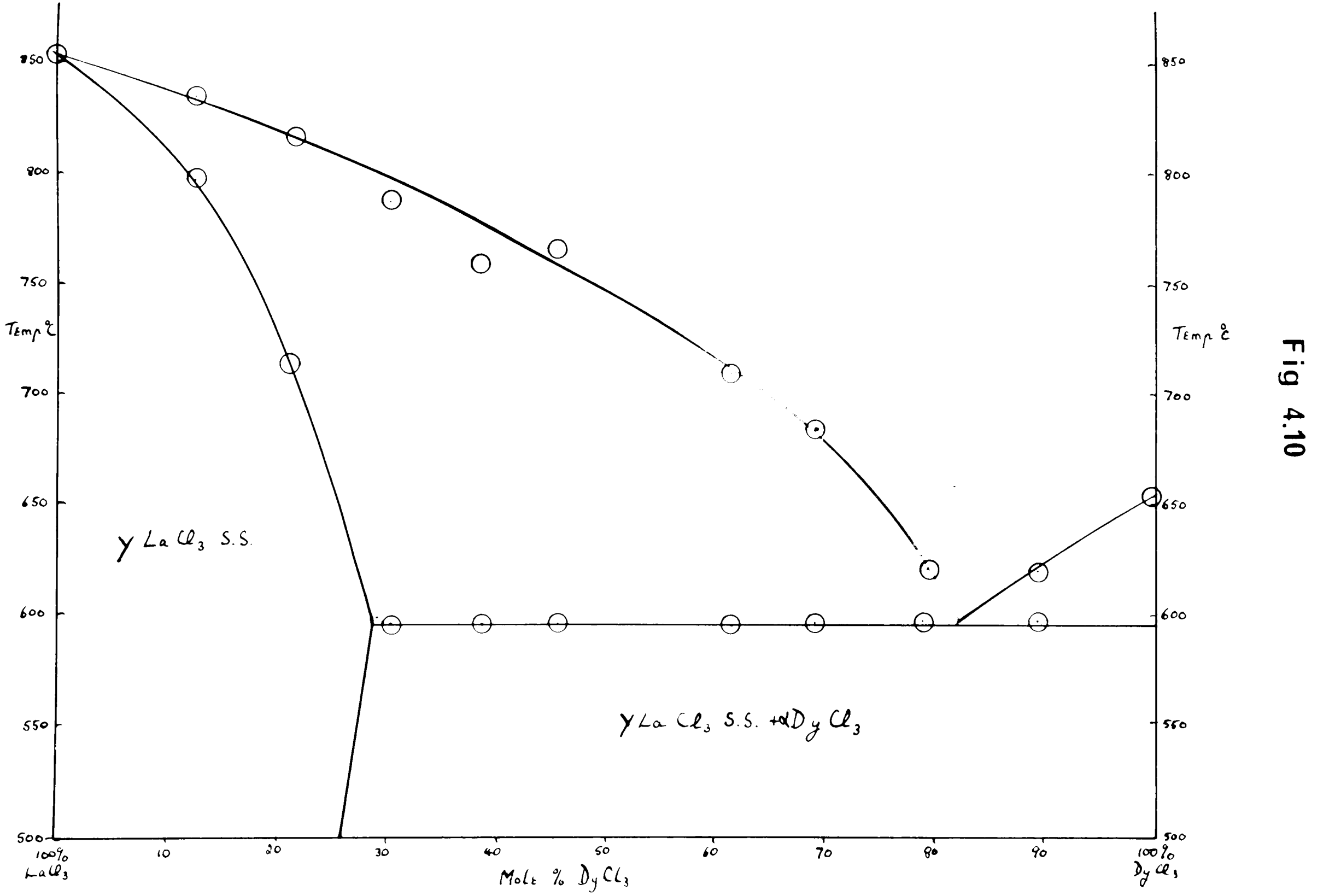

850
800
750
Temp °C
700
650
600
550
500
100% LaCl3
10
20
30
40
50
60
70
80
90
100% DyCl3
Mole % DyCl3
yLaCl3 S.S.
yLaCl3 S.S. + αDyCl3

Fig 4.10

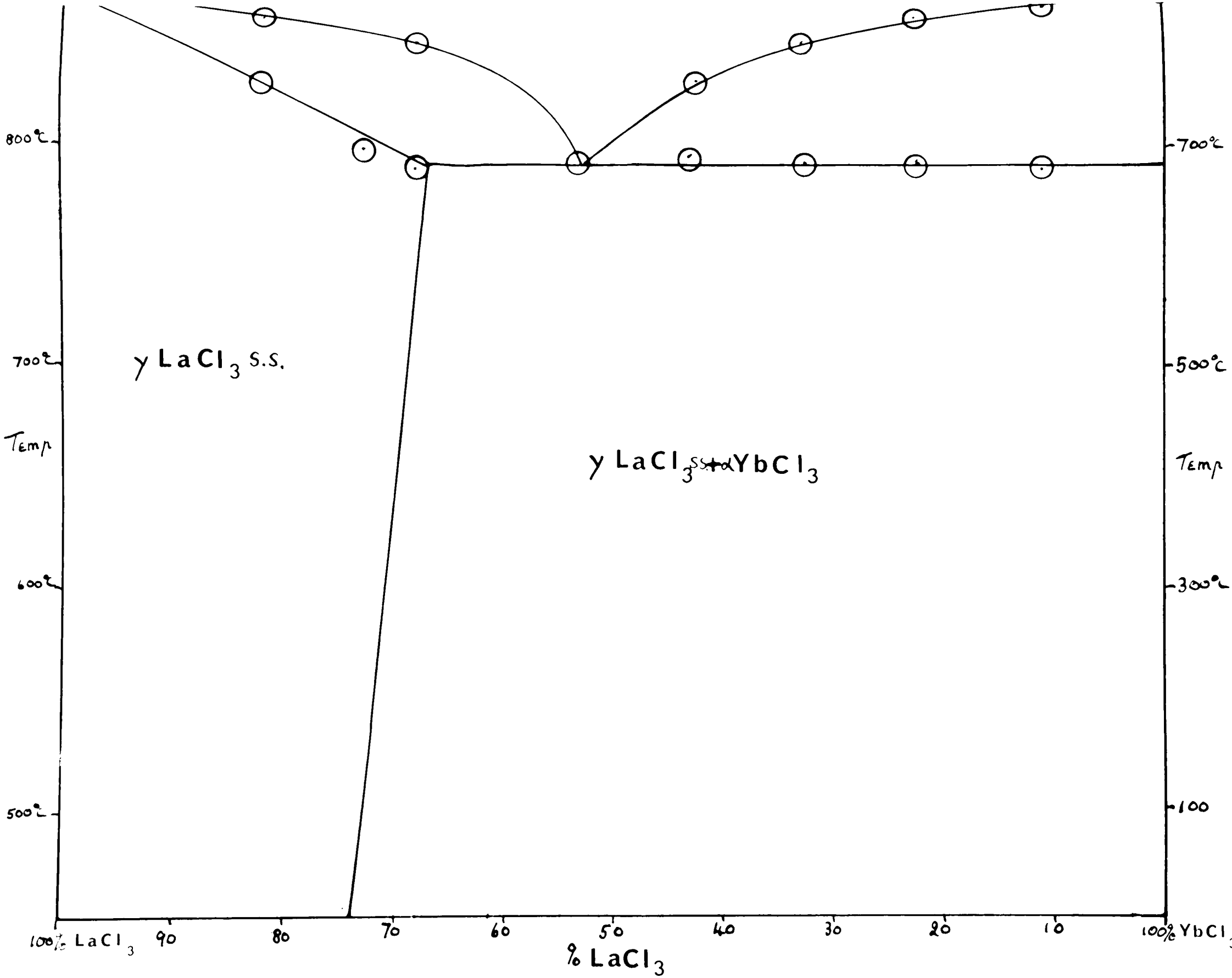

800°C
700°C
700°C
500°C
Temp
Temp
γ LaCl3 S.S.
γ LaCl3 SS + αYbCl3
600°C
300°C
500°C
100
100% LaCl3
90
80
70
60
50
40
30
20
10
100% YbCl3
% LaCl3

Fig 4.11

$YbCl_3$ is undectable by X-ray and thermal measurements. The solid solubility of the other rare-earth ion in $LaCl_3$ decreases from 59% ($TbCl_3$) to 30% ($YbCl_3$). The phase transition of $TbCl_3$ is observed at the same temperature as in pure $TbCl_3$. The phase transition of $DyCl_3$ was not observed.

The systems $CeCl_3/EuCl_3$ and $TbCl_3/EuCl_3$ were investigated only briefly, by the X-ray powder method alone. D.T.A. gave inconsistent results due to decomposition of $EuCl_3$ near the melting-point. The system $CeCl_3/EuCl_3$ forms a continuous series of solid solutions with no sign of any new phases due to a reaction:-

$$CeCl_3 + EuCl_3 \longrightarrow EuCl_2 + CeCl_4$$

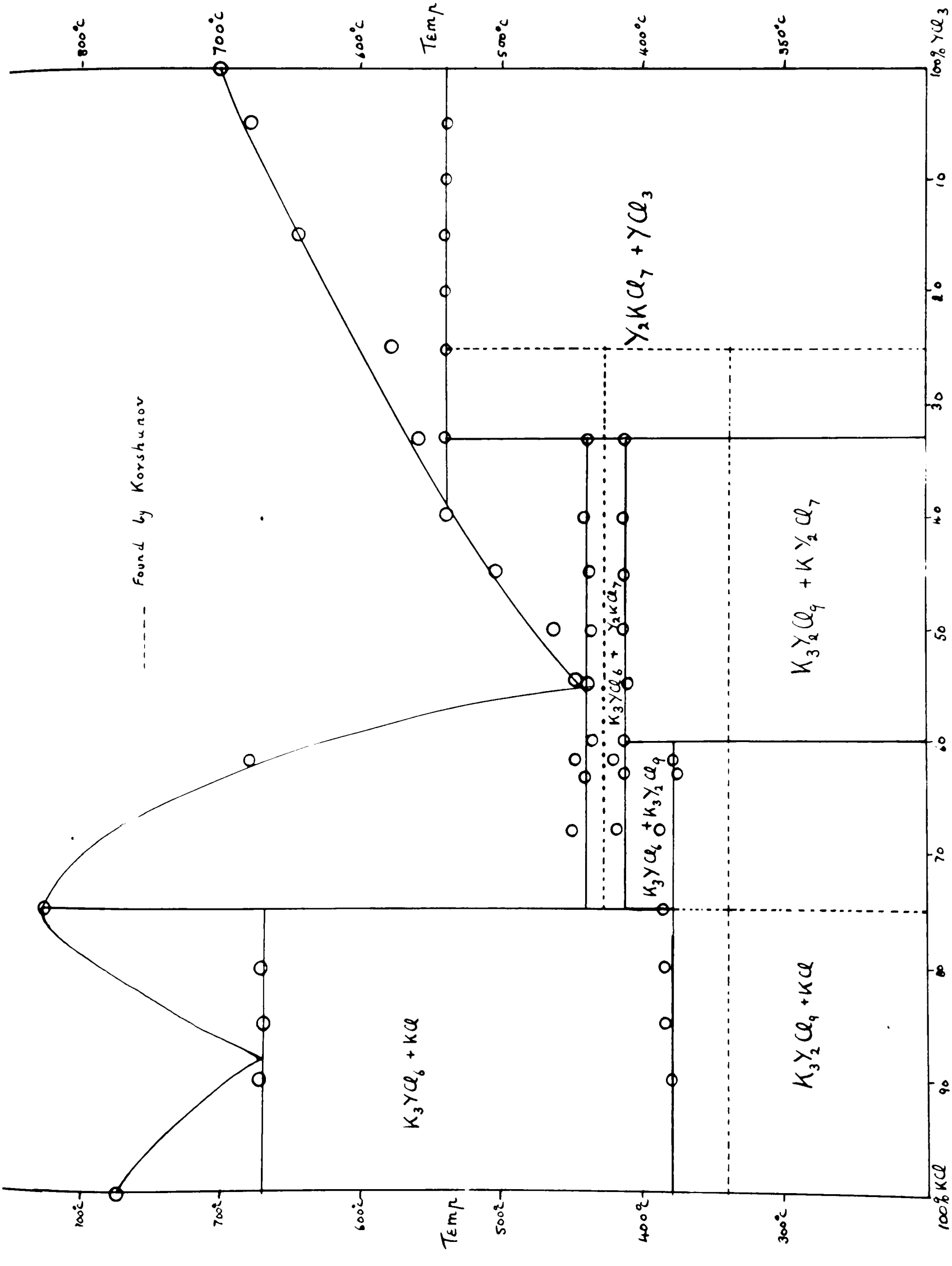
The system $TbCl_3/EuCl_3$ was similar to the $TbCl_3/GdCl_3$ system and likewise showed no interesting effects.

4.3c. Systems containing rare-earth chlorides and alkali metal chlorides.

The phase diagrams of the systems KCl/YCl_3 and $NaCl/YCl_3$ have been determined by Russian workers using thermal analysis (11).

The phase diagram of KCl/YCl_3 has been redetermined, and the results disagree with the published data (Fig.4.12).

Fig 4.12


800°C
700°C
600°C
Temp
500°C
400°C
350°C
100% YCl3
10
20
30
40
50
60
70
80
90
100% KCl
% of KCl
Found by Korshunov
Y2KCl7 + YCl3
K3YCl6 + K2KCl7
K3Y2Cl9 + KCl
K3YCl6 + K3Y2Cl9
K3Y2Cl9 + KCl
100°C
700°C
600°C
Temp
500°C
400°C
300°C

The Russian workers did not use any X-ray methods to check the formulae of their compounds, and it would appear that the sensitivity of their thermal analysis equipment was not good enough to separate thermal effects occurring at temperatures only a few degrees apart. The liquidus points on their diagrams were calculated, not observed.

The compound K_3YCl_6 cannot be grown as a single crystal from the melt due to its decomposition below 380°C into KCl and $K_3Y_2Cl_9$, and KY_2Cl_7 cannot be grown as a single crystal from the melt due to its incongruent melting-point.

The phase-system $LiCl/YCl_3$ (Fig.4.13) forms one compound only Li_3YCl_6. This compound has been grown as a single crystal. The crystallographic properties will be described in Chapter 6. This substance may provide a useful host lattice for the study of the physical properties of rare-earth ions.

4.3(d). The Systems $CsCl/CeCl_3/Cl_2$ and $CsCl/ZrCl_4$.

$CeCl_4$ has not been made in the solid state. It was hoped that compound formation between $CeCl_4$ and CsCl might stabilise the oxidised phase, in the same way that NaF will stabilise PrF_4 by formation of $NaPrF_5$ etc. (See Section 4.3 (a)) The phase system $CsCl/ZrCl_4$ forms the compound Cs_2ZrCl_6, which has a cubic structure [18]. Before attempting to grow a single crystal of this compound it was necessary to check the

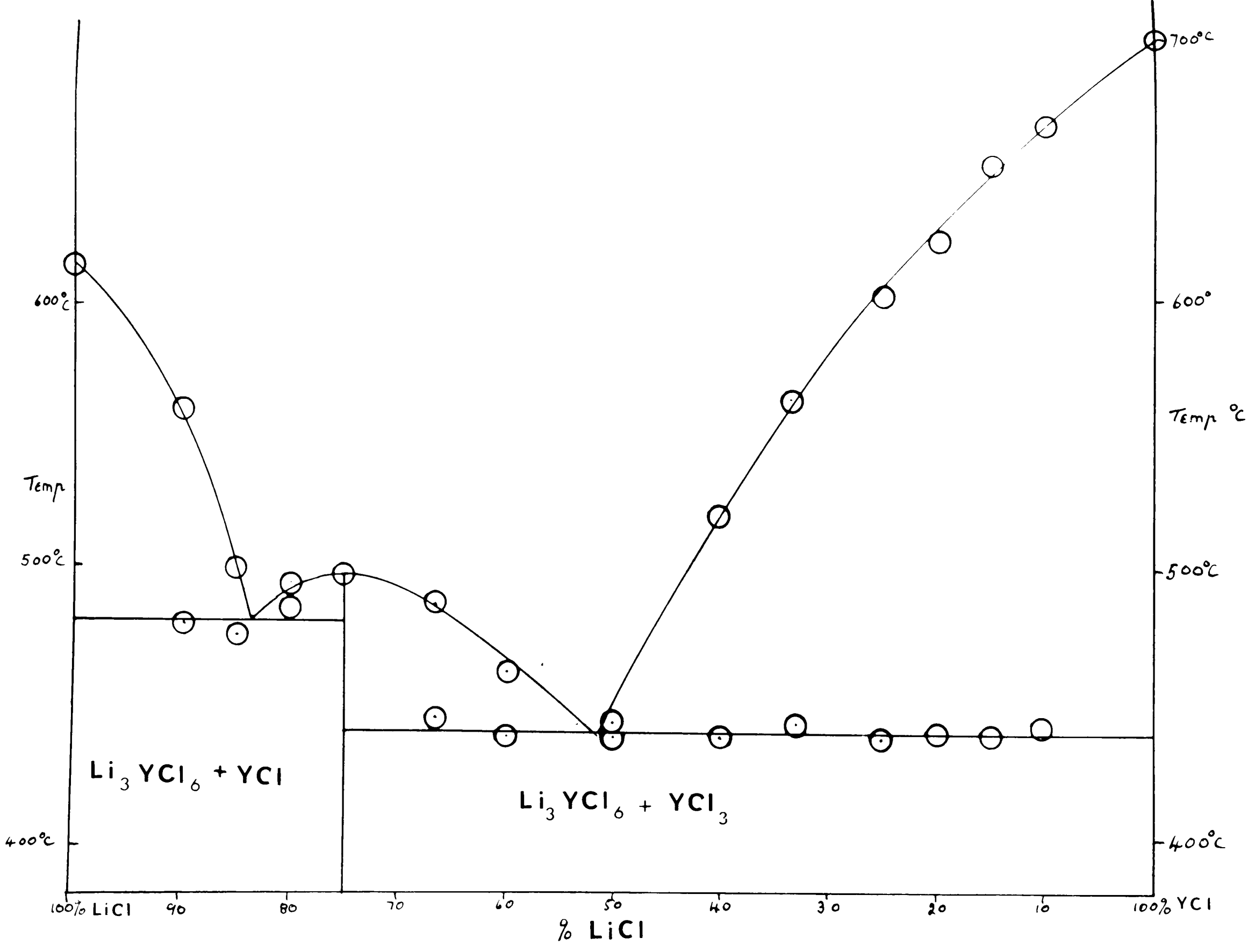

700°C
600°C
600°
Temp °C
Temp
500°C
500°C
$Li_3YCl_6 + YCl$
$Li_3YCl_6 + YCl_3$
400°C
400°C
100% LiCl
90
80
70
60
50
40
30
20
10
100% YCl
% LiCl

Fig 413

previous work on this system.

In order to study the system $CsCl/CeCl_3/Cl_2$, stoichiometric mixtures of anhydrous CsCl and $CeCl_3$ were made up in the molar ratios 1:1, 2:1 and 3:1 and fused together in the normal way. X-ray powder diffraction patterns were used to identify the phases present. Dry chlorine gas was passed over the finely powdered samples at 450°C, and the samples were slowly cooled to room temperature in an atmosphere of chlorine over a period of five hours. The X-ray powder diffraction patterns did not change after chlorination, although the solids now had an orange appearance, and liberated iodine from KI solution.

Quantitative iodometry showed the presence of up to 6% Ce^{4+}, only if dilute acid was added to the solution. The oxidised phase was assumed to be CeO_2, formed by the presence of oxygen in the chlorine gas. The A.C.susceptibility of the powder at liquid helium temperatures showed the presence of 7% Ce^{4+}

Cesium chloride and zirconium tetrachloride from a compound Cs_2ZrCl_6. This compound could be used as a host lattice for U^{4+} and other tetravalent ions such as Ce^{4+}, Pr^{4+}, Tb^{4+}, which might be stabilized in the lattice in small amounts. An X-ray powder diffraction pattern of a 2:1 molar

mixture agreed well with previous data (Table 4.8). A D.T.A. run gave the melting-point as $815^{o} \pm 20^{o}C$. The accuracy was low due to sublimation of $ZrCl_4$ in the apparatus.

For large-scale crystal-growth experiments the commercially available $ZrCl_4$ was sublimed at 300-350°C at 10 microns pressure to free it from oxide and oxychloride impurities. A single crystal was grown in the normal way, but contained some specks of carbon which had not been removed by distillation.

4.4. Summary. A variety of phase systems containing rare-earth chlorides and fluorides have been investigated, with the intention of finding new compounds which can be grown as single crystals. The only new compound of any interest is Li_3YCl_6. Phillips (17) has shown that the following rare-earths form similar compounds, Dy, Ho, Er, Tm, Yb and Lu. It is hoped that these compounds may be used as a host lattice for the study of the behaviour of rare-earth ions at low temperatures.

Table 4.8.

Cs_2ZrCl_6. (Cu K_α)

Reflection hkl.	Intensity	$Sin^2\theta$ obs. x 10^4.	$Sin^2\theta$ calc. x 10^4
111	M	167	165
22	S	440	439
222	S	658	658
320	W-	704	713
400	S	878	878
422	S	1324	1317
551	W	1488	1481
440	S	1754	1756
620	M-	2191	2195
622	M-	2410	2414
444	W+	2631	2634
642	M	3067	3073

CHAPTER 5.

PREPARATION OF SAMPLES FOR PHYSICS EXPERIMENTS AND DESCRIPTION OF SOME PHYSICS EXPERIMENTS.

5. 1(a) Introduction: The preparation of rare-earth halides in single crystal form has been described in Chapters 2 and 3. This chapter will describe the preparation and mounting of crystal fragments of suitable size, shape and orientation for various physical measurements at low temperatures. Techniques have been developed to protect the hygroscopic crystals during the considerable handling necessary in the preparation of the sample, and its subsequent transfer to the cryostat

Optical methods of orienting crystals have been used as much as possible because of their speed. However, for the most exacting work, the more accurate method of orienting crystals by Laué back-reflection X-ray photographs has been used.

The following properties of the crystals were measured at low temperatures:- specific heat, A.C. magnetic susceptibility and D.C. magnetic moment, and optical absorption and fluorescence spectra, and also electron para magnetic resonance spectra (19). The types of sample-holder varied considerably in design owing to the differing designs of

cryostat in existing pieces of apparatus. The author collaborated with other workers in the measurements of specific heat and A.C. magnetic susceptibility, and these measurements will also be described.

Some discussion of the crystal structures of lanthanon halides is necessary before describing the methods of preparing the samples.

5.1(b). The YCl_3 Structure. The lanthanon trichlorides which crystallize with this structure (20) are tabulated in Table 5.1. (See also Figs. 5.1., 5.2., and 5.3.) The Ycl_3 monoclinic unit cell has the dimensions:-

$a = b.92\mathring{A}$ $b = 11.94\mathring{A}$ $c = 6.44\mathring{A}$ $\beta = 111.0^{\circ}$.

The unit cell dimensions of isomorphous lanthanon trichlorides are given in Table 5.1. The space group is C2/m. The chloride ions are approximately cubic close-packed, and occupy the 4 (i) (m) and 8 (j) (1) $\pm$ $(x_2 y_2 z_2)(x_2 \bar{y}_2 z_2)$ positions (Nomenclature of International Tables for X-ray Chrystallography).

$x_1 = 0.211$ $\quad$ $x_2 = .299$

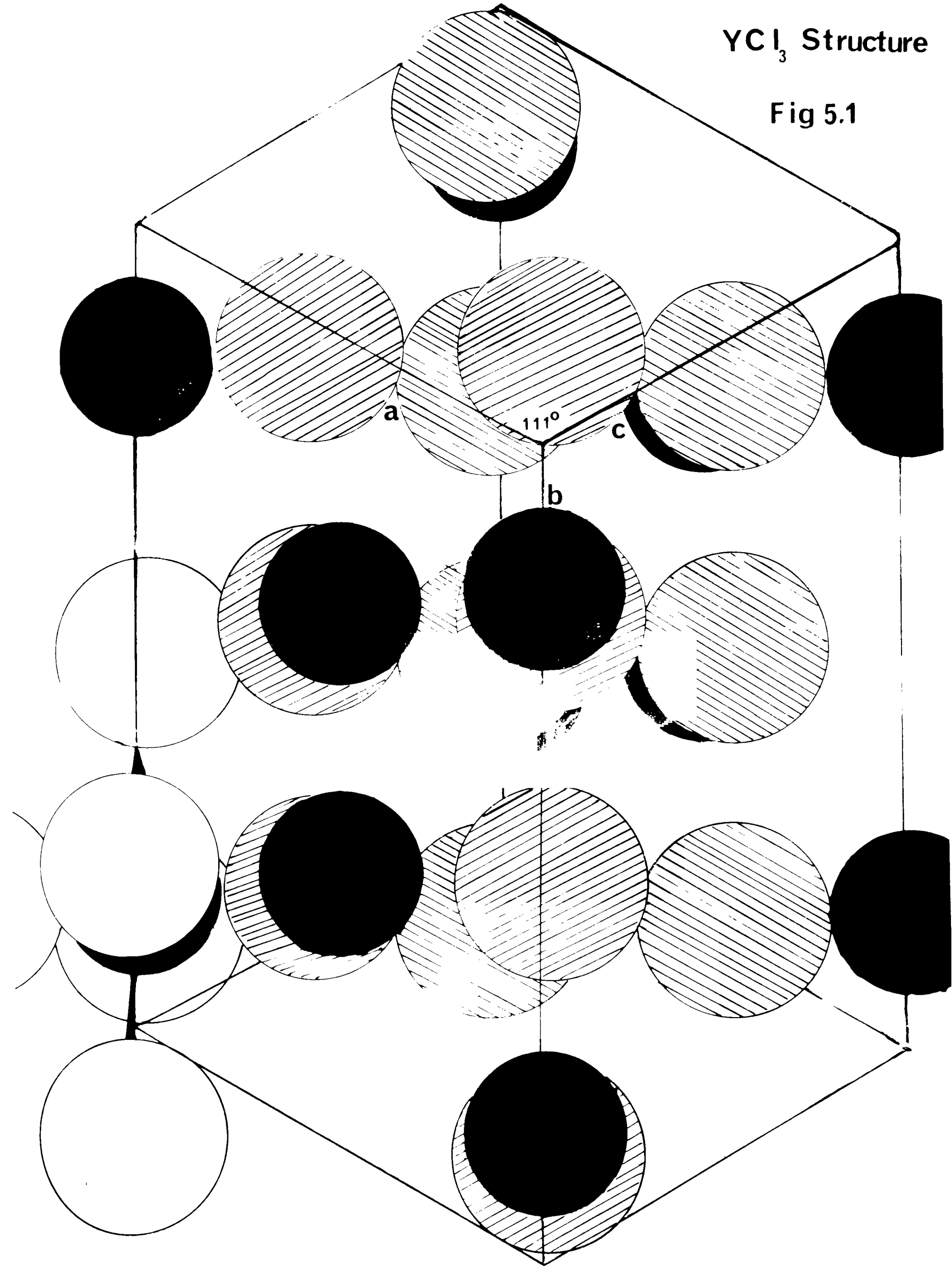
$z_1 = 0.247$ $\quad$ $y_2 = .179$

$z_2 = .760$

The metal ions lie in $\frac{2}{3}$ of the octahedral holes between alternate layers of chloride ions, in the 4(g)(2) $\pm$ $(00z_3)$

YCl_3 Structure

Fig 5.1



[010] Projection

○ Cl^- $y_j = .179$

◯ Y^{3+} $y_g = .166$

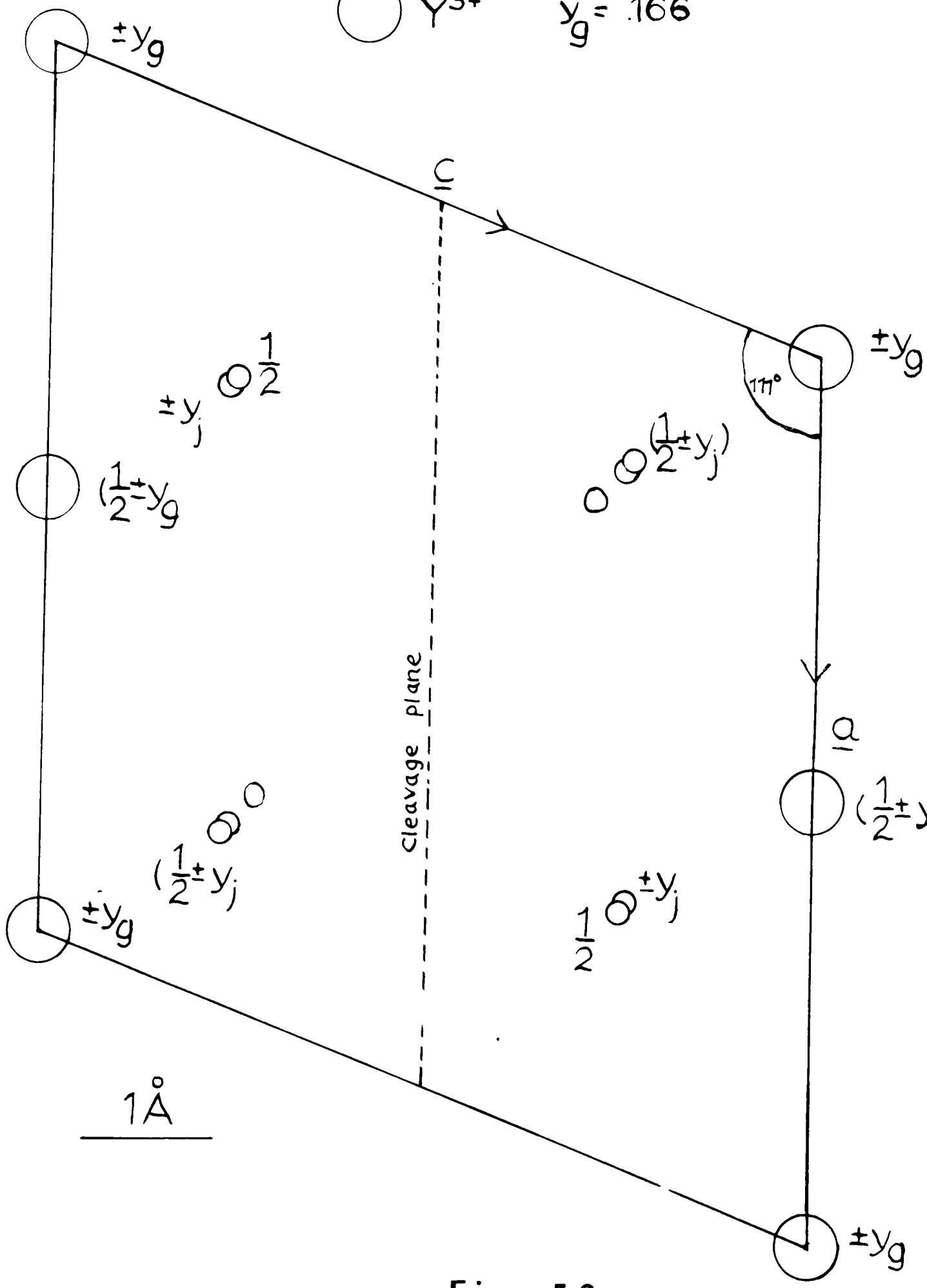


Fig 5.2

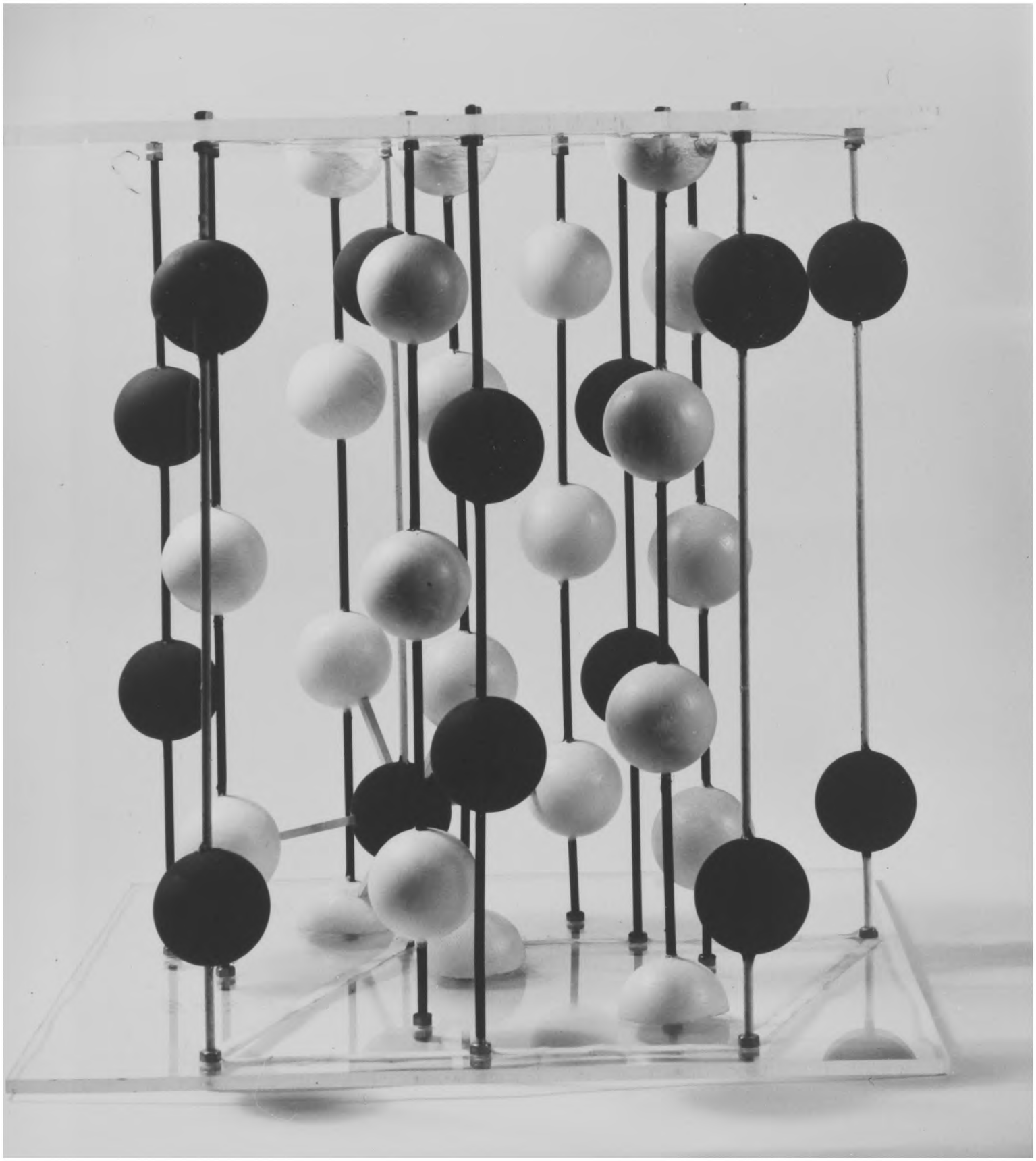


Fig. 53.

Table 5.1.

	Str.	Ionic R.	aÅ	bÅ	cÅ	β°	MPt.°C
$LaCl_3$	$LaCl_3$	1.061	7.468	-	4.366		852
$CeCl_3$	$LaCl_3$	1.034	7.450	-	4.315		802
$PrCl_3$	$LaCl_3$	1.013	7.422	-	4.275		776
$NdCl_3$	$LaCl_3$	0,995	7.381	-	4.231		760
$SmCl_3$	$LaCl_3$	0.964	7.378	-	4.171		678
$EuCl_3$	$LaCl_3$	0.950	7.369	-	4.133		623
$GdCl_3$	$LaCl_3$	0.938	7.363	-	4.105		609
$TbCl_3$	$PuBr_3$	0.925	3.84	11.74(5)	8.51		588
$DyCl_3$	YCl_3	0.908	6.91	11.97	6.40	111.2	654
$HoCl_3$	YCl_3	0.894	6.84	11.85	6.39	110.8	718
$ErCl_3$	YCl_3	0.881	6.80	11.79	6.39	110.7	774
$TmCl_3$	YCl_3	0.869	6.75	11.73	6.39	110.6	821
$YbCl_3$	YCl_3	0.858	6.73	11.63	6.38	110.4	854
$Lu\ Cl_3$	YCl_3	0.848	6.72	11.60	6.39	110.4	892
YCl_3	YCl_3	0.88	6.92	11.94	6.44	110.0	700

positions, $z_3 = .166$. Each metal ion has a pair of chloride ions at each of the following distances, 2.58Å, 2.63Å, 2.69Å. There are four molecules per unit cell, and all metal ions are magnetically equivalent. The crystals have a well defined (001) cleavage plane, perpendicular to an (010) plane of symmetry.

5.1.(c) The $LaCl_3$ structure. The lanthanon chlorides which crystallize with the $LaCl_3$ structure are tabulated in Table 5.1 (21). The unit cell has hexagonal symmetry, space group $P6_3/m$. The dimensions of the unit cells are given in Table 5.1. There are two molecules per unit cell, the positions of the ions in $LaCl_3$ being:-

2 La ions in position 2(d) at $(\frac{2}{3},\frac{1}{3},\frac{1}{4})$ and $(\frac{1}{3},\frac{2}{3},\frac{3}{4})$.

6 Cl ions in position 6(h) at $(x,y,\frac{1}{4})$, $(\bar{x},\bar{y},\frac{3}{4})$, x=.29 y=.38.

The lanthanum ions are symmetrically 9-coordinated; the La-Cl distance is 2.97Å. A projection down the (001) axis of the $LaCl_3$ unit cell is shown in Fig. 5.4. Both the lanthanum ions are crystallographically and magnetically equivalent. The crystals have no well-defined cleavage plane but the crystals as grown tend to be striated, the striations lying along the direction of the c axis.

5.2. Sample Preparation.

(a) Anhydrous lanthanon chlorides are extremely hygroscopic and the crystals must be protected from atmospheric moisture while

$LaCl_3$ Structure

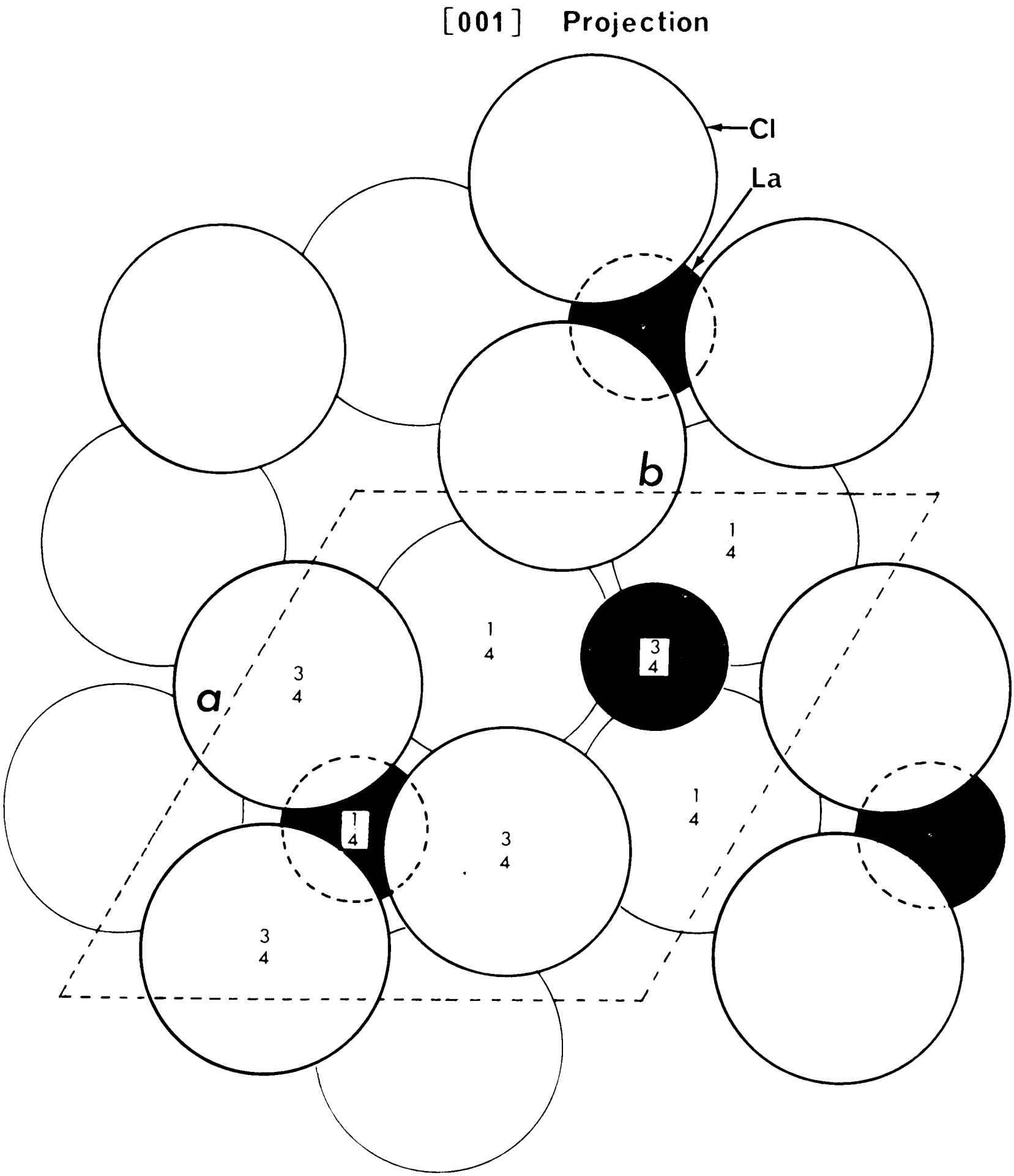


FIG. 5.4

being shaped and oriented. The crystals were kept under liquid paraffin, (Light, density .83 - .87) and were cut and polished while covered with a film of paraffin. Where necessary unprotected crystals were handled in a drybox.

The crystals were shaped by making use of the natural cleavage of the crystal, or by rubbing down with fine emery paper, using liquid paraffin as a lubricant.

5.2.b. Preparation of samples for specific heat experiments. The specific heat experiments were carried out in the absence of a magnetic field, therefore the crystals were not oriented. A piece of crystal, weighing between .5 and 5 gms. was cleaved or cut from a single crystal boule. After the crystal was weighed it was stuck on to the calorimeter with G.E. varnish. A further layer of varnish served to protect the outside of the crystal while the apparatus was being assembled.

5.2.c. Preparation of samples forA.C. susceptibility and D.C. magnetic Movement Measurements. Experiments of this type were done on crystals of $DyCl_3$ and $HoCl_3$ only. Crystal fragments of known shape and orientation weighing between 10 mg. and 40 mg. were required. Identical sample-holders were used for both types of experiment. (Fig.5, 6, A and B).

The orientation of these crystals was facilitated by two

useful properties. There is a well-defined (001) cleavage plane. Also, if a crystal flake is viewed by a microscope perpendicular to the cleavage face using convergent plane-polarised light and a Bertrand lens, interference images, similar to those shown in Fig. 5.5.A., are seen. The optic plane was shown to contain the b axis by X-ray oscillation photographs. The optic plane was parallel to the b axis for all chlorides with the YCl_3 structure.

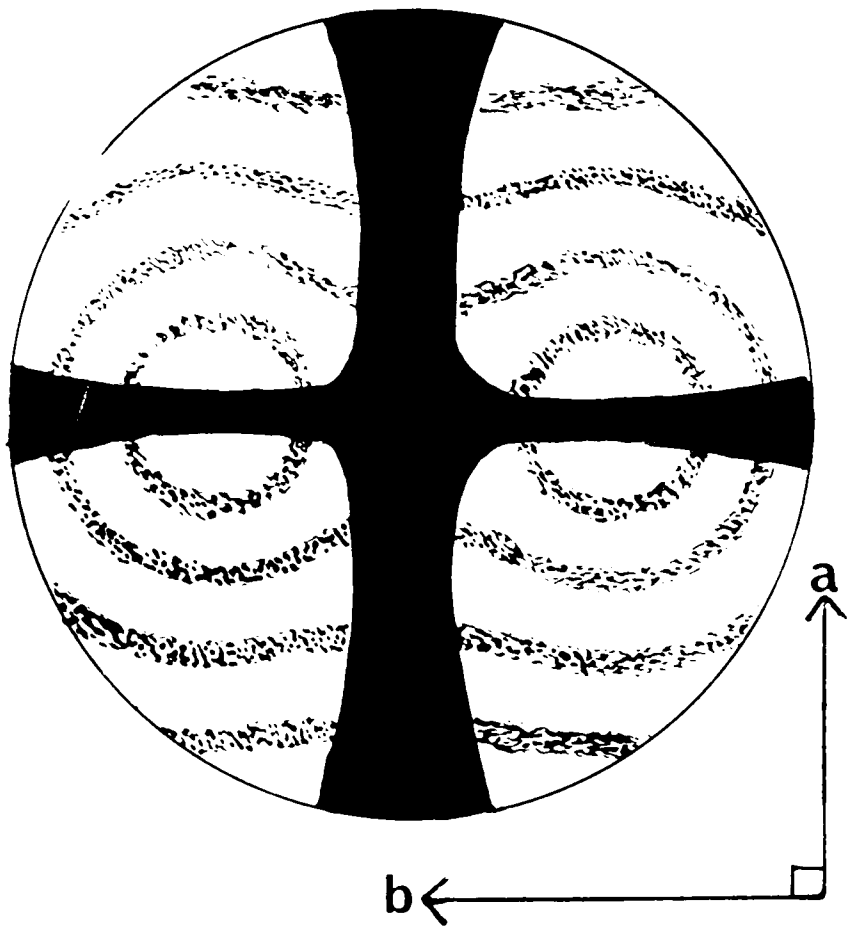
A crystal flake about .5mm. thick was cut from the main boule with a scalpel, and the crystal axes were identified optically. Three crystal orientations were required. The two axes in the cleavage plane, a and b were required to be along the axis of the apparatus (Fig. 5.6.A and 5.6.B). The third direction of measurement was perpendicular to the cleavage plane. In the case of the first two orientations the crystal flake was cut so that the required axis lay along the length of a rectangular crystal fragment about 5 mm. x 2 mm. x $\frac{1}{2}$ mm. thick. The dimensions were then determined optically using a calibrated eyepiece. The crystal fragment was then weighed after the liquid paraffin had been washed away with dry petroleum ether.

A diagram of the sample-holder is given in Figs. 5.6A and 5.6B. Both pieces are of circular cross-section. The

Key to Fig. 5. 5.

B

A Araldite
B Vacuum Seal
C Sample Rod
D Glass window
E Rotatable crystal mount
H Crystal mount
L Rubber bung
M Crystal



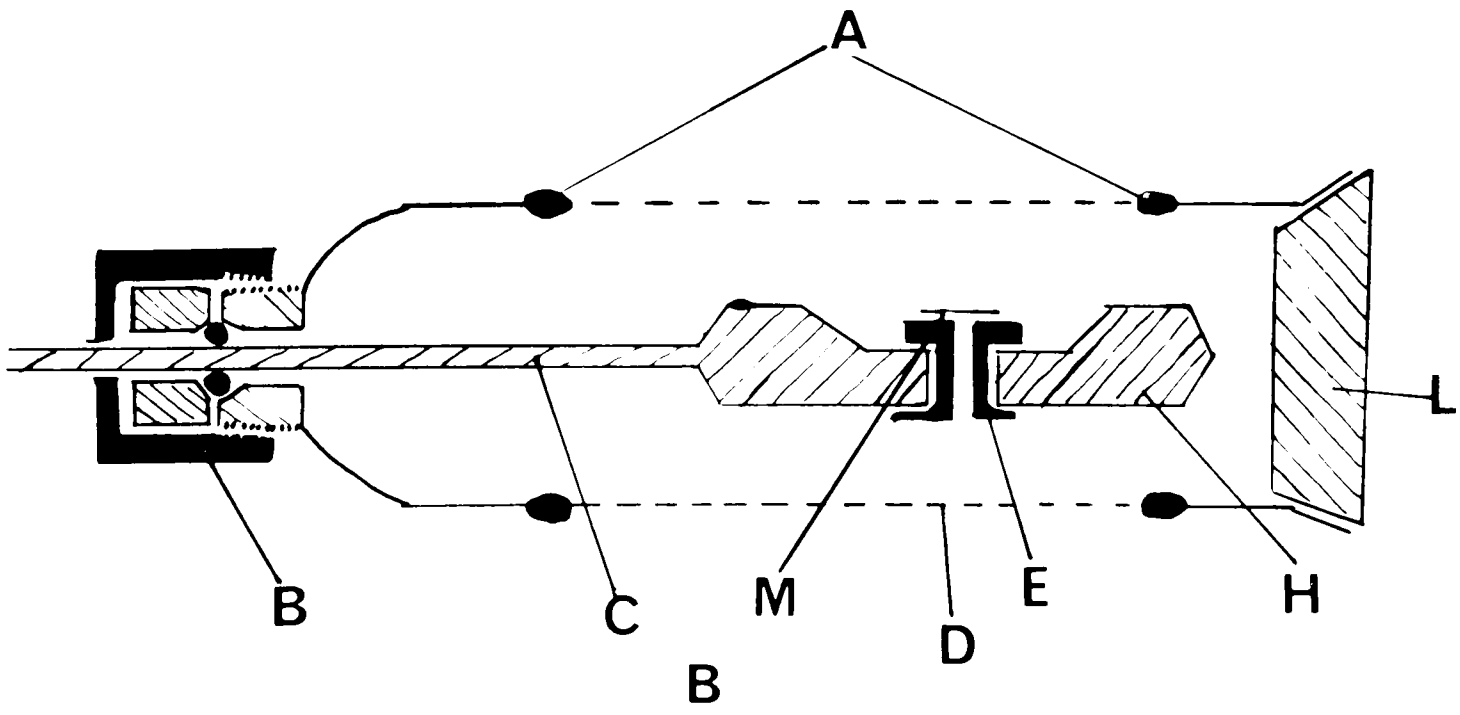


Fig 5.5

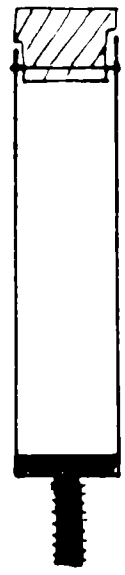
Key to Fig. 5. 6.

A

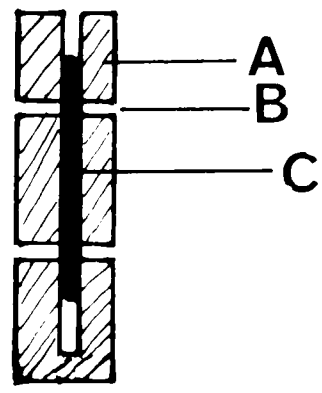
A P.T.F.E. cylinder
B Sight hole
C Crystal

C

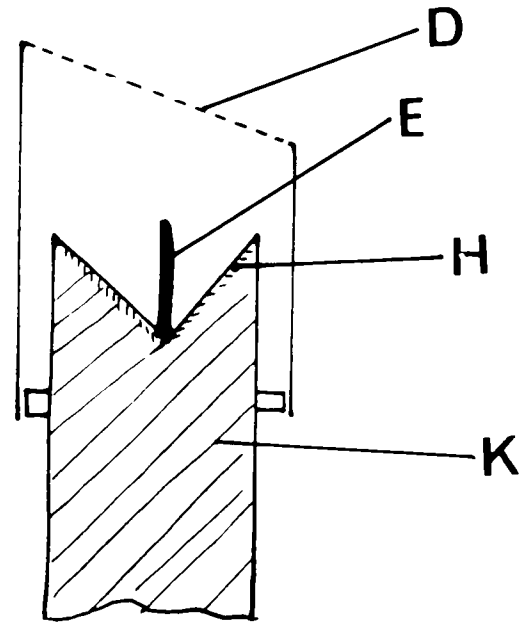
D Saranwrap window
E Crystal
H Mirror
K Tufnol mount stem



B



A



C

Fig 5.6

crystal, covered with liquid paraffin, was placed in the slot in the insert, and held in place with vacuum grease. The crystal was then oriented so that the required crystal axis lay along the axis of the holder. This was achieved by means of plane-polarised light which passed through the small holes in the insert. The insert was placed in the holder and held in place with the lid.

Samples which had the cleavage plane perpendicular to the axis of the apparatus were cut from crystal flakes using a No. 1 cork-borer to give thin discs which fitted closely in the tube (Fig. 5.6.B). The discs were kept in place with cotton-wool.

5.2(d) Preparation of samples for resonance experiments.

Crystals of $LaCl_3$ containing 1% of $NdCl_3$ were used for electron paramagnetic resonance experiments. An optically clear piece, about 3mm cube, was cleaved from the boule under liquid paraffin. The c axis was identified by the striations. The crystal was then placed on a circular perspex disc, which acted as a sample-holder in the cryostat. The crystal was stuck in place using Apiezon grease, and the position of the crystal was adjusted until the striations were parallel to the surface of the disc. The crystal was then oriented more accurately using Laué back-reflection

X-ray photographs. The crystal was protected by painting the surface with a mixture of paraffin-oil and vaseline which had been homogenized by warming to approximately 60°C.

The experiments for which the crystals were used were only in the nature of trial runs, therefore approximate orientation sufficed. A more accurate procedure for orienting crystals for this type of experiment has been described by the author elsewhere (22).

5.2.e. Preparation of samples for optical spectroscopy. The preparation of crystals for optical experiments had to satisfy two requirements not needed in the other preparative methods. Firstly, the crystals had to be of extremely good optical quality, and the surfaces had to be flat and polished. Secondly, the surfaces, had to be free of liquid paraffin, since the paraffin rendered the crystal opaque on cooling to liquid helium temperatures. Therefore, methods had to be devised for polishing the crystals and for transferring to the apparatus. In no case was an apparatus specifically designed to aid the transfer of hygroscopic crystals into the cryostat.

Crystals which crystallize with the YCl_3 structure cleave along an (001) plane. An optically clear crystal flake about .1 mm. thick or less, was prepared by carefully

cleaving a large crystal fragment with a scalpel. If this was done carefully, no polishing was necessary. The crystal axes were identified as in Sec. 5. 2(c), and the crystal flake was cut so that the crystal axes could be identified without further reference to the microscope.

The crystal was transferred to the drybox, and the liquid paraffin was removed with petroleum ether. The crystal was then stuck to the holder with Durofix (Fig. 5.5.B). The crystal was rotated on its base until the required axis was perpendicular to the axis of the holder. For accurate measurements the orientation was checked using the polarising microscope. The holder was then placed in the outer container which was airtight, and which served as a transfer vessel.

Those crystals which crystallize with the hexagonal $LaCl_3$ crystal structure were made into optically clear flakes about $\frac{1}{2}$ mm. thick by grinding and polishing on successively finer grades of emery paper finishing with grade 6/0 or 3/0. Liquid paraffin protected the crystals and also served as a lubricant while polishing. The flakes were oriented optically, or when required for more accurate work, by Laué back-reflection X-ray photographs.

Three methods of mounting these crystals were used, depending on the apparatus in which the experiment was to be

carried out. One holder was the same as that described in the previous section (Fig. 5.5.) Another type of holder is shown in Fig.5.6.C. The crystal was stuck in place between the mirrors by Apiezon grease, and was protected during transfer to the apparatus by the "box" with the "Saranwrap" window. A third type of cryostat enabled the crystal to be sealed in a glass envelope. The crystal was polished and cleaned in the normal way, and was stuck over a 2mm. diameter hole in a strip of aluminium, which was a sliding fit inside a 7mm. bore glass tube. The crystals for these experiments were not oriented. The crystal was sealed in the glass envelope under $\frac{1}{3}$ atmosphere of dry helium gas. The crystals remained optically clear for some months, even after they had been repeatedly cooled to liquid helium temperatures.

Physical Measurements on $DgCl_3$, $HoCl_3$ and $ErCl_3$.

5.3.(A). Introduction.

The experiments described in this section are only two of a number of physical experiments being performed on rare-earth halides in this laboratory. Wyatt (3) and Shore (22) found that the A.C. susceptibility of powdered $DyCl_3$ and $HoCl_3$ indicated that these substances ordered magnetically in the liquid helium temperature range. As a continuation of this work, it was decided to investigate these substances

more closely because of their potential interest.

The two types of experiment with which the author has been personally concerned have been the measurement of the A.C. susceptibility of oriented single crystal specimens, and the measurement of the specific heat of these substances. The variation of the A.C. susceptibility with temperature for various crystal orientations should indicate both the approximate temperature at which the substance orders magnetically, and in what way it orders. The measurement of the specific heat would give the true temperature at which the substance orders, and can also be used to estimate the entropy and dipole-dipole interactions.

5.3.(B). Measurement of A.C.Susceptibility.

(a) Apparatus. The apparatus was similar to that used by McKim and Wolf (23) for measuring the paramagnetic susceptibility of small specimens at temperatures between $77^{o}K$ and $1.8^{o}K$ (Fig.5.7). The measurements are made in terms of the change of mutual inductance ΔM produced by moving the specimen inside a coil system using a Hartshorn bridge to measure the mutual inductance.

The crystal consists of two concentric Dewars D, containingrespectively liquid hydrogen C, and liquid helium H.

Key to Fig. 5.7.

A Sample Shift

B Vacuum seal

C Liquid Hydrogen

D Sample Rod

E Vacuum spaces

I Large He^4 can.

H Needle Valve

J Small He^4 can

K Secondary Coils

L Sample

M Primary coil

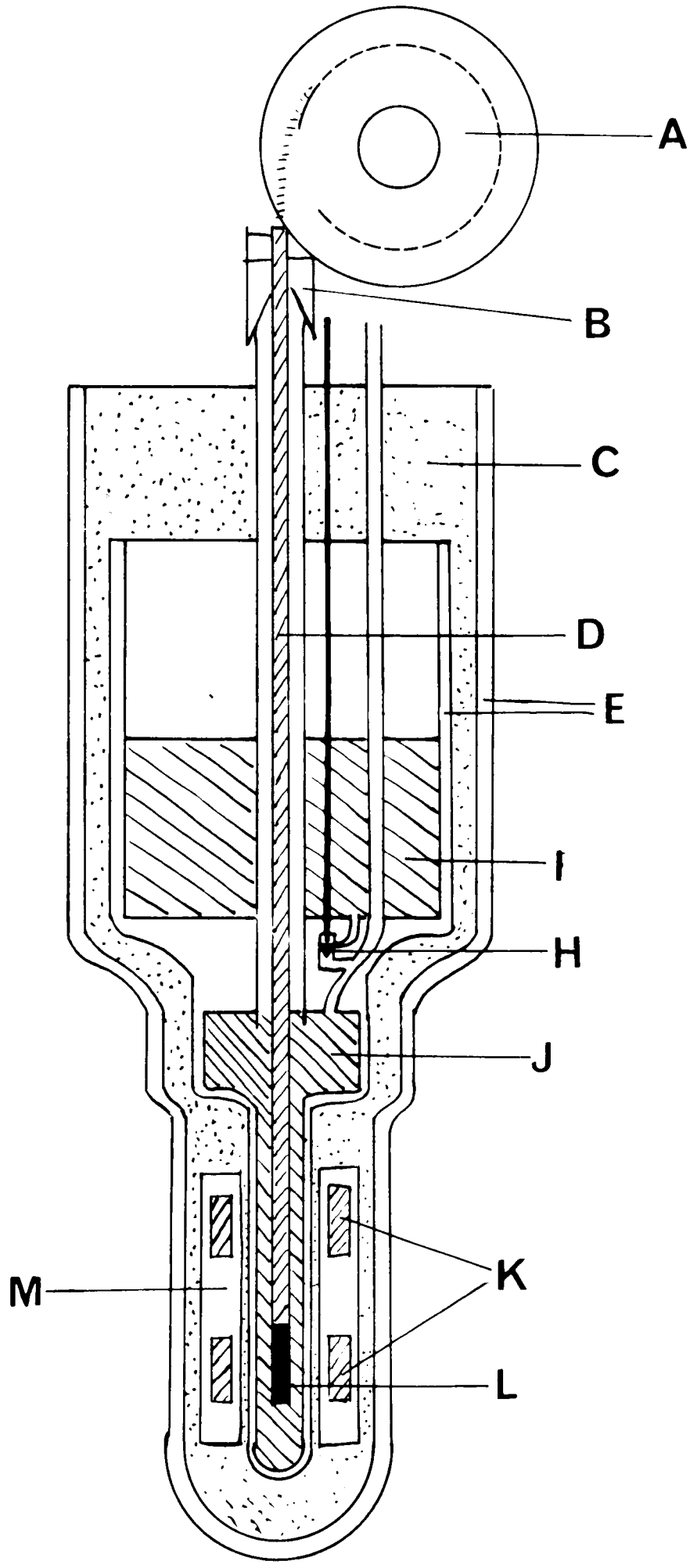


Fig 5.7

The temperature is lowered below 4.2°K by pumping off the helium gas through the outlet J. The pressure of the He gas is measured by a mercury or oil manometer attached to L and is a measure of the absolute temperature, which can be found from standard vapour pressure tables. The specimen holder F is screwed onto the end of the Tufnol rod M. The specimen can be moved between the two secondary inductance coils G by means of the flexible coupling N and the dial which moves between the adjustable stops A. The primary coil is wound round the outside of the secondary coils. Thermal comtact clips B ensure that the Tufnol rod is in thermal equilibrium with the hydrogen Dewar, and thus stops heat being conducted down the rod to the specimen. Thermal contact between the specimen and the helium dewar is made by filling the specimen space with low pressure helium gas.

The block diagram of the electrical circuit is shown in Fig. 5.8. The primary circuit contains an oscillator O which oscillates at 175 c/s. This signal is amplified by the power amplifier R and goes through the accurately variable mutual inductance I and the primary coil C. The secondary circuit is composed of two mutual inductance coils S which are wound in the opposite sense. The out-of-balance signal is amplified in the tuned amplifier D and shown on the cathode ray oscilloscope (C.R.O). The standard mutual inductance

Key to Fig. 5.8.

O	Oscillator
A	Amplifier
I	Decade inductance
P	Potentiometer
T	Amplifier
c.r.o	Cathode Ray Oscillograph
S	Sample
C	Coil System

Electrical Circuitry of Susceptibility Apparatus.

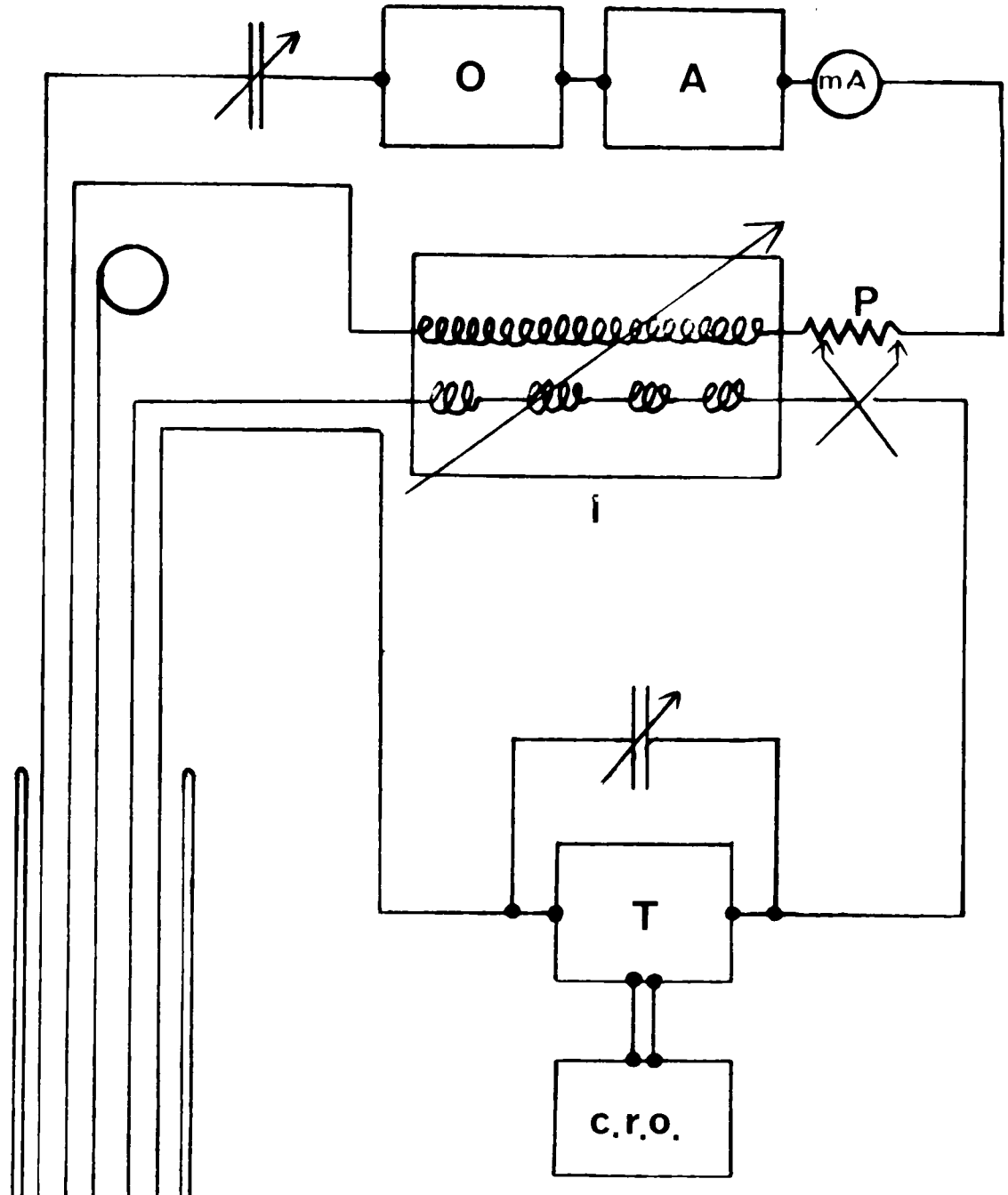


Fig 5.8

is then adjusted until the out-of-balance signal is a minimum. The potentiometer P is used to balance the out-of-phase component between the primary and secondary currents. The machine is calibrated using manganous ammonium sulphate, since the magnetic behaviours of this substance is well understood. By using this substance a conversion factor to convert ΔM into susceptibility units can be found.

(b) Measurements and results. The crystal was cut, weighed and oriented as described previously (5.2.d), and introduced into the apparatus. The readings of ΔM for various stop positions were taken until a maximum ΔM was obtained. The stops were then clamped. Under the conditions the system had the greatest sensitivity and also the small setting errors were minimised. Readings were always taken by moving the specimen from the bottom coil to the top so that thermal equilibrium was not upset by introducing a relatively warm section of rod into the helium. The helium vapour pressure was read from a mercury or oil manometer, and the temperature found from standard helium vapour pressure tables. The pressure over the liquid helium was reduced by pumping and further readings of ΔM taken at lower temperatures. The rate of pumping was governed by a manostat, and thus the temperature was maintained constant while readings were taken.

The A.C. susceptibility of $DyCl_3$ and $HoCl_3$ were measured in three mutually perpendicular directions, along the a and b axes, and perpendicular to the (001)(cleavage) plane. The graphs obtained are shown in Figs. 5.9. and 5.10. The graphs were reasonably reproducible, but occasionally crystals gave unusual results. This was eventually traced to a crystallographic phase change (See Chapt.4). Measurements of D.C. magnetic moment, in which the author did not participate, showed even less reproducibility. This was found to be due to both large relaxation effects and also to a crystallographic phase change.

When the materials based on the mineral elpasolite (Chapter 8) became available, the powder A.C. susceptibilities of Cs_2KGdCl_6 and Cs_2KDyCl_6 were measured in order to determine whether the substances exhibited any cooperative phenomena. These two substances were chosen because they are both Kramer's salts, and also have a large effective magnetic moment.

Cs_2KGdCl_6 exhibits no interesting phenomena in the liquid helium temperature range (Fig.5.10.A), and the variation of susceptibility is given by:-

$$X = \frac{7.68}{T.}$$

Cs_2KDyCl_6 also obeys a Curie Law (Fig.10.A).

$$X = \frac{8.47}{T + 0.150.}$$

A.C. susceptibility of

$DyCl_3$

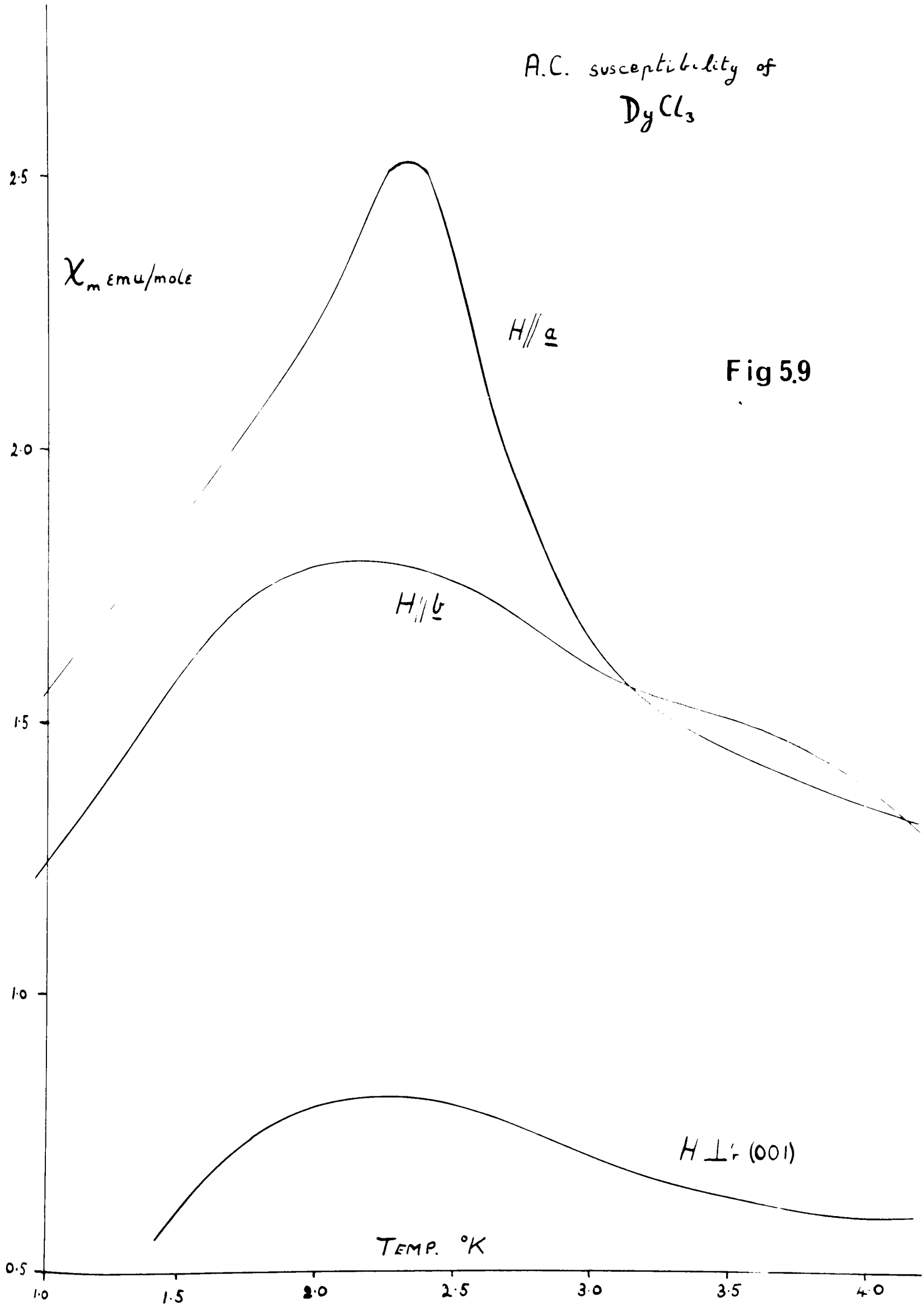


Fig 5.9

A.C. Susceptibility of $HoCl_3$

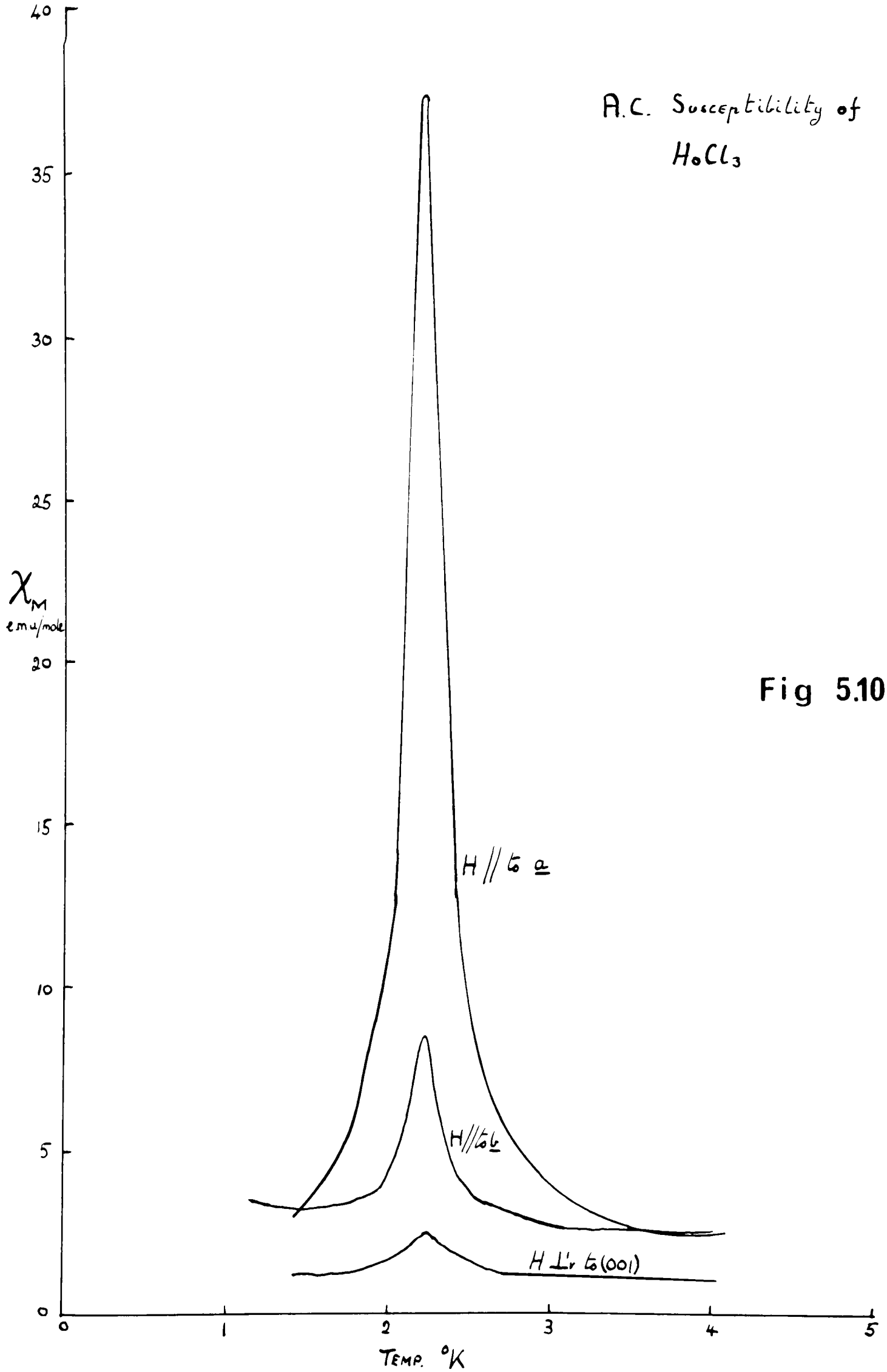
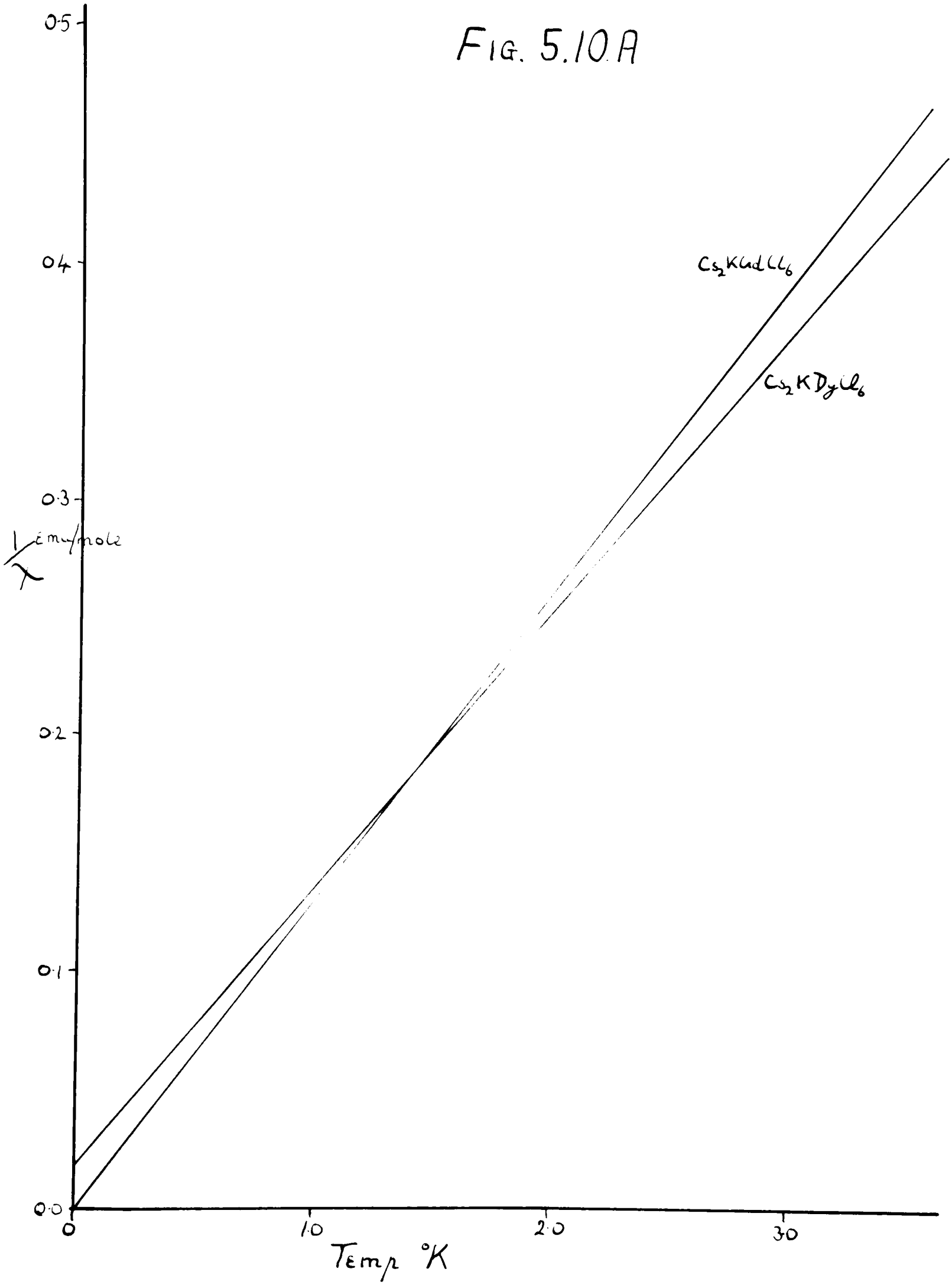


Fig 5.10

FIG. 5.10A


0·5
0·4
0·3
0·2
0·1
0·0
1/χ emu/mole
0
1·0
2·0
3·0
Temp °K
Cs₂KGdCl₆
Cs₂KDyCl₆

Since neither of these compounds orders in the liquid helium temperature range, it is unlikely that any other rare earth analogue will show interesting cooperative phenomena. The reason for this is probably that the rare-earth ions are too far apart, about 7.8Å, for them to interact.

5.3.C. Measurement of Specific Heats.

(a) Apparatus. The basis of the experimental method was to measure the temperature rise produced in a thermally isolated calorimeter by an amount of heat Δq supplied electrically.

A diagram of the apparatus is shown in Fig.5.11. Much of the detail is omitted for clarity. An outer glass dewar contains liquid hydrogen. Inside this is a can containing liquid He^4, which has a radiation shield suspended from the bottom. Inside this latter space is a smaller He^4 can which can be pumped. The small He^4 can is filled from the larger by means of a needle valve. Inside the small He^4 can is the He^3 can, which contains the calorimeter suspended by threads. The calorimeter can be brought into thermal contact with the He^3 can by means of a mechanical heat switch. (Fig.5.12).

The He^3 can is filled with liquid by condensing in gas from a cylinder. Liquid helium and hydrogen are syphoned into the other cans. Each of the vacuum spaces between the

Key to Fig. 5.11.

A Liquid Hydrogen
B Large He^4 Can
C Needle valve
D Small He^4 can
E He^3 can
F Heat Switch
H Calorimeter
J Radiation Shields

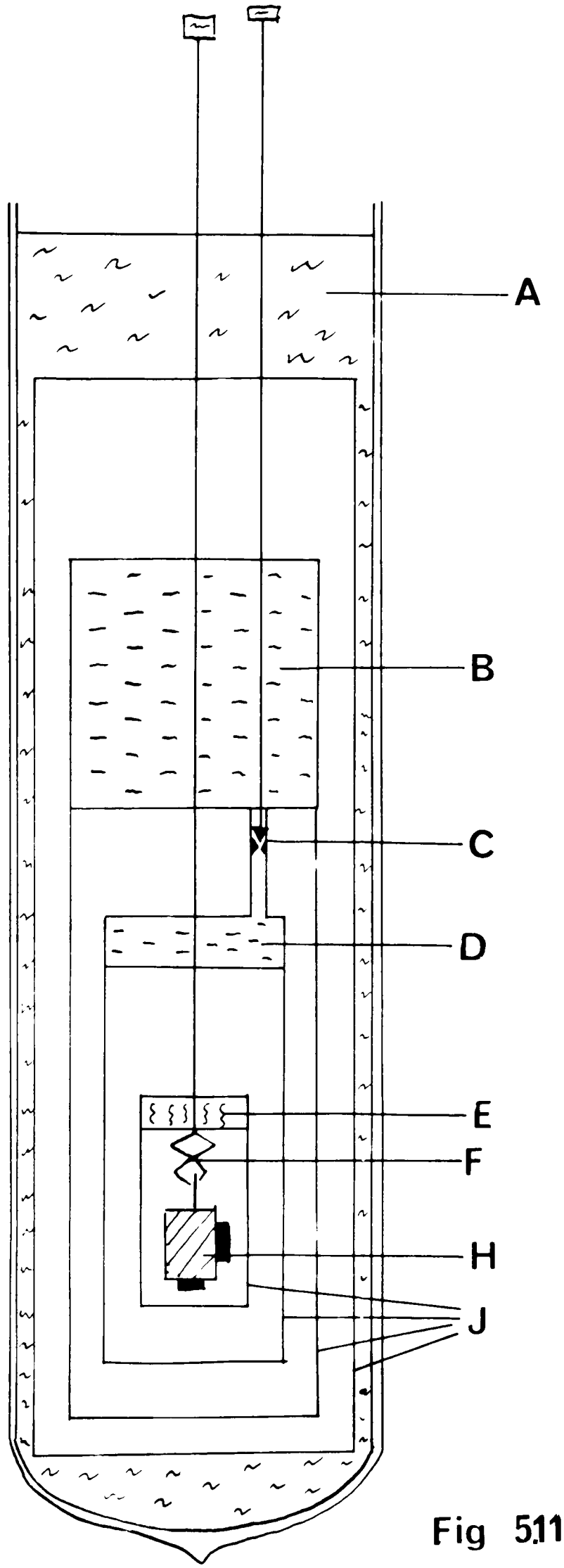


Fig 5.11

heat shields can be filled with helium exchange gas for thermal contact, or evacuated for thermal isolation.

Two types of calorimeter were used to obtain good thermal contact. One type, Fig.5.12. was closed and contained the substance to be measured in the presence of a few millimetres of He^3 and He^4 exchange gas. The heater and germanium resistance thermometer were soldered on the outside. The other design (Fig.5.12) consisted of two copper plates with the heater stuck between them with G.E. varnish. The sample and thermometer were stuck to the outside with varnish.

The apparatus was cooled using standard techniques. The resistance of the germanium resistance thermometer was measured by an A.C. Wheatstone bridge, which measured the resistance to 1 part in 10^4. The current passing through the heater was determined using a potentiometer and a standard 100w resistance. The resistance of the heater as a function of temperature was measured by the Wheatstone bridge. The time of heating was determined mechanically by connecting the microswitch controlling the current to a stopwatch.

The germanium resistance thermometer was calibrated once by measuring the resistance at various temperatures which were obtained from standard vapour pressure tables. The specific heat of the empty calorimeter was measured before measuring

Key to Fig. 5.12.

A

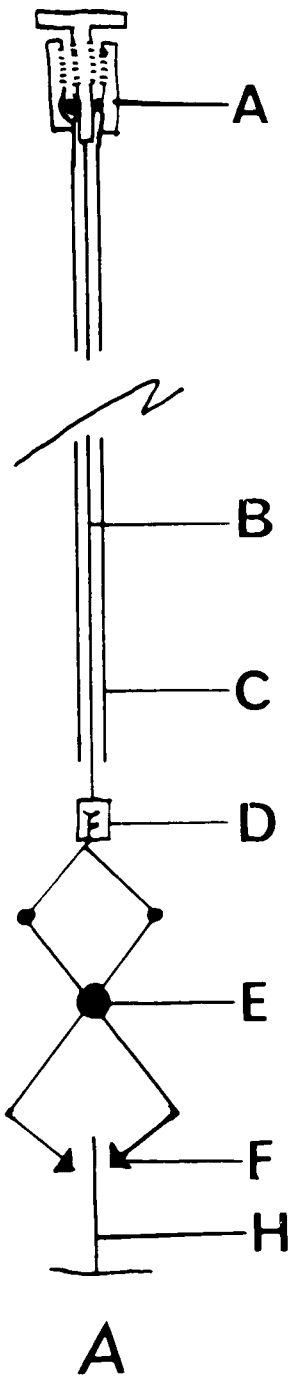
A Vacuum Seal
B Tight wire to open switch
C Outer tube
D Spring
E Fixed hinge
F Gold-plated jaws
H Gold-plated wire to calorimeter

B

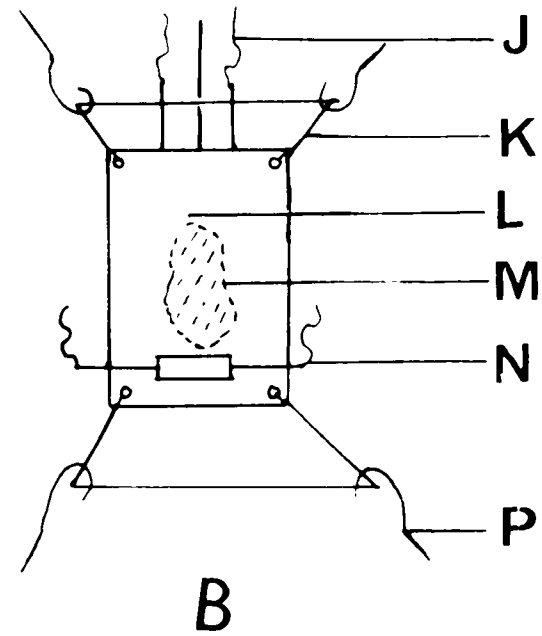
J Heater leads
K Taut cotton support
L Copper plate.
M Crystal
N Thermometer
P Hooks fixed to inside of radiation shield

C

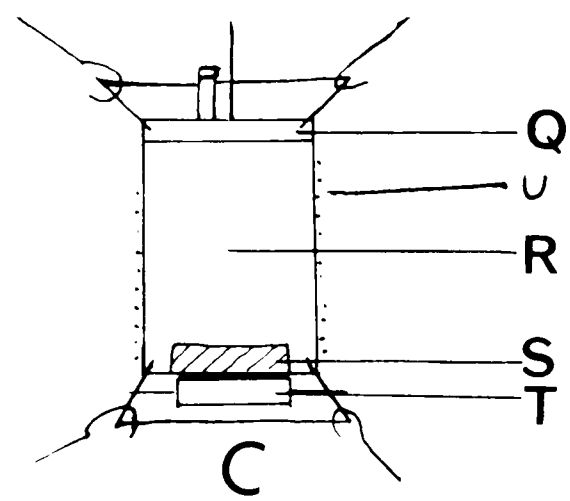
Q Lid with gas inlet
U Heater wire
R He^3 exchange gas
S Sample
T Thermometer



A



B



C

Fig 5.12

the specific heat of the sample. The specific heat of the G.E. varnish used to stick the sample to the calorimeter was known to be negligible.

The apparatus was cooled down to 20°K with hydrogen gas in all the vacuum spaces for good thermal contact, and when cool the gas was pumped out. Helium was then syphoned into the large helium can, and some admitted to the small can via the needle valve, and pumped down to 1°K. He^3 was then condensed into the He^3 can and pumped down to .35°K. The sample, when it had reached this temperature, was thermally isolated by opening the mechanical heat switch.

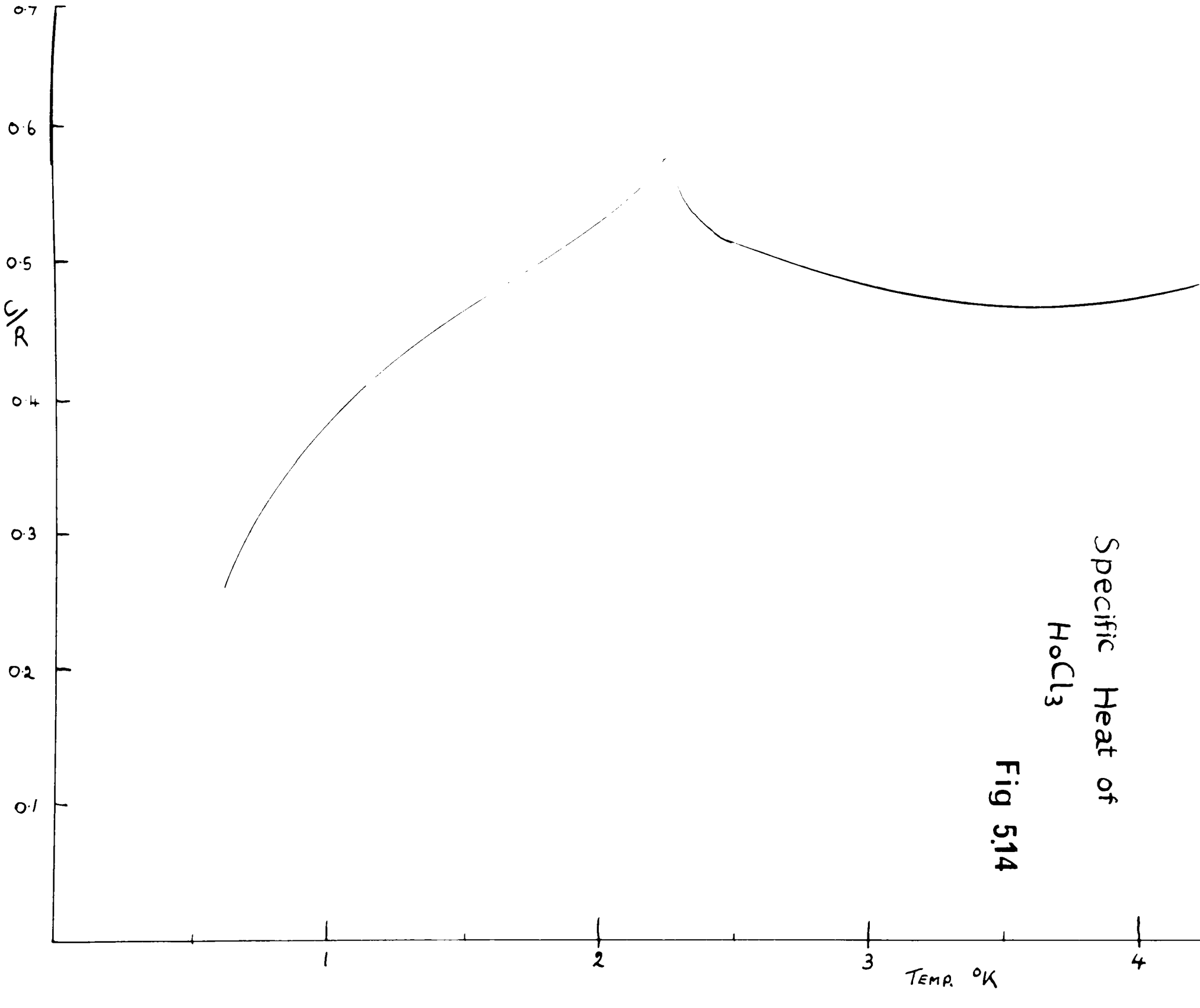
The drift rate of the resistance thermometer was then plotted graphically, and when it was linear, the calorimeter was heated for a measured time with a measured current. The resistance drift rate was again plotted, and another heating period commenced when the drift rate was again linear. The temperature rise (10-100 millidegrees) was measured by extrapolating the drift rates before and after the heating period into the middle of the heating period.

(b) Measurements and Results. Certain difficulties were experienced in measuring the specific heats of $DyCl_3$ and $HoCl_3$. The length of time taken for the drift rates to become linear was prohibitively long in the regions of large specific

heat, due to poor thermal contact and microcrystallinity. A calorimeter filled with exchange gas was tried, but this gave spurious peaks due to He^4 condensing in the calmrimeter. Final measurements were made with He^3 exchange gas. This was satisfactory down to 0.7°K, before He^3 started to condense. Also the specific heat graphs of $HoCl_3$ and $DyCl_3$ were never completely reproducible. This was subsequently traced to a crystallographic phase change. Because of this the results have little significance. The graphs showing the variation of specific heat with temperature, of $DyCl_3$ $HoCl_3$ and $ErCl_3$ are given in Figs. 5. 14, 15 and 16.

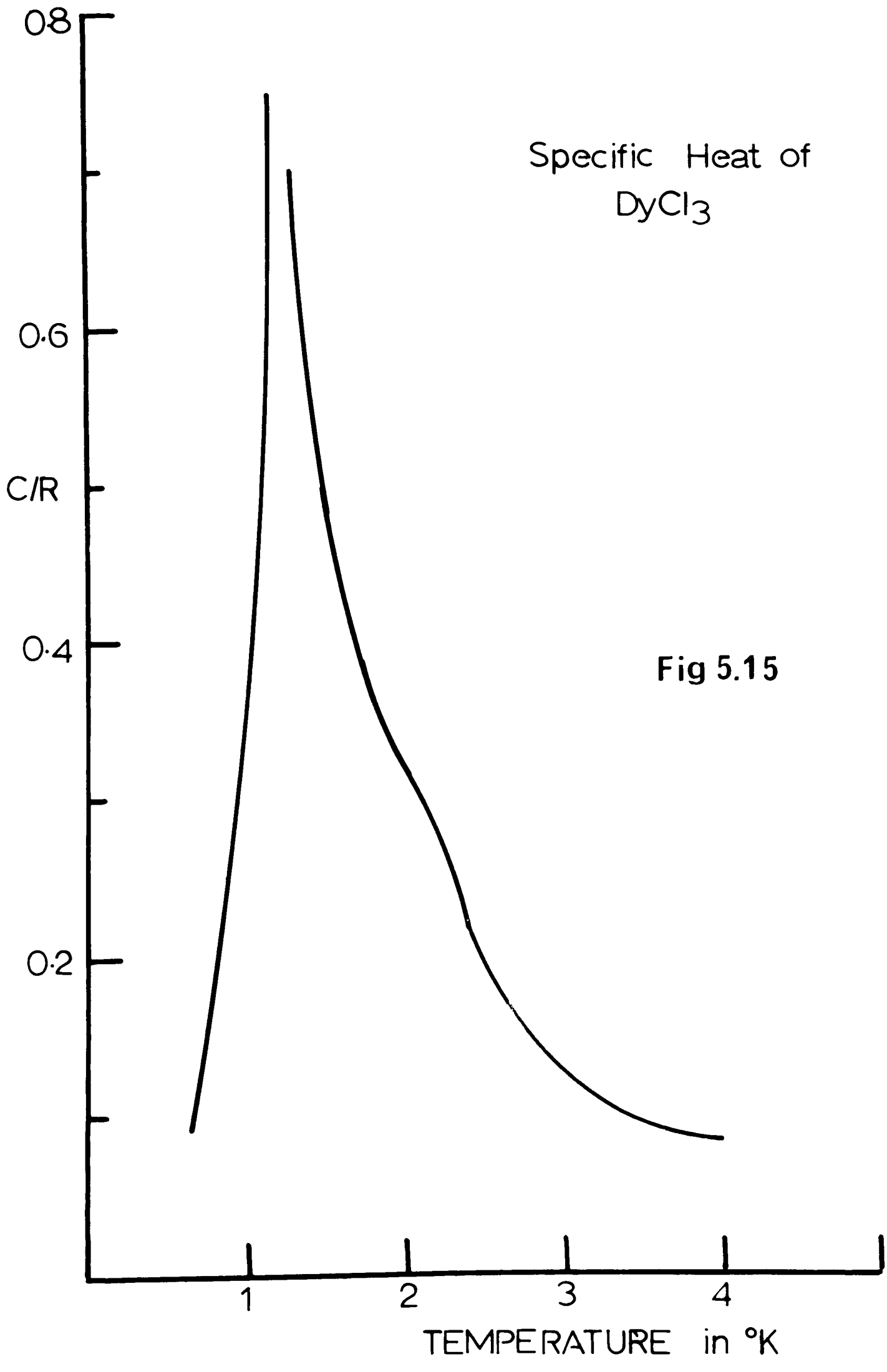
(c) Discussion. X-ray powder photographs of several samples of $DyCl_3$ after they had been used for experiments at liquid helium temperature showed that the samples consisted of a mixture of at least two unknown crystalline forms in different proportions. Therefore, since the substances measured were never of the same crystalline form, the non-reproducibility of the results is explained.

The results of the susceptibility and specific heat experiments do not correspond, in that the latter experiments show large effects when the former show small ones, and vice-versa. These effects cannot be explained except in terms of the crystalline forms present. The specific heat of $ErCl_3$ shows no evidence of cooperative phenomena in the temperature range investigated.



Specific Heat of $HoCl_3$

Fig 5.14



Specific Heat of
$DyCl_3$

Fig 5.15

Specific Heat of
$ErCl_3$

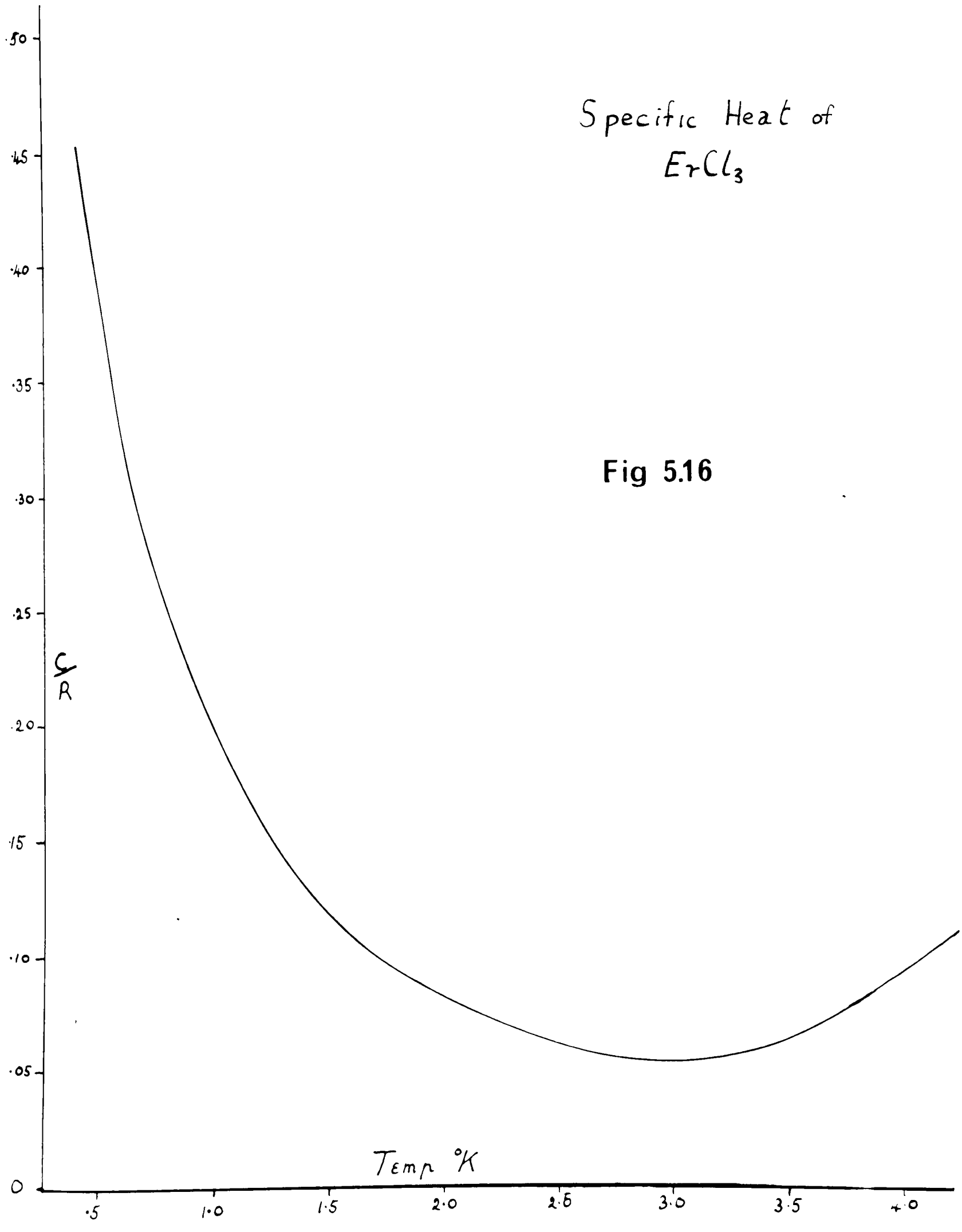


Fig 5.16

CHAPTER 6.

SOME X-RAY DIFFRACTION STUDIES OF SOME LANTHANON COMPOUNDS.

A. $TbCl_3$.

(1) Introduction. Terbium trichloride was previously known to be dimorphic (5). The high temperature form is isomorphous with YCl_3 and $DyCl_3$. The low temperature form is not isomorphous with the hexagonal $GdCl_3$ and prior to the beginning of this work its structure was unknown.

Some single-crystal fragments of the low temperature form of $TbCl_3$ were available as a result of unsuccessful attempts to grow a large single crystal by the Bridgman-Stockbarger method (Chapter 3). Although of poor quality these crystals gave sufficiently good reflections for a determination of the crystal structure to be attempted.

Before this work was complete, a report of the determination of the crystal structure of $TbCl_3$ was published by Forrester et al (24) and further refinement of the structure was not pursued. The results of the author are in close agreement with those of Forrester, and fully confirm the fact that the low temperature form of $TbCl_3$ has a similar structure to that of plutonium tribromide.

(2) Structure Determination. The crystals were prepared by the methods described in Chapters 2 and 3. They were in the form of flat needles, about 3-5 mm. long and $\frac{1}{10}$ mm. across. Observation of the crystals with a polarising microscope showed them to be twinned, the orientation of the crystal twins differing by up to 5^{o}. A crystal which gave the best Weisenberg photograph was selected by trial and error, although even with this crystal the spots were elongated. The crystals were suitable for oscillation about the needle axis, which coincided with a crystal axis, but any other mounting was not possible. Due to the hygroscopic nature of the crystals, they were handled under liquid paraffin, and the crystal selected was sealed in a Lindemann glass capillary for protection. Relative intensities were estimated by visual comparison with a strip prepared by exposing one spot for varying lengths of times.

Oscillation and zero and first-layer Weissenberg photographs were taken about the needle axis, taken as a, using Nickel-filtered CuK_{α} radiation. The lattice dimensions were found to be :-

$a = 3.81\text{Å}$(needle axis). $b = 11.76\text{Å}$ $c = 8.50\text{Å}$.

The films were calibrated by superimposing a pattern of sodium chloride on the film.

Consideration of the oscillation and Weissenberg photographs showed the presence of three mutually perpendicular planes of symmetry. The Laue group is therefore m m m and the unit cell orthorhombic. The density was measured using an S.G. bottle and found to be 4.59gm/cc corresponding to four formula units per unit cell. (Calculated density 4.59 gm/cc).

The spectra were indexed on the basis of this unit cell, by means of a Weissenberg chart and the reciprocal lattice construction. The following conditions were found to govern the reflections.

(hkl) only occurs when h + k = 2n.
(hol) " " " l = 2n (h = 2n).

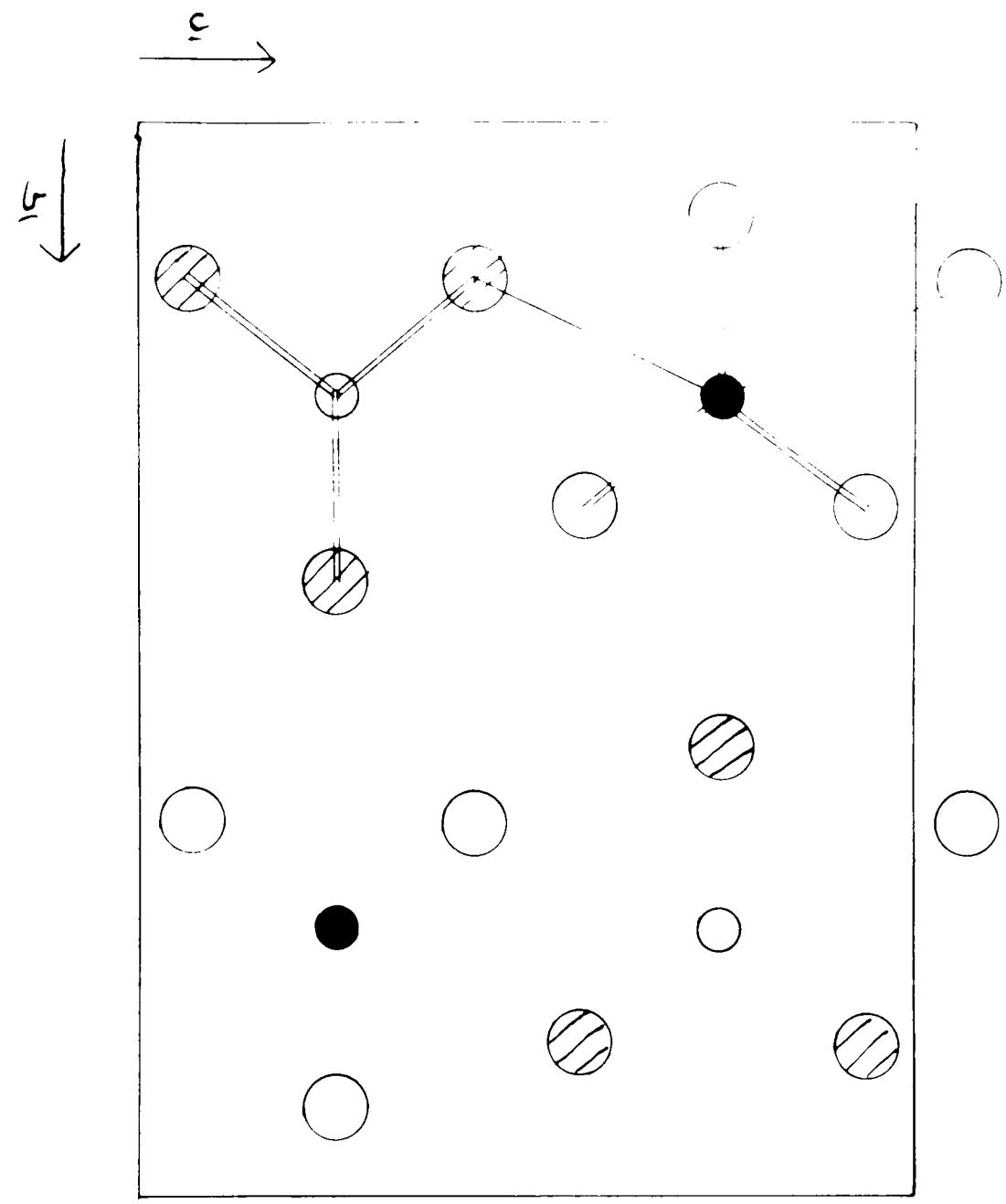
From the general condition that (hkl) is only present when h + k = 2n, the unit cell must be centred on the C face. The condition (hOl) only present when l = 2n indicates a c glide plane. The diffraction symbol is therefore m m m C c c. Only three space-groups are possible, Cmc2, C2cm and Cmcm. The last space-group is centrosymmetric, and in the absence of piezo and pyro-electric tests was adopted with the usual reservations.

At this stage it was noticed that the data bore a marked resemblance to those obtained for the $PuBr_3$ structure.[3] Several lanthanon bromides and iodides crystallize with this

structure (Table 8.1) A Patterson synthesis on a plane perpendicular to a could be interpreted on the basis of this structure (Fig. 6.1. and 6.2), using the parameters published for $PuBr_3$ (Table 6.1). Values of F(hko) were calculated from these parameters, and the signs given to the observed values. An electron density synthesis on a plane perpendicular to (100) was then used to determine the positions of the Tb and Cl ions (Fig. 6.3.). The peaks due to the chlorine ions were not sharp, and it was difficult to determine their positions accurately.

At this stage the computations were transferred to a computer. The first calculations were done by Dr. K. Watson, using Mercury, and later refinement was computed by the author using K.D.F.-9. Both computers utilised basically the same routines, and after a final refinement of all parameters by the method of least squares over five cycles the disagreement factor, $R = \frac{\Sigma(|Fo| - |Fc|)}{\Sigma|Fo|}$ was reduced to .22. This is not as good as the value of .18 obtained by Forrester, but this can be attributed to several possible factors:-

1) The crystal was of extremely poor quality, and the spots were elongated on the film, making accurate estimation of the relative intensity of the spots difficult.



○ METAL ION AT O ◯ HALIDE ION AT O

● METAL ION AT ½ ⊘ HALIDE ION AT ½

$PuBr_3$ STRUCTURE TYPE

Fig 6.1

$TlCl_3$ Patterson Projection On [100]

CONTOURS EVERY 25 UNITS TO 100, THEN EVERY 100 UNITS

SCALE:- 5 cms ≡ 1Å

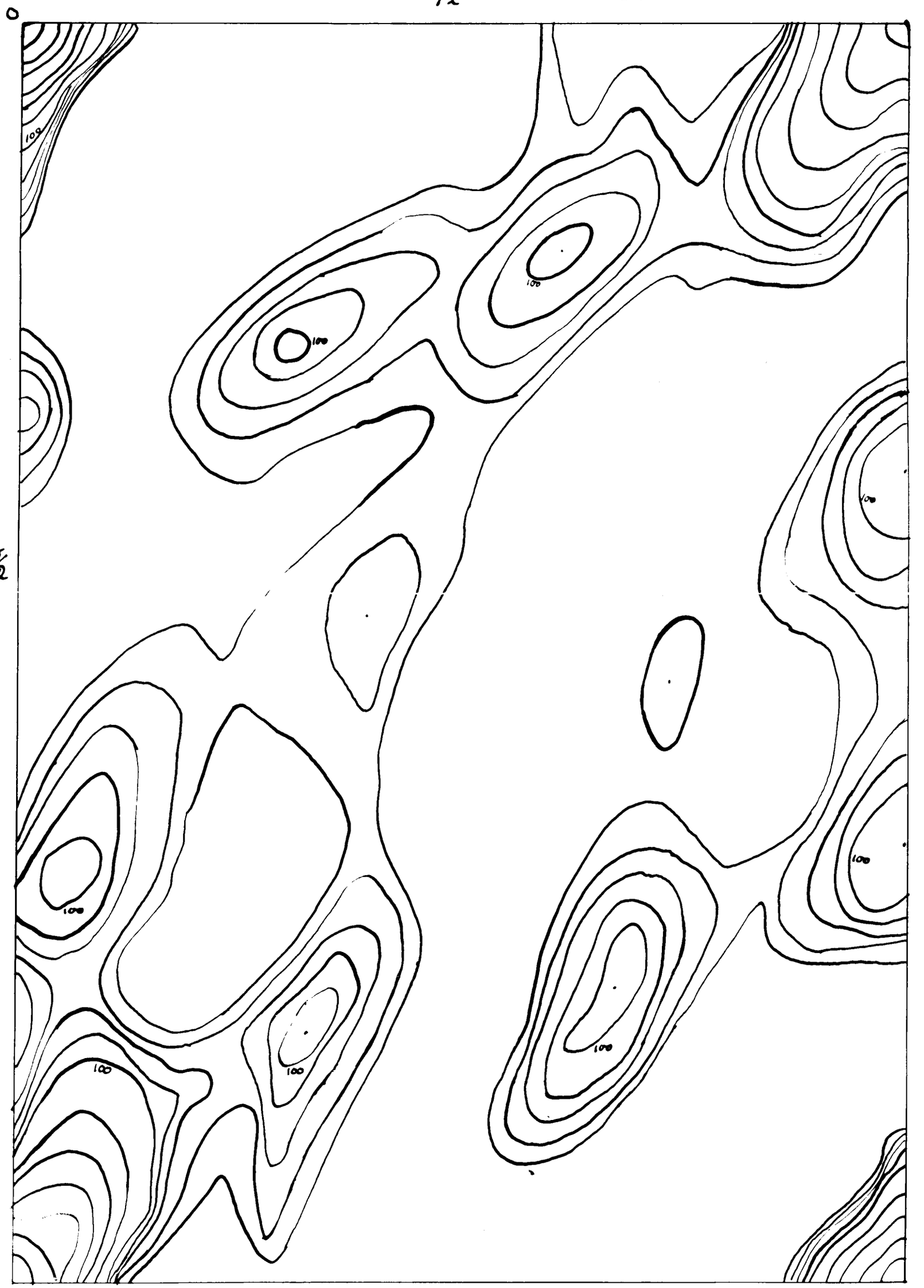


Fig 6.2

$TbCl_3$ Fourier Projecton On [100]

CONTOURS EVERY 25 UNITS TO 100, THEN EVERY 100 UNITS

SCALE: 5 cms ≡ 1Å

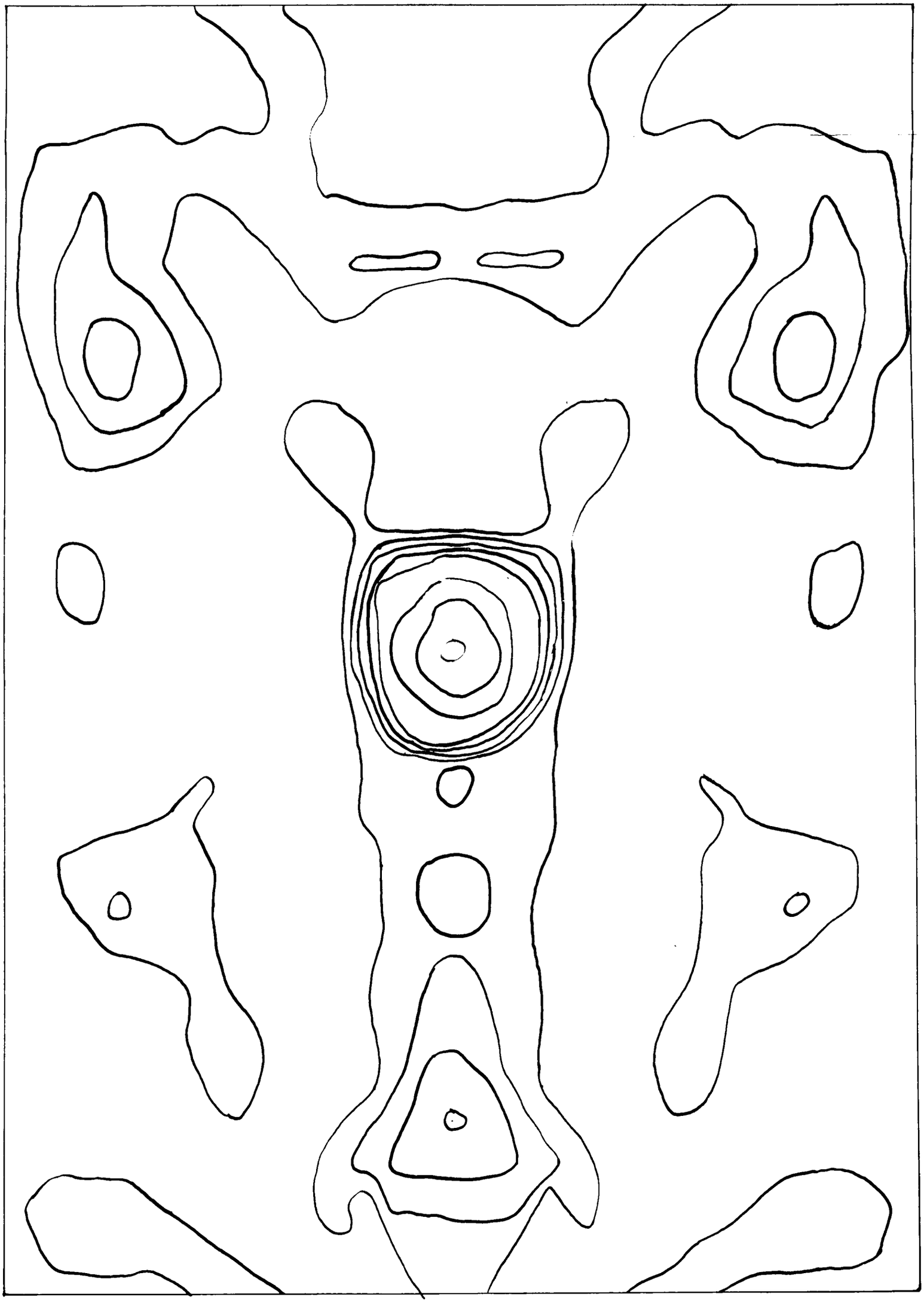


Fig 6.3

2) $TbCl_3$ absorbs X-rays very heavily. An attempt was made to correct for this by manually estimating the path through the irregularly shaped crystal, but the improvement was not very good. Corrections for absorption could have been obtained from the computer if the analysis had been continued.

3) The ions were assumed to be vibrating isotropically. This is almost certainly incorrect in this unusual structure, and corrections could possibly have been made if the analysis had proceeded.

At this stage the paper by Forrester et al was published. It was decided not to proceed further with the refinement of the structure, in view of the close agreement between the two sets of results. The powder photograph data are tabulated in Table 6.3.

Table 6.1.

Atomic Posn.	$PuBr_3$	$TbCl_3$ (Forrester)	$TbCl_3$ (Author).
4 M in 4(c)	x = 0	x = 0	x = 0
0 y $\frac{1}{4}$; o $\bar{y}$ $\frac{1}{4}$	y = .250	y = .256	y = .256
	z = .250	z = .250	z = .250
4 X_1 in 4(c)	x = 0	x = 0	x = 0
	y = -.07	y = -.083	y = -.084
	z = .250	z = .250	z = .250
8 X_2 in 8(f)	x = 0	x = 0	x = 0
o y z ; o $\bar{y}$ z ;	y = .36	y = .354	y = .353
o y $\frac{1}{2}$-z; o $\bar{y}$ $\frac{1}{2}$+z	z = -.05	z = -.069	z = -.064

Table 6.2.

Plane nkl.	F. obs.	F.Calc.	Plane nkl.	F.obs.	F.Calc.
002	88	100	0410	132	142
004	89	110	060	1110	76
006	100	110	061	361	308
008	32	45	062	1381	1175
0010	23	64	063	No	No
020	93	118	064	957	852
021	176	126	065	317	326
022	239	816	066	557	576
023	639	719	067	N.O.	N.O.
024	809	770	068	608	728
025	N.O.	N.O.	069	No	No
026	730	679	0610	217	375
027	631	248	080	1011	751
028	330	411	081	623	471
029	173	233	082	680	478
0210	130	384	083	NO	NO
040	558	441	084	560	516
041	192	164	085	620	493
042	127	110	086	616	510
043	222	159			
044	798	727	087	245	191
045	132	171	088	281	261

Table 6.2. (continued).

Plane nkl.	F. Obs.	F.Calc.	Plane nkl.	F.Obs.	F.Calc.
046	423	400	089	N.O.	N.O.
047	N.O.	N.O.	0.8.10	389	306
048	510	634	0.10.0	387	747
049	No	No	0.101	No	No
			0 14 3	484	344
0 10 2	358	307	0 14 4	430	263
0 10 3	N.O	N.O	0 14 5	N.O	N.O
0 10 4	494	418	0 14 6	N.O	N.O
0 10 5	N.O	N.O	0 14 7	N.O	N.O
0 10 6	573	509	0 14 8	N.O	N.O
0 10 7	N.O	N.O	0 14 9	N.O	N.O
0 10 8	N O	N.O	0 14 10	N.O	N.O
0 10 9	N.O	N.O			
0 10 10	249	307			
0 12 0	687	585			
0 12 1	N.O	N.O			
0 12 2	749	537			
0 12 3	470	408			
0 12 4	459	504			
0 12 5	N.O	N.O			
0 12 6	486	452			
0 12 7	N.O	N.O			

(N.O. are spots too weak to be observed).

Table 6.2 (continued).

Plane hkl.	F. obs.	F. Calc.	Plane hkl.	F. obs.	F. Calc.
0 12 8	347	355			
0 12 9	N.O	N.O			
0 12 10	306	301			
0 14 0	171	119			
0 14 1	295	278			
0 14 2	389	294			

Table 6. 3.

$TbCl_3$ Powder Photograph, CuK_α .

Intensity.	Plane hkl.	$\sin^2\theta$ obs. x 10^4	$\sin^2\theta$ Calc. x 10^4
S+	020	172	172
M	002	330	330
M+	022	502	503
M-	111	529	523
W	040	690	692
W+	041	774	779
W+	130	792	787
S-	131	874	869
M	023	913	913
S	042	1017	1021
M+	113	1186	1192
W+	004	1315	1317
W+	024) 150)	1488	14 86 1491
M-	060	1556	1553
W	061	1631	1635
W-	114	1777	1783
W-	220	1811	1812
M+	062	1880	1883
W+	044	2005	2005

Table 6. 3. (continued).

Intensity.	Plane hkl.	Sin^2 obs. x 10^4	Sin^2 Calc. x 10^4
W-	134	2110	2105
W-	170	2521	2526
W+	171	2596	2593
W+	080	2754	2757
M-	081	2838	2843
W+	064 135	2861	2858 2867
W	204	2956	2955
W	082	3081	3082
W-	224 026	3135	3141 3134
W+	083	3486	3481
W+	155	3536	3529
W-	065	3607	3609
W-	191	3967	3961
W-	330	4080	4083
W-	0,10,0	4301	4304
W-	0,10,2.	4621	4615

3) Description of the Structure. The unit cell (Fig. 6.1) of $TbCl_3$ is orthorhombic, with four molecules per unit cell, space-group C m c m. The unit cell dimensions are:-

$$a = 3.81 \pm 0.01\text{Å} \quad b = 11.76 \pm 0.01\text{Å} \quad c = 8.50 \pm 0.01\text{Å}.$$

The positions of the atoms as determined by the author are given in Table 6.1, together with the parameters determined by Forrester et al, and the parameters of the atoms in $PuBr_3$, for purposes of comparison.

The coordinates given by Forrester et al in their paper refer to a different origin, but have been converted to the same origin in the table.

The structure contains terbium atoms at the centre of triangular prisms of 6 chlorine atoms. The prisms share triangular faces to form columns of terbium and chlorine atoms $(TbCl_3)_x$, parallel to a. Each terbium atom has three other near chlorine neighbours on lines out through the centres of the prism faces. Two of these are the same distance (2.81Å) as the apical chlorine atoms, but the third, (in the (010) direction) is considerably farther away. The coordination of each terbium atom is similar to the coordination of gadolinium in gadolinium trichloride, but whereas the latter has nine equidistant chlorine nearest

neighbours, the former has only eight, the ninth chlorine atom being squeezed out because of the smaller ionic radius of terbium. In the series $GdCl_3$, $TbCl_3$, α-$DyCl_3$, the coordination number of the metal ion decreases from 9 to 8(+1) to 6 as the cationic radii decrease.

The mechanical properties of the crystal are in accord with the structure of low temperature $TbCl_3$. There is a strong tendency to fibrous cleavage in the direction of the columns of $TbCl_3$. Cleavage along the (010) plane is to be expected, since there are no strong bands across that plane. Cleavage along the (001) plane is apparently the result of repulsion between chlorine ions in adjacent columns of $(TbCl_3)_x$.

β-$DyCl_3$

It is convenient at this point to include the powder data for β-$DyCl_3$, which is isomorphous with β-$TbCl_3$. (Chapter 4). The powder data were obtained from photographs of several samples of impure β-$DyCl_3$ obtained in several ways. The observed data always agreed within experimental error, but were averaged for the purpose of finding the lattice parameters. The powder data are tabulated in Table 6.3.A. The lattice parameters are of low accuracy, because it was not possible to observe any high angle lines.

Table 6. 3. A.

$DgCl_3$

Orthorhombic form. CuK_α .

Intensity.	Index hkl.	$Sin^2\theta$ Obs. x 10^4	$Sin^2\theta$ Calc. x 10^4
S	020	170	170
M	002	329	330
M	022	498	500
S	111	534	534
S	131	874	874
M	023	912	913
M	042	1012	1010
M	113	1192	1194
M	004	1319	1320
W	024	1490	1490
M	133	1535	1534

a = 3.81 Å

b = 11.82 Å

c = 8.49 Å

B. Determination of the Positions of the Yttrium atoms in Li_3YCl_6

1) Introduction. A compound Li_3YCl_6 which has not been reported previously was identified in the $LiCl/YCl_3$ phase diagram (Chapter 4) and a preliminary investigation of its unit cell size and symmetry was made. No crystal structure determination of any similar compounds has been attempted.

2) Determination of unit cell size and symmetry. A good quality single crystal of Li_3YCl_6 was grown by methods described in Chapters 2 and 3. The crystal did not cleave easily in any direction. Examination of crystal fragments by a polarizing microscope showed them to be anisotropic. Small crystal fragments were obtained by cleaving large crystals under paraffin oil and were then mounted in Lindeman glass capillaries which were sealed with black wax.

X-ray photographs were taken using Ni-filtered CuK_α radiation. An oscillation photograph was taken about an axis found to be 6.01 Å. A Weissenberg photograph taken about this axis showed hexagonal symmetry, the other two axes being both 11.18 Å. First and second layer Weissenberg photographs were also taken. The spectra were indexed by means of a Weissenberg chart, and the following condition was found to govern reflections.

(h k 0) only occurs when $-h + k = 3n$.

Oscillation and Weissenberg photographs taken about the 11.18 Å axis confirmed that the unit cell was hexagonal, with the following dimensions:-

$$a = 11.18\ \text{Å} \pm 0.05\ \text{Å} \qquad c = 6.01\ \text{Å} \pm 0.02\ \text{Å}$$

The density was measured with a specific gravity bottle, and found to be 2.45 gm/cc, corresponding to 3 formula units per unit cell (Calculated density 2.47 gm/cc).

A powder photogtaph was also taken of Li_3YCl_6, using Ni-filtered Cu K_α radiation and a Philips 11.483 cm diameter camera. The pattern could be indexed on the basis of a hexagonal unit cell,

$$a = 11.20\ \text{Å} \pm 0.05\ \text{Å} \qquad c = 6.01\ \text{Å} \pm 0.02\ \text{Å}.$$

The powder pattern is given in Table 6.4.

3) Determination of the positions of the Yttrium atoms.

Two Patterson syntheses were calculated, one on a plane perpendicular to c (Fig. 6.4) and the other on a plane perpendicular to a (Fig. 6.5). Fig. 6.4. shows a strong peak at $\frac{2}{3}, \frac{1}{3}$, and Fig. 6. 5. peaks of similar height at $\frac{1}{3}$,0 and $\frac{2}{3}$.0. Therefore, the three Yttrium atoms lie in the following positions:- $\frac{1}{3}, \frac{2}{3}$ 0, $\frac{2}{3}, \frac{1}{3}$,0 and 0,0,0.

Li_3YCl_6 Patterson Projection On [001]

Scale:- 2cms ≡ 1 Å

Peak Heights on Arbitrary Scale

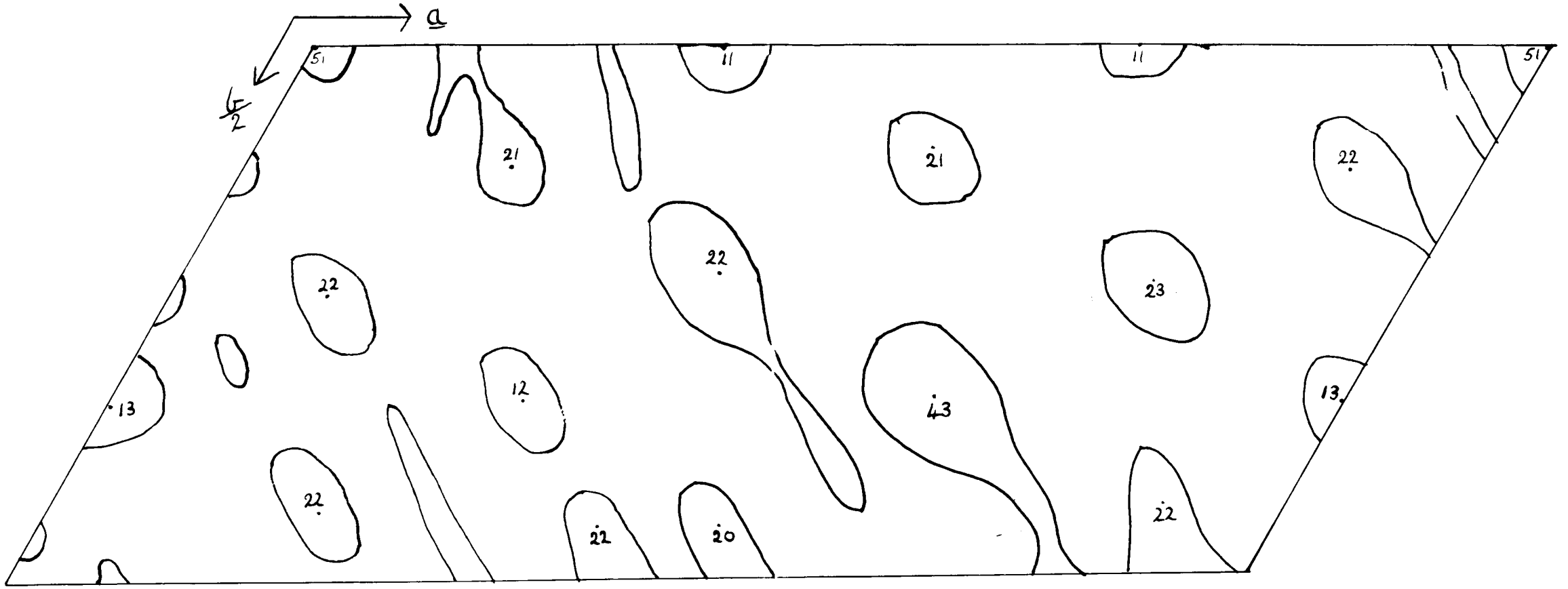


Fig 6.4

Li_3YCl_6 PATTERSON PROJECTION ON [100]

SCALE :- 2 cms ≡ 1 Å

PEAK HEIGHTS ON ARBITRARY SCALE

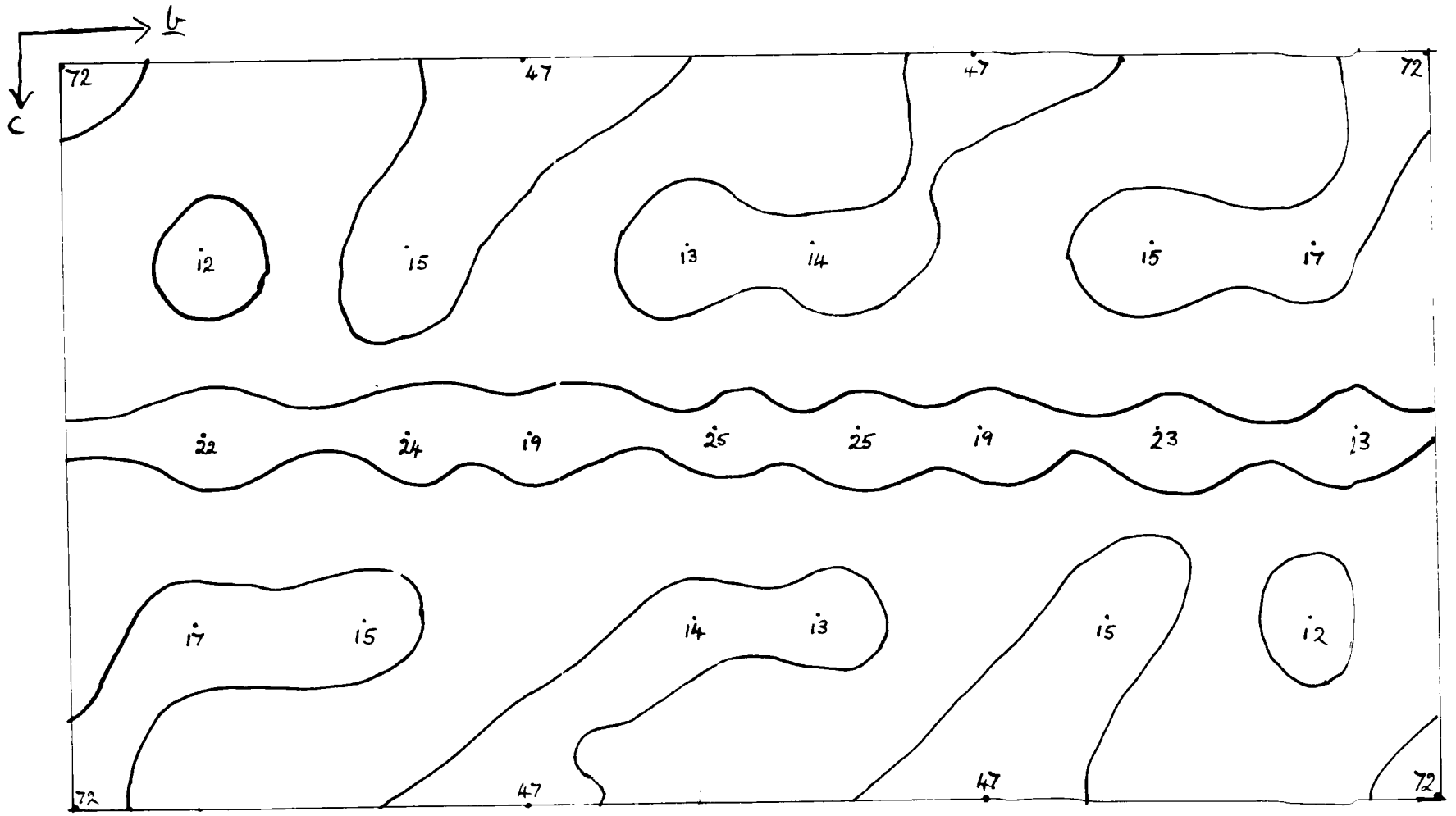


FIG. 6.5

The structure determination was not proceeded with any further for the following reasons. The Weissenberg photographs showed that the crystals, however small, absorbed heavily. It was not possible to correct for the absorption since at the time no computer programme was available to do this. In addition, since there are no general selection rules governing reflections, the choice of space groups is rather wide, and the correct space group could only be arrived at by trial and error.

Table 6. 4.

Powder data for Li_3YCl_6 Ni-filtered Cu α radiation.

Intensity.	Plane (hkl)	$Sin^2\theta$ Calc. x 10^4.	$Sin^2\theta$ Obs. x 10^4.
S	110	190	194
S-	200	253	252
M	201	417	394
W-	002	657	662
S	301	733	741
M-	112	847	846
W=	311	986	969
S	302	1226	1239
W-	222	1415	1416
S	330	1706	1714
W	412	1984	1988
M-	303	2048	2040
W=	332	2363	2367
M-	520	2465	2450
W=	512	2616	2613
M-	602	2932	2936
W	522	3122	3134
W-	711) 603)	3766) 3754)	3764
W-	623) 523)	3943) 3944)	3940
W-	631) 105)	4146) 4171	4178
W	534	4335	4332
W	632	4639	4641

C. Crystal Structure of $GdBr_3$.

1) Introduction. No work on the structure of $GdBr_3$ has been published, although $EuBr_3$ has been reported to crystallize with the $PuBr_3$ structure (21). Since the A.C. powder susceptibility of $GdBr_3$ shows an anomaly in the liquid helium temperature range[3], it was decided to attempt a structure determination of $GdBr_3$ because of its potential interest.

2) Attempted Structure Determination. A poor quality single crystal of $GdBr_3$ was grown by the methods described in Chapters 2 and 3. The crystal cleaved easily into thin plates. The plates were not of a fibrous nature, and the crystal plates extinguished polarised light. The plates were cut into narrow needles, which were mounted in thin-walled capillary tubes in the normal way. Oscillation photographs were taken about two axes in the cleavage plane, using Ni-filtered CuK_α radiation. The lengths of the axes obtained were:-

$$\underline{a} = 7.2\ \text{Å} \qquad \underline{b} = 12.4\ \text{Å}$$

The photographs were of poor quality, and the accuracy of the measurements was low. Attempts were made to take Weissenberg photographs, but the spots were very streaky, and it was not possible to interpret the photographs at all. Many crystals were tried, and were handled very carefully, but the results were always bad. Therefore, an attempt was

made to index the powder photograph, first making some assumptions about the structure. Table 8.1. shows all the known structures of the rare earth bromides. It would appear that $GdBr_3$ should crystallize with the $PuBr_3$ structure, or possibly with the YCl_3 type structure. Both possibilities were investigated in the light of all available information.

The length of the a axis obtained from oscillation photographs is not the length expected for one of the axes if $GdBr_3$ has the $PuBr_3$ structure. Also the cleavage properties of the crystal were similar to those of crystals having the YCl_3 structure, and unlike those of $TbCl_3$.

The powder photograph was indexed successfully on the basis of a monoclinic unit cell, starting with the approximate values of the axial lengths obtained from the oscillation photographs, and assuming the monoclinic angle to be about 110^{o}. Using those powder lines which could be indexed unequivocally, the lattice parameters could be refined by the method of least squares. An attempt was made to index the powder pattern on the basis of an orthorhombic unit cell, of a size expected from a $PuBr_3$ structure type, but this was not possible.

Therefore $GdBr_3$ crystallizes with the YCl_3 type structure ,

$a = 7.3\ \mathring{A}$ $b = 12.6\ \mathring{A}$ $c = 6.7\ \mathring{A}$ $\beta = 106^{\circ}$.

It was not possible to estimate the errors in the lattice parameters, but they are probably large, roughly $0.1\mathring{A}$, due to the fact that only lines of low Bragg angle were measurable. The data are given in Table 6.4.

The following selection rule governs all reflections:- (hkl) only when h + k = 2n. The possible space groups are C2, Cm and C2/m. The latter space group is centrosymmetric, and the space-group allotted to the YCl_3 structure. The measured density is 4.4gm/cc, giving 4 molecules per unit cell (calculated density 4.8 gm/cc).

Description of the Structure. Since the single crystal photographs were of such poor quality, and only a few lines of the powder photograph could be indexed unequivocally, it was not possible to attempt a full structure determination. It must therefore be assumed that the atomic parameters are approximately the same as for YCl_3, and the description of the structure is essentially the same as that described in Chapter 5.

Table 6. 4.

Powder data for $GdBr_3$, Ni-filtrated CuK_α radiation.

Plane hhl.	$Sin^2\theta \times 10^4$ Calc.	$Sin^2\theta \times 10^4$ obs.	Intensity.
001	145	140	VS
110	158	159	W
$11\bar{1}$	228	224	W
021	295	305	VW
002	579	561	W
112) 040)	587) 598)	596	W
$22\bar{1}$ } 220 }	630) 635)	638	W
022 } 041 }	729) 743)	731	S
201	780	793	W
$22\bar{2}$	914	914	W
$31\bar{1}$ } 150 }	1049) 1056)	1054	W
$13\bar{2}$) 113)	1187) 1236)	1210	W
241	1378	1384	W
061 } $13\bar{3}$ }	1491) 1536)	1513	W

C. $CeCl_3 \cdot 7\ H_2O$.

Introduction. A partial determination of the structure of $CeCl_3 \cdot 7\ H_2O$ was attempted in order to estimate the positions of the Cerium atoms. Further structural information was not needed, for the data was only used to help the interpretation of magnetic measurements (25).

An attempt was made previously to determine this structure (26) but due to difficulties experienced in obtaining a good crystal, only the unit cell size and symmetry were determined. (Table 6.5).

Structure Determination. Small crystals were selected from a mass of small crystals supplied by Dr. Weber. They were hygroscopic and were mounted in Lindemann glass capilliaries. Some of the crystals cracked after mounting but finally uncracked crystals were found by trial and error. Relative intensities were estimated by visual comparison with a strip prepared by exposing one spot for varying lengths of times.

Oscillation and Weissenberg photographs were taken about two axes, using Ni-filtered CuK_α radiation. The lattice dimensions are given in Table 6.5. The powder photograph could also be indexed on the basis of this unit cell (Table 6.6.) The density was mesured using an S.G. bottle and found to be 2.24 gm/cc corresponding to four molecules per unit cell (Calculated density 2.29 gm/cc.

The spectra were indexed on the basis of a monoclinic unit cell, and the following conditions were found to govern the reflections:-

(hkl)	only	occurs	when	h + k = 2n.
hol	"	"	"	(h = 2n)
okl	"	"	"	(k = 2n)

The possible space groups are C2, Cm and C2/m. In accordance with normal procedure the centrosymmetric space-group C2/m was chosen with the usual reservations.

Two Patterson syntheses were calculated, one on a plane perpendicular to b, (Fig. 6.6.) the other on a plane parallel to (001) (Fig. 6.7). The Cerium atoms are located at:-.

0.222, 0, 0.174

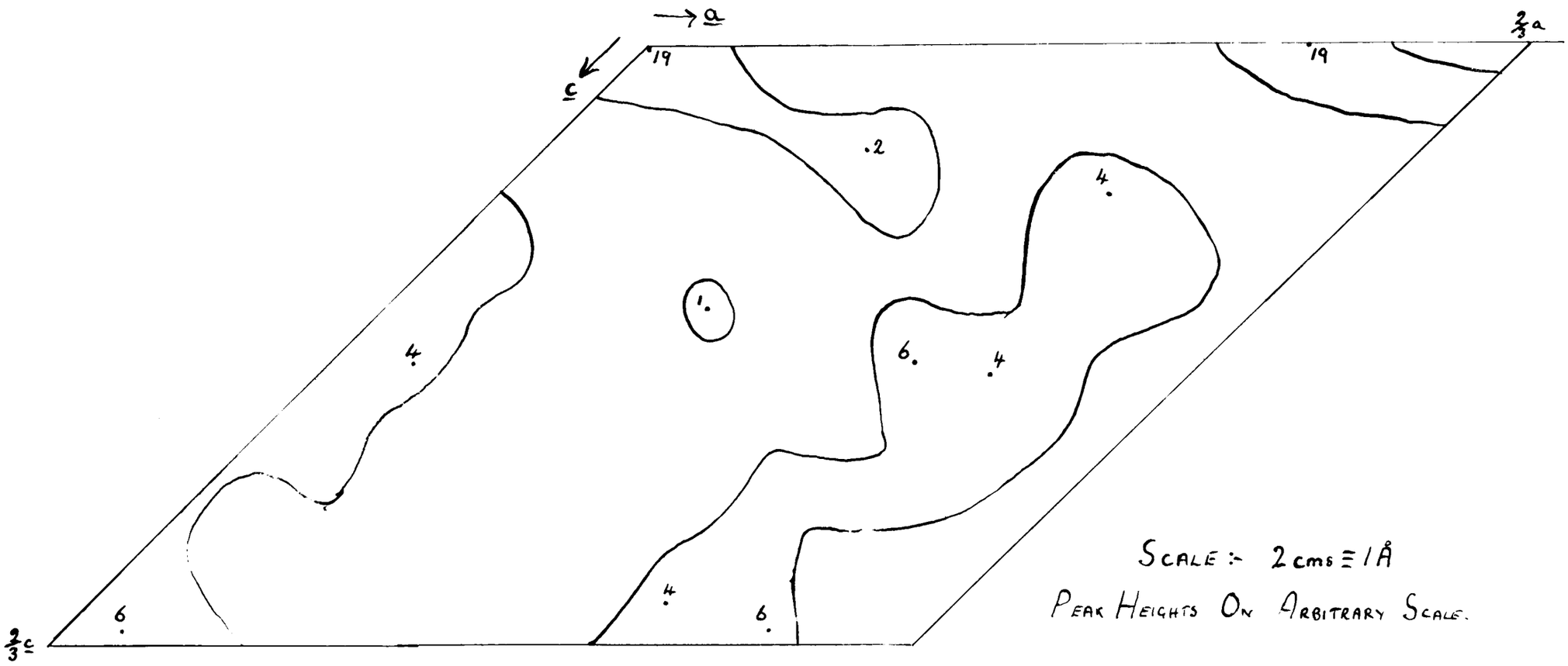
0.722, 0.5. 0.174.

0.278, 0, 0.826

0.778, 0.5, 0.826

since it is only in these positions that the peaks on the Patterson maps and the demands of the possible space groups can be satisfied.

$CeCl_3.7H_2O$ Patterson Projection On [010]



Scale :- 2 cms ≡ 1Å

Peak Heights On Arbitrary Scale.

Fig 6.6.

$CeCl_3.7H_2O$ Patterson Projection On [001]

Scale:- 2 cms ≡ 1 Å

Peak Heights On Arbitrary Scale.

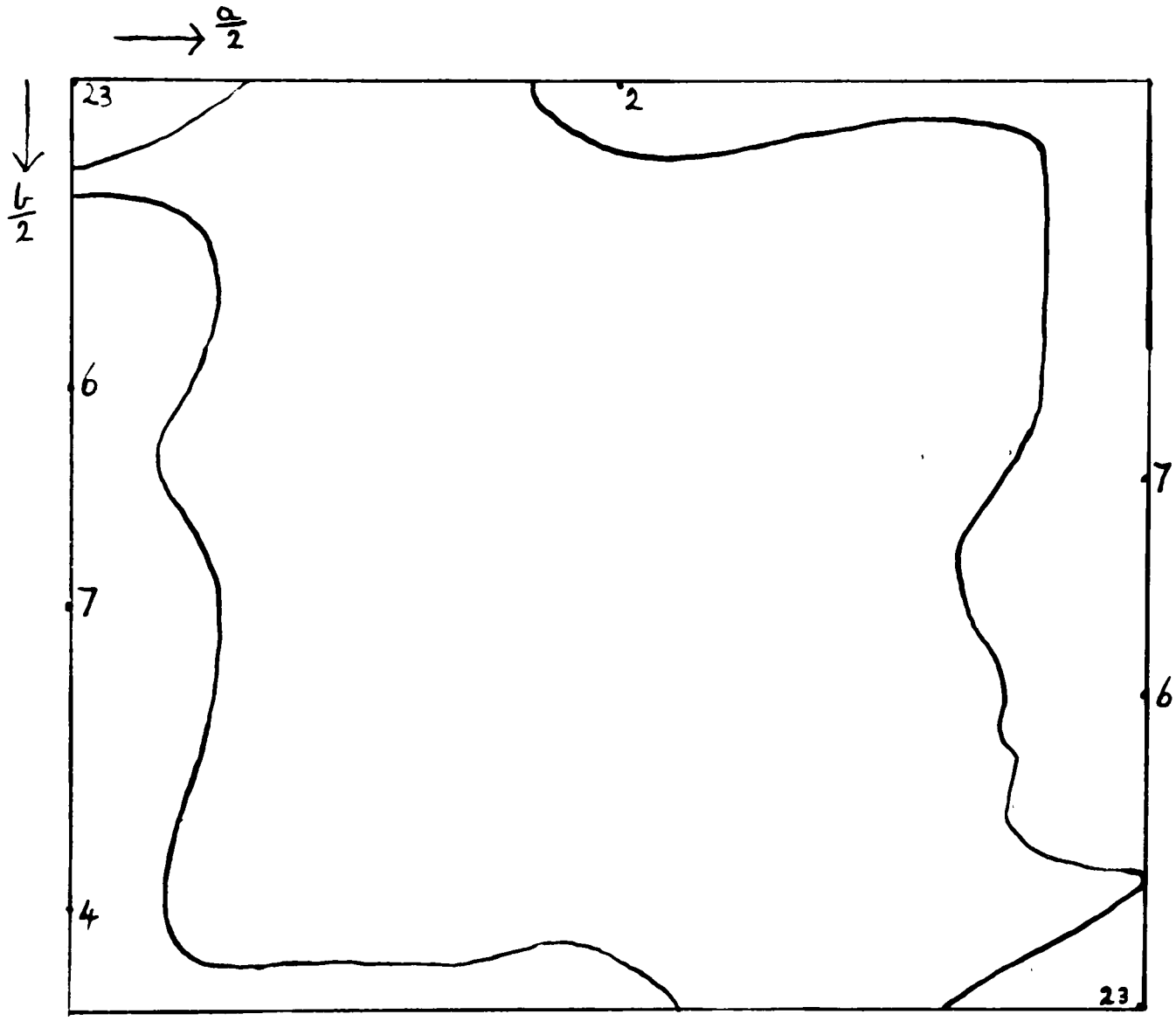


Fig. 6.7.

Table 6. 5.

Unit Cell Dimensions Å.

	Weber's Data.	Present Data	
		Single Crystal.	Powder
a	12.2	12.29 ± 0.05	12.26
b	10.4	10.56 ± 0.05	10.60
c	12.0	11.95 ± 0.05	11.91
β	137°	135.6° ± 0.4°	135.40

Table 6. 6.

Powder data for $CeCl_3 . 7H_2O$. Ni-Filtered CuK_α Radiation.

Intensity	Plane (hkl)	$Sin^2\theta$ obs. x 10^4.	$Sin^2\theta$ calc. x 10^4
M	001	85	85
M	$11\bar{1}$	97	100
S	110	134	133
W	$20\bar{2}$	189	190
M	020	210	212
M	$11\bar{2}$	236	238
M	021	296	297
M	200	320	321
M	111) 002)	338	(336 (340
M	$20\bar{3}$) $22\bar{1}$)	377	(380 (383
M	$22\bar{2}$	396	402
M	$31\bar{2}$	412	409
M	$11\bar{3}$	545	545
M	$22\bar{3}$	599	592
S	$31\bar{4}$) $20\bar{4}$)	722	(723 (740
M	$13\bar{1}$) $40\bar{4}$)	761	(759 (762
W	310	788	775

Table 6. 6. (continued).

Intensity	Plane (hkl)	$Sin^2\theta$ obs. x 10^4.	$Sin^2\theta$ calc. x 10^4.
W	040) 42$\bar{3}$) 221)	845	(847 (849 (853
W	22$\bar{4}$) 13$\bar{3}$)	1959	(952 (968
W	40$\bar{5}$	1050	1056
W	13$\bar{2}$) 202)	1129	(1131 (1132
W	330	1202	1198
W	24$\bar{1}$) 51$\bar{5}$)	1238	(1230 (1243
W	20$\bar{5}$	1276	1270

CHAPTER 7.

SOME POWDER X-RAY DIFFRACTION STUDIES OF SOME GROUP III B COMPOUNDS.

7.1. Introduction. The X-ray powder diffraction pattern of a substance is characteristic of that substance, and forms a "fingerprint" by which that substance can be identified (27). These characteristic patterns can be used both for identification, and for quantitative and qualitative analysis. Quantitative analyses were not used in this work.

The particular advantage of diffraction analysis is that it discloses the presence of a substance as that substance actually exists in a sample, and not in terms of the constituent elements. This is important when mixtures are analysed. Only extremely small quantities of material are used, and are not destroyed during the experiment. The method will, however, sometimes break down if insufficient data of known materials are available for comparison.

The compounds studied have been compounds of Gp.III elements Ga, I and Y, which have recently been prepared in the Inorganic Chemistry Laboratory, Oxford.

7.2. Gallium Hypophosphite Complexes. Some complex hypophosphites of Ga^{III}, of general formula $Ga(H_2PO_2)_3.GaX_3$ where X = Cl, Br, I, have been made by Reddy (28). The composition of these substances was proved by chemical analysis, but it was not possible to show whether the compounds existed as a complex compound, or as two or more coprecipitated phases. However, since, as stated in Sec. 7.1. each phase has a characteristic powder pattern it should be possible to confirm Reddy's assumption that the precipitates were one phase.

The complexes were identified as follows. The X-ray powder photographs were taken on a 9 cm. diameter Unicam camera, using Ni-filtered CuK_α radiation. Powdered samples were sealed in .2 mm. Lindemann glass tubes. The deliquescent halides were handled in a drybox. In addition to the compounds themselves , photographs were taken of the simple trihalides, and the only known gallium hypophosphite. The interplanar spacings are tabulated in Table 7.1.

Table 7.1.

$Ga(H_2PO_2)_3.GaCl_3$		$GaCl_3$		$Ga(H_2PO_2)_3.GaBr_3$		$GaBr_3$		$Ga(H_2PO_2)_3.GaI_3$		GaI_3		$GaH_3(PO_2)_2$	
I	d_{hkl}(A)	I	d_{hkl}(A)	I	d_{hkl}(A)	I	d_{hkl}(A)	I	d_{hkl}(A)	I	d_{hkl}(A)	I	d_{hkl}(A)
S	9.18												
M	5.69			W	5.96								
W	5.45	M	5.45	M	5.74			M	5.65			S	5.54
S	4.86	W	4.83	M	5.17	M	5.15	W	5.39			S	5.24
M	4.66			S	4.88	M	4.92	W	5.23				
W	4.06	W	4.38	W	4.72			W	4.95				
W	3.611	W	3.773	W	4.41	M	4.48	M	4.63				
W	3.454	W	3.504	W	3.866	M	4.12	W	4.48			S	4.42
W	3.307	W	3.462	W	3.733	M	3.94	W	4.32			S	3.907
W	3.232	W	3.339	W	3.666	W	3.537	M	3.764			S	3.715
S	3.127	W	3.054	S	3.324	M	3.307	M	3.557				
S	2.875			S	3.147	S	3.196	M	3.469	S	3.446	S	3.386
S	2.794	W	2.794	W	3.060	W	3.040	S	3.286			W	3.212
W	2.714	W	2.710	W	2.990	W	2.940	M	3.119				

I	d_{hkl}(A)	I	d_{hkl}(A)	I	d_{hkl}(A)	I	d_{hkl}(A)	I	d_{hkl}(A)	I	d_{hkl}(A)	I	d_{hkl}(A)
W	2.580	W	2.570	S	2.899	M	2.795	W	3.008	M	3.020	M	2.990
W	2.561			M	2.729	M	2.736	M	2.918				
M	2.466	W	2.499	M-	2.596	W	2.682	W	2.782			M	2.847
M	2.275			M-	2.483	W	2.626	W	2.689			S	2.800
M	2.181	W	2.162	M-	2.281	W	2.557	W	2.534			W	2.703
M	2.127			M	2.198	W	2.473	W	2.333			S	2.477
W	2.109	W	2.086	M	2.149	W	2.378	M-	2.213			M	2.397
W	2.052			W	2.101	W	2.299	W	2.143	M	2.142	M	2.358
W	2.029	W	2.019	S	2.026	W	2.030	W	2.091	M	2.113	M	2.303
S	1.983			W	1.971	M	1.992	W	2.035			S	2.177
M	1.921			M	1.938	S	1.966	M-	1.964	W	1.990	W	2.107
M	1.873			M	1.895	W	1.911	M-	1.921	W	1.917	W	2.049
W	1.794			W	1.853	W	1.881	W	1.853	M	1.830	M	1.980
W	1.774			W	1.794	W	1.837	W	1.771	W	1.792	M	1.936
W	1.737	W	1.749	M	1.752	W	1.794	W	1.747	M-	1.733	M	1.858
W	1.720			W	1.734	W	1.764	W	1.713			M	1.774

Table 7.1. (continued)

I	d_{hkl}(A)	I	d_{hkl}(A)	I	d_{hkl}(A)	I	d_{hkl}(A)	I	d_{hkl}(A)	I	d_{hkl}(A)	I	d_{hkl}(A)
W	1.694	W	1.687	W	1.717							M	1.739
M	1.669			M	1.677	S	1.692	W	1.674			W	1.712
W	1.663	W	1.653	M	1.655	S	1.663					W	1.677
W	1.641					W	1.648					M	1.622
M	1.622	W	1.622	W	1.620							W	1.596
W	1.609					M	1.605						
M	1.574	W	1.588	M	1.588	W	1.597						
W	1.524	W	1.532	W	1.574	W	1.532			W	1.520	M	1.510
W	1.498	W	1.499	W	1.536	W	1.504	W	1.487			M	1.464
W	1.478			W	1.531	W	1.468					W	1.429
W	1.441	W	1.462	W	1.466	W	1.413	W	1.427			S	1.397
M-	1.406			W	1.456							S	1.634
M-	1.386			W	1.436							W	1.334
W	1.352			W	1.399			W	1.397				
W	1.329			W	1.367	W	1.376	W	1.367	W	1.394	W	1.312
W	1.318			W	1.335					W	1.377		

Table 7.1. (continued)

I	d_{hkl}(A)	I	d_{hkl}(A)	I	d_{hkl}(A)	I	d_{hkl}(A)	I	d_{hkl}(A)	I	d_{hkl}(A)	I	d_{hkl}(A)
W	1.296			W	1.312							W	1.292
W	1.282			W	1.291	W	1.294						
M	1.257			W	1.266	W	1.280			W	1.256	W	1.274
W	1.224			W	1.246	W	1.263					M-	1.252
W	1.203			W	1.217	W	1.151			M-	1.237	M-	1.239
W	1.178			W	1.164					W	1.220		
W	1.162					W	1.135			W	1.173		
M	1.151												

Table 7.1. (continued)

The complex gallium hypophospites, which had the analytical formulae $Ga(H_2PO_2)_3.GaX_3$ could be regarded as existing as one of the following:-

(a) A mixture of $Ga(H_2PO_2)_3$ and GaX_3. No lines due to gallium halides appear, nor is there a set of lines common to all complexes, (corresponding to an as yet unknown compound, $Ga(H_2PO_2)_3$.

(b) A mixture of $GaH_3(PO_2)_2$ (the only known gallium hypophosphite) together with another compound containing hypophosphite and halogen. However, no lines due to $Ga\ H_3(PO_2)_2$ appear.

(c) Compounds of the formulae postulated. In the absence of any contrary data, this would appear to be the correct conclusion. In addition each compound gives a series of strong lines which are unequivocally characteristic of that compound, giving positive identification.

The powder patterns of all the new compounds were extremely complicated, and it was not possible to index them.

7.3. Indium Oxyhalides and OxyPseudohalides. In OCl and InOBr have been made by Forsberg (2). McColm (30) in extending this work has prepared InOF, InOCl, InOBr, InOI and InOCN by an entirely different method. The X-ray powder diffraction

patterns were used to identify the substances only. It was possible to index all the patterns, but none of the compounds had a simple unit cell. The thermal stability was poor, and it would appear that single crystals of these compounds cannot be made easily.

The X-ray powder diffraction patterns were obtained with a Unicam 9 cm. diameter camera, using nickel-filtered $Cu K_\alpha$ radiation, $\lambda = 1.542$ Å. Sodium chloride was used as an internal standard, $\underline{a} = 5.627$ Å.

In OCl and InOBr. The diffraction patterns agreed well with the data published by Forsberg. (Tables 7.2. and 7.3).

In OI. The diffraction pattern Table 7.4, could be indexed on the basis of an orthorhombic unit cell.

$\underline{a} = 5.05 \pm 0.02$ Å $\quad \underline{b} = 3.71 \pm 0.02$ Å $\quad c = 9.49 \pm 0.05$ Å.

The space-group, as determined from the systematic absences is P m m n. The density is 6.17 (calculated 6.00) giving two molecules per unit cell. InOI is therefore isostructural with InOCl and InOBr.

In OCN. This could not be prepared pure, but contained about 50% In_2O_3. Only a few lines were therefore observed. (Table 7.6). The pattern could be indexed on the basis of an orthorhombic unit cell,

$\underline{a} = 5.01 \pm 0.05$ Å, $\quad \underline{b} = 3.71 \pm 0.05$ Å $\quad \underline{c} = 9.03 \pm 0.1$ Å

The space group is P m m n, and InOCN is probably isostructural with InOCl. etc.

InOF. The powder diffraction pattern, Table 7.5. could be indexed on the basis of a hexagonal unit cell,

$$\underline{a} = 10.83 \pm 0.02 \text{ Å} \qquad \underline{c} = 11.75 \pm 0.02 \text{ Å}.$$

The measured density is 3.9 gm/cc, giving 18 molecules per unit cell (calculated density 3.75 gm/cc).

7.4. $In(CN)_3$, $Y(CN)_3$ $In(SCN)_3$. Rare earth tricyanides have not been prepared, but if they can be prepared as single crystals, could be used for the study of rare-earth ions in another type of lattice. McColm (30) has prepared $In(CN)_3$, $Y(CN)_3$ and $In(SCN)_3$, but was unable to investigate the preparation of these compounds on a large scale. It has not been possible to investigate the possibilities of making single crystals of these compounds owing to the small quantities available. Attempts to make $Er(SCN)_3$ have produced an amorphous product.

$In(CN)_3$. The X-ray powder diffraction pattern, Table 7.7., could be indexed on the basis of a monoclinic unit cell.

$$\underline{a} = 6.80 \pm 0.03 \text{Å} \qquad \underline{b} = 11.90 \pm 0.05 \text{Å} \qquad c = 6.97 \pm 0.03 \text{Å}$$

$$\beta = 116.8 \pm 0.5^{\circ}$$

The possible space-groups are C2, Cm and C2/m. $InCl_3$ crystallizes with the space-group C2/m, and $In(CN)_3$ is probably isostructural with it.

$Y(CN)_3$. The X-ray powder diffraction pattern can be indexed on the basis of an orthorhombic unit cell (Table 7.9.)

$$a = 4.22 \pm 0.01\text{Å} \quad b = 12.97 \pm 0.05\text{Å} \quad c = 9.10 \pm 0.02\text{Å}.$$

$In(SCN)_3$. The X-ray powder diffraction pattern can be indexed on the basis of a cubic unit cell (Table 7.8).

$$a = 12.00 \pm 0.05\text{Å}.$$

Table 7.2.

InOCl. ($Cu K_\alpha$)

Present Data.			Forsberg's Data.	
Reflection hkl.	$Sin^2\theta$ obs. x 10^4	Intensity.	$Sin^2\theta$ obs. x 10^4	Intensity.
001	80	S	90	W+
002	-	-	359	vvw.
101	448	S	449	S
011	569	M	568	W
102	718	W	722	W
110) 012)	837	S	836 841	M+ M+
111	931	M	928	W-
103	1170	W	1177	vvw
013	1295	W	1294	VW
200) 004)	1435	S	1437	M
201	1528	W	1528	W
113	1664	M	1656	W
020	1921	M	1914	M+
021) 211)	2008	M	2004	M
005) 022) 212) 114)	2277	S	2276	M
121	2367	M	2363	M
105) 122)	2631	W	2638	W-
023) 213) 015)	2729	W	2735	W-
220)	-		-	V.

123) 115)	3098	W	3090	VW
221	3431	W	3439	W

Table 7.3.

Incor. ($Cu K_\alpha$)

Rosberg's Data.			Present Data.	
Reflection hkl.	$Sin^2\theta$ obs. x 10^4	Intensity.	$Sin^2\theta$ obs. x 10^4	Intensity.
001	79	W	75	W
101	441	S	440	S
102	680	VW	699	W
012	772	M+	763	M
111	896	S	897	S
200	1447	M	1455	W+
201) 113)	1530	M	1510	M
020	1820	M	1846	M
212	2220	M	2218	W+
121	2261	M-	2263	W
220	3267	M-	3269	W
301) 221)	3336	W	3336	VW

Table 7.4.

InOI. ($Cu K_\alpha$)

Reflection hkl.	Intensity.	$Sin^2\theta$ Obs x 10^4	$Sin^2\theta$ Calc. x 10^4
001	W+	70	66
101	S	438	428
011	M	482	498
102	S	693	696
111	S	863	860
013	M	1020	1036
112) 004)	M	1055	(1058 (1056
113	M	1388	1398
104	M	1431	1418
005	M	1646	1650
020	M	1721	1728
211	W	1953	1946
212) 121)	S	2152	(2144 (2156
213	W	2474	2484
106	W	2747	2738
116) 223)	M	3179	3170) 3176)
215	W	3566	3530
206) 303)	W	3842	3824 3865
032	W	4178	4152

Table 7.4. (continued).

InOI.

Reflection hkl.	Intensity.	$\sin^2\theta$ Obs. x 10^4	$\sin^2\theta$ Calc. x 10^4.
131) 304) 313)	W	4293	4316 4314 4294
314	W	4737	4746
134	W	5311	5306
232) 306)	W	5625	5600 5634
135) 233)	W	5919	5900 5940

Table 7. 5.

InOF. ($Cu K_\alpha$)

Reflection hkl.	Intensity.	$Sin^2\theta$ obs. x 10^4.	$Sin^2\theta$ calc. x 10^4.
110	M	204	204
200	M	271	272
201	W	318	315
003	S+	387	388
202	W	431	445
210	M	476	478
212) 203) 301)	W	659	{659 660 665
220	M	814	817
221	M	850	860
311	W	936	928
400	W	1087	1090
223	W	1213	1205
006) 215)	M	1553	{1551 1554
323	W	1689	1681
330	M	1848	1839
324	W	1992	1983
216) 332)	W	2013	2029) 2011)
422	W	2066	2079

Table 7.5. (continued).

InOF.

Reflection hkl	Intensity.	$\sin^2\theta$ obs. x 10^4.	$\sin^2\theta$ calc. x 10^4
107) 333)	W	2194	2180) 2226)
207) 226) 325)	W	2373	2384) 2368) 2371)
600	W	2449	2452
226) 610)	W	2933	2929) 2928)
612	W	3092	3101
407	W	3205	3202
524 308	W	3351	3346) 3371)
702	W	3507	3509
516	W	3668	3663
710) 711)	W	3900	3882) 3925)
606	W	3986	4003
229) 630) 0010)	W	4292	4308) 4290) 4310)
21 10) 329)	W	4793	4787 4785
811	W	5021	5034

Table 7. 6.

InOCN. ($Cu K_\alpha$)

Reflection hkl.	Intensity.	$Sin^2\theta$ obs. x 10^4	$Sin^2\theta$ calc. x 10^4
001	M	68	73
101	S	438	442
111	S	878	874
004	W	1167	1166
200	S	1478	1476
202 020	M-	1748	1768 1728
210	M	1903	1908
114 211	M	1973	1967 1981

Table 7. 7.

In(Cu) . ($Cu K_\alpha$)

Reflection hkl.	Intensity.	$Sin^2\theta$ obs. x 10^4	$Sin^2\theta$ calc. x 10^4
001	M	153	154
020	W	170	168
110	M-	206	203
$11\bar{1}$	M	217	215
021	S	314	322
002	M-	606	615
200	M	639	645
$20\bar{1}$) 040)	W+	664	658) 672)
022	S	793	783
131	W	840	834
201	W+	934	941
112	M-	1104	1102
$24\bar{1}$	W	1191	1187
$15\bar{1}$) $31\bar{1}$)	W-	1233	1223) 1223)
$31\bar{2}$	W	1258	1268
$24\bar{2}$	W=	1360	1365
060) $15\bar{2}$)	W=	1534	1511) 1542
$33\bar{2}$	M	1585	1594

Table 7. 8.

$In(CNS)_3.(CuK_\alpha)$

Reflection hkl	Intensity.	$Sin^2\theta$ obs. x 10^4	$Sin^2\theta$ calc. x 10^4
111	W	136	124
200	S+	165	165
220	S	329	330
300	W	365	371
311	W	457	454
222	M	501	495
420	s	824	825
422	S	990	990
440	M	1319	1320
531	M	1441	1444
600) 442)	M-	1497	1485
620	W	1646	1650
622	W	1812	1815

Table 7. 9.

$Y(CN)_3$. ($Cu\ K_\alpha$)

Reflection hkl.	Intensity.	$Sin^2\theta$ obs. x 10^4	$Sin^2\theta$ calc. x 10^4
020	M-	143	141
002) 030)	W	304	287) 318)
110	S	373	367
101	W-	401	405
111	M+	449	440
032	W	610	605
041	S+	639	637
013	W	693	681
131	W-	723	723
122	W	750	762
050) 140)	S	894	884) 899)
132	M	930	930
113	M	1011	1014
150) 043)	M+	1215	1217) 1211)
060	W	1261	1273
211	S	1434	1440
104	W-	1489	1481
005	M-	1789	1794

Table 7. 9. (continued).

Reflection hkl.	Intensity.	$Sin^2\theta$ obs. x 10^4	$Sin^2\theta$ calc. x 10^4
063	M+	1912	1918
223) 105)	W	2129	2120) 2127)
163	W	2239	2252
064	M-	2433	2421
016	W	2619	2619
300	W	3003	2999

7.5 Barium Chloride Fluoride.

Barium Fluoride Chloride is a possible host lattice for divalent rare-earth ions, such as Eu^{2+}. No crystallographic data has been published previous to this work.

Fragments of single crystals were supplied by Dr. W. Hayes of this department. The fragments tended to cleave into rectangular flat plates, which when viewed with polarised light, were isotropic perpendicular to the cleavage plane, but not in any other direction.

A small crystal fragment was mounted in a capillary, and oscillation and zero and first layer Weissenberg photographs were taken using Ni-filtered $Cu_{K\alpha}$ radiation.

The spectra could be indexed on the basis of a tetragonal unit cell;

$$a = 4.37\text{Å} \pm 0.02 \qquad c = 7.28\text{Å} \pm 0.05\text{Å}.$$

The following condition was found to govern the reflections:-

hko only occurs when h + k = 2n.

The two possible space groups are therefore P 4/n (No.85) and P 4/nmm (No. 129).

The density was measured with a specific gravity bottle and found to be 4.60 gm/cc, corresponding to 2 formula units/unit cell (calculated density 4.58 gm/cc).

The data found for the BaClF is very similar to that found for PbClF (31) which has been given the same space-group. It is therefore likely that BaClF is isostructural with PbClF, since the morphological properties are very similar.

7.6. Summary. Several compounds of gallium, indium and yttrium have been studied by X-ray powder diffraction. The only potentially interesting compounds are the tricyanides, which could provide sites for transition metal or lanthanon ions in very strong crystal fields. McColm[4] has found that the chemical properties are similar to those of the halides, i.e. fairly volatile and extremely hygroscopic. However, the tricyanides could prove even more difficult to handle than the trihalides due to their toxicity.

Chapter 8.

Materials based on the Mineral Elpasolite.

The naturally occurring mineral elpasolite, K_2NaAlF_6 has a cubic lattice in which trivalent ions occupy octahedral sites (35, 36). Subsequent work on synthetic materials, such as K_2NaGaF_6 (37) and K_2NaCrF_6 (38) has shown that these compounds are cubic, space group Fm3m.

Hukin (39) in a comprehensive survey of compounds of this type, has shown that it is possible to prepare the rare-earth analogues by using Cesium and Potassium to replace potassium and sodium. All the rare earths form compounds of the type Cs_2KLnF_6. A limited single crystal structure determination by Cox (40) has shown that in the compound Cs_2KYF_6 the atoms are in the following positions of Fm3M.

8 Cs in 8c, $\frac{1}{4},\frac{1}{4},\frac{1}{4}$.

4 K in 4b, o o o.

4 Y in 4a, $\frac{1}{2}\ \frac{1}{2}\ \frac{1}{2}$

24 F in 24e $\pm x$,oo x = 0.264

It was therefore suggested that perhaps a similar series of compounds might be formed by the respective chlorides. Therefore, a compound of composition Cs_2KYCl_6

was prepared by weighing out stoichiometric quantities of the constituent chlorides and fusing under dry helium. The product was homogeneous and contained some optically isotropic crystals up to $1mm^3$. An X-ray powder photograph and a diffractometer trace showed the product to consist of a cubic, face-centred phase, a = 11.094Å (Tables 8.2. and 8.2.A). Oscillation and Weissenberg photographs of a small single crystal fragment confirmed the indexing of the powder photograph.

The density was measured using a specific gravity bottle, and found to be 2.98 gm/cc. (Calculated for 4 molecules/unit cell, 2.95 gm/cc).

The intensities of ten reflections were measured from a diffractometer chart using a planimeter. After correction for Lorentz, Polarization and multiplicity factors, the intensities were used to determine the chlorine x-parameter using a least squares procedure. The final paramater obtained was 0.27, giving an R-factor $\left(\frac{\Sigma\Delta F}{\Sigma|F_o|}\right)_o$ of 13% The K-Cl distance is 3.0Å, the Y-Cl distance 2.6A. (See Table 8.2.A).

The structure factors calculated for a chlorine parameter of 0.27 are compared with the observed intensities obtained

from the powder photograph in Table 8.2. All missing reflections had very low calculated structure factors.

The complete series of elpasolite-type compounds was made using each rare-earth. In each case the X-ray powder diffraction patterns could be indexed on the basis of a face-centred unit cell (Tables 8.1 - 8.16). By analogy with the other similar compounds with the Elpasolite structure, these compounds were assumed to be isostructural, with the space-group Fm3m.

In order to determine the range of composition of these elpasolite-type compounds with respect to the alkali metal and the halogen, the following mixtures were fused in the normal way:-

$2CsCl:1NaCl:1YCl_3$

$2RbCl:1KCl:1YCl_3$

$2CsCl:1RbCl:1YCl_3$

$2CsBr:1KBr:1GdBr_3$

Only the first mixture gave a compound of the elpasolite structure, (Table 8. 1. and 8.7.a.). Cs_2NaYCl_6 is cubic, a = 10.705.

Table 8. 1.

Material	Lattice Dimension (Å)
Cs_2 K Y Cl_6	11.094
Cs_2 K La Cl_6	11.326
Cs_2 K Ce Cl_6	11.278
Cs_2 K Pr Cl_6	11.254
Cs_2 K Nd Cl_6	11.217
Cs_2 K Sm Cl_6	11.202
Cs_2 K Eu Cl_6	
Cs_2 K Gd Cl_6	11.15 0
Cs_2 K Tb Cl_6	11.112
Cs_2 K Ho Cl_6	11.083
Cs_2 K Er Cl_6	11.067
Cs_2 K Tm Cl_6	11.030
Cs_2 K Yb Cl_6	11.023
Cs_2 K Lu Cl_6	11.019
Cs_2 Na Y Cl_6	10.705

Table 8. 2.

Cs_2KYCl_6			Cu K_α	Ni filter.
I	F calc.	Plane hkl.	$\sin^2\theta$ obs. x 10^4	$\sin^2\theta$ calc. x 10^4
M	15	111	146	145
W	9	200	194	193
S+	58	220	387	386
W-	7	311	531	531
S-	54	222	579	579
S	90	400	773	773
Vw	11	420	968	966
S-	47	422	1160	1159
W	(13 (3	511) 333)	1303	1304
W	9	531	1692	1690
M	42	620	1929	1931
W+	25	622	2124	2124
M-	52	444	2320	2318
W-	(5 (12	711) 551)	2463	2462
M	35	642	2703	2704
VW	(3 (9	731) 553)	2849	2849
W	41	800	3089	3090
M-	(30 (32	822) 660)	3474	3476

Table 8. 2 (continued).

I	F calc.	Plane hkl	$\sin^2\theta$ obs.x.10^4	$\sin^2\theta$ calc.x 10^4
W+	36	840	3862	3863
W-	28	664	4248	4249
VW	6	931	4398	4394
W	31	844	4634	4635

Cubic a = 11.094Å

Table 8. 2.A.

Diffractometer Trace of Cs_2KYCl_6.

Plane hkl	F obs.	F calc.
220	66	58
222	54	54
400	111	90
422	48	47
440	60	66
531	7	9
620	38	42
622	18	25
444	46	52
642	30	35

$R = 13\%$

$x_{Cl} = 0.27.$

Table 8. 3.

$Cs_2K\ La\ Cl_6$ — Cu_α — Ni filter.

I	Plane hkl.	Sin θ obs. x 10^4	$Sin^2\theta$ cal. x 10^4.
W+	111	140	139
S+	220	374	371
W-	311	514	510
W	222	560	556
S-	400	742	742
W-	331	885	880
S	422	1115	1112
W	333) 511)	1256	1251
M	440	1488	1483
W-	531	1622	1622
M-	620	1852	1853
M-	642	2596	2594
W-	822) 660)	3336	3336

Cubic a = 11.326 Å

Table 8. 4.

$Cs_2K\ Ce\ Cl_6$ — Cu_α — Ni Filter.

I	Plane hkl	$\sin^2\theta$ obs. x 10^4	$\sin^2\theta$ calc. x 10^4
M-	111	142	140
S+	220	378	374
W+	311	518	514
M-	222	564	561
S	400	751	748
W	331	893	888
S	422	1124	1121
W+	511) 333)	1264	1262
S-	440	1497	1495
W+	531	1638	1635
M	620	1868	1869
W-	533	2011	2009
W+	444	2247	2243
W	711) 551)	2386	2383
M+	642	2616	2617
W	731) 553)	2761	2758
W-	800	2982	2990
M-	822) 660)	3363	3364

Table 8. 4. (continued).

I	Plane hkl.	$\sin^2\theta$ obs. x 10^4	$\sin^2\theta$ calc. x 10^4
W-	751) 555)	3505	3504
W	840	3733	3738
W	664	4108	4112

Cubic. a = 11.278 Å

Table 8.5.

Cs_2K rr Cl_6 — CuK_α — Ni filter.

I	Plane hkl	$Sin^2\theta$ obs. x 10^4	$Sin^2\theta$ calc. x 10^4
M-	111	140	141
S+	220	375	375
W+	311	516	516
M-	222	564	563
S-	400	751	751
W-	331	892	892
S-	422	1125	1126
W+	333) 511)	1268	1270
M+	440	1502	1502
W	531	1641	1642
M-	620	1876	1877
W	444	2252	2252
W-	711) 551)	2395	2393
M-	642	2627	2628

Cubic a = 11.254 Å

Table 8. 6.

$Cs_2K\ Nd\ Cl_6$ — Cu_α — Ni-filter.

I	Plane hkl	$\sin^2\theta$ obs. x 10^4	$\sin^2\theta$ calc. x 10^4
W+	111	144	142
S+	220	380	378
M	311	522	517
W+	222	570	567
S-	400	760	756
S	422	1136	1134
W	511) 333)	1276	1275
M+	440	1514	1512
M	531	1654	1653
M-	620	1889	1889
W	444	2268	2267
VW	711) 551)	2415	2409
M	642	2643	2645
W-	731) 553)	2789	2787
W+	822) 660)	3402	3401
W	840	3774	3779

Cubic a = 11.217Å

Table 8. 7.

$Cs_2K\ Sm\ Cl_6$ — Cu_α — Nickel Filter.

I	Plane hkl.	$Sin^2\theta$ obs x 10^4	$Sin^2\theta$ calc. x 10^4
W+	111	145	143
S+	220	384	380
W	311	527	523
W+	222	573	571
S	400	765	761
S	422	1145	1141
W+	511) 333)	1289	1284
S-	440	1526	1522
W+	531	1668	1664
M+	620	1907	1902
W	444	2285	2283
W-	711) 551)	2427	2425
M+	642	2662	2663
VW	731) 553)	2800	2806
W-	800	3046	3043
M-	822) 660	3422	3424
W+	840	3798	3804

Cubic a = 11.202 Å

Table 8.

Cs_2NaYCl_6 Cu-α

Reflection hkl.	Intensity.	$Sin^2\theta$ obs. x 10^4.	$Sin^2\theta$ obs. x 10^4
111	W+	156	156
220	S+	415	415
222	S-	624	622
400	S	831	830
422	M	1244	1245
333) 511)	VW	1401	1400
440	M+	1659	1660
531	VW	1818	1815
620	W+	2074	2074
622	W+	2283	2282
444	W+	2487	2489
642	M-	2905	2904
800	W-	3320	3319
822) 660)	W	3731	3734
840	W	4142	4149

Cubic, a = 10.705 Å.

Table 8. 9.

Cs_2KGdCl_6 — α_1 — Ni filter.

I.	Planes hkl.	$Sin^2\theta$ obs. x 10^4	$Sin^2\theta$ calc. x 10^4
W+	111	148	143
S+	220	383	382
W+	311	526	526
M-	222	574	574
S	400	764	765
VW	331	909	908
S-	422	1147	1147
W+	511) 333)	1290	1291
M+	440	1532	1530
W+	531	1677	1673
M	620	1913	1912
W-	533	2055	2055
W-	622	2108	2103
W+	444	2297	2294
W	711) 551)	2440	2438
M	642	2674	2677
W-	731) 553)	2821	2820
W	800	3059	3059
M-	822) 660)	3440	3442
W+	840	3826	3824
W	664	4206	4206
W-	844	4582	4589

Cubic a = 11.150Å

Table 8. 10.

Cs_2K Tb Cl_6 — Cu K_α — Ni filter.

I	Planes hkl	$Sin^2\theta$ obs. x 10^4	$Sin^2\theta$ calc. x 10^4
M-	111	144	144
S+	220	386	385
W+	311	529	529
M-	222	578	578
S	400	772	770
W-	331	919	914
S-	422	1157	1155
W+	333) 511)	1302	1300
M+	440	1543	1540
W+	531	1684	1685
M	620	1929	1925
M-	622	2118	2117
W+	444	2312	2310
W	711) 551)	2457	2455
M	642	2696	2695
W1	731) 553)	2842	2840
W-	800	3081	3080
W+	822) 660	3462	3465
W+	840	3848	3850

Cubic a = 11.112Å

Table 8. 11.

Cs_2K Dy Cl_6 — Cu α — Ni Filter.

I	Planes hkl.	$\sin^2\theta$ obs x 10^4	$\sin^2\theta$ calc. 10^4
W+	111	146	145
S+	220	388	386
W-	311	534	531
W	222	518	579
S	400	774	772
S-	422	1160	1157
W-	511) 333)	1302	1302
M+	440	1544	1543
W-	531	1687	1688
M-	620	1929	1929
W	444	2318	2315
M	642	2697	2701
VW	800	3092	3087
W	822, 660)	3469	3472
W	840	3856	3858

Cubic a = 11.101Å

Table 8. 12.

$Cs_2K\ HoCl_6$ — CuK_α — Ni filter.

I.	Planes hkl.	$\sin^2\theta$ obs. x 10^4	$\sin^2\theta$ calc. x 10^4
W+	111	146	145
S+	220	388	387
W-	311	535	532
M-	222	582	581
S	400	776	774
S-	422	1163	1161
W-	511) 333)	1309	1306
M+	440	1551	1548
W-	531	1692	1693
M-	620	1939	1935
W	444	2320	2322
W+	642	2709	2709
W-	660	3480	3484

Cubic $a = 11.083\text{Å}$

Table 8. 13.

$Cs_2K\ ErCl_6$ — Cu_α — Ni filter.

I	Planes hkl.	$Sin^2\theta$ obs. x 10^4	$Sin^2\theta$ calc. x 10^4
W+	111	147	146
S+	220	390	388
W	311	536	534
W+	222	585	582
S-	400	777	776
S	422	1166	1164
W	511) 333)	1312	1310
M+	440	1553	1553
W	531	1702	1698
M	620	1941	1941
W+	444	2328	2329
W-	711) 531)	2475	2474
M	642	2717	2717
W-	731) 553)	2863	2863
W-	800	3103	3105
W	660	3490	3493
W	840	3882	3881

Cubic. a = 11.067Å

Table 8. 14.

$Cs_2K\ Tm\ Cl_6$ — $C\text{-}\alpha$ — Ni filter.

I	Planes hkl.	$Sin^2\theta$ obs. x 10^4	$Sin^2\theta$ calc. x 10^4.
M-	111	149	147
S+	220	394	391
W	311	540	537
W	222	588	586
S	400	784	782
W-	331	930	928
S-	422	1176	1172
W+	333) 511)	1319	1319
M+	440	1564	1563
W	531	1714	1710
M-	620	1955	1954
W-	444	2344	2345
W-	711) 551)	2494	2491
W+	642	2735	2736
W-	731) 553)	2881	2882
W	800	3127	3126
W-	822) 660)	3512	3517
W-	840	3902	3908

Cubic a = 11.030. Å

Table 8. 15.

$Cs_2K\ YbCl_6$ — Cu-α — Ni-filter.

I	Planes hkl	$Sin^2\theta$ obs. x 10^4	$Sin^2\theta$ calc. x 10^4
M-	111	148	147
S+	220	394	391
W+	311	539	539
W+	222	589	587
S	400	784	782
W-	331	932	929
S-	422	1176	1174
W+	511) 303)	1325	1320
M+	440	1569	1565
W+	531	1714	1712
M	620	1956	1956
W-	533	2103	2103
W-	622	2152	2152
W+	444	2350	2347
W	711) 511	2500	2494
M	642	2743	2739
W	553) 731)	2809	2885
W	800	3129	3130
M-	822) 660)	3521	3521
W-	751) 555)	3663	3668
W+	840	3911	3912
W-	911) 753	4055	4059
W-	664	4301	4304
W-	931	4448	4450
W	844	4693	4695

Cubic a = 11.023.

Table 8. 16.

$Cs_2K\ LuCl_6$ — $Cu_{K\alpha}$ — Ni filter.

I	Planes hkl.	$Sin^2\theta$ obs. x 10^4	$Sin^2\theta$ calc. x 10^4
M	111	147	147
S+	220	393	392
W+	311	541	538
M-	222	588	587
S	400	783	783
W-	331	732	730
S-	422	1176	1175
W+	511) 333)	1324	1321
M	440	1569	1566
W	531	1715	1713
M-	640	1957	1958
W	440	2347	2349
W-	711) 551)	2500	2496
M	642	2740	2741
W-	731) 553)	2885	2887
W-	800	3134	3132
W	822) 660)	3521	3524
W	840	3916	3915

Cubic a = 11.019.

Chapter 9.

DISCUSSION.

Some discussion of the results has been given at the end of each previous chapter. It is now appropriate to discuss the significance of the work as a whole.

Much of the experimental work described in previous sections has been concerned with the preparation and properties of three lanthanon chlorides of particular interest, namely $TbCl_3$, $DyCl_3$ and $HoCl_3$, and the behaviour of the compounds will be discussed first.

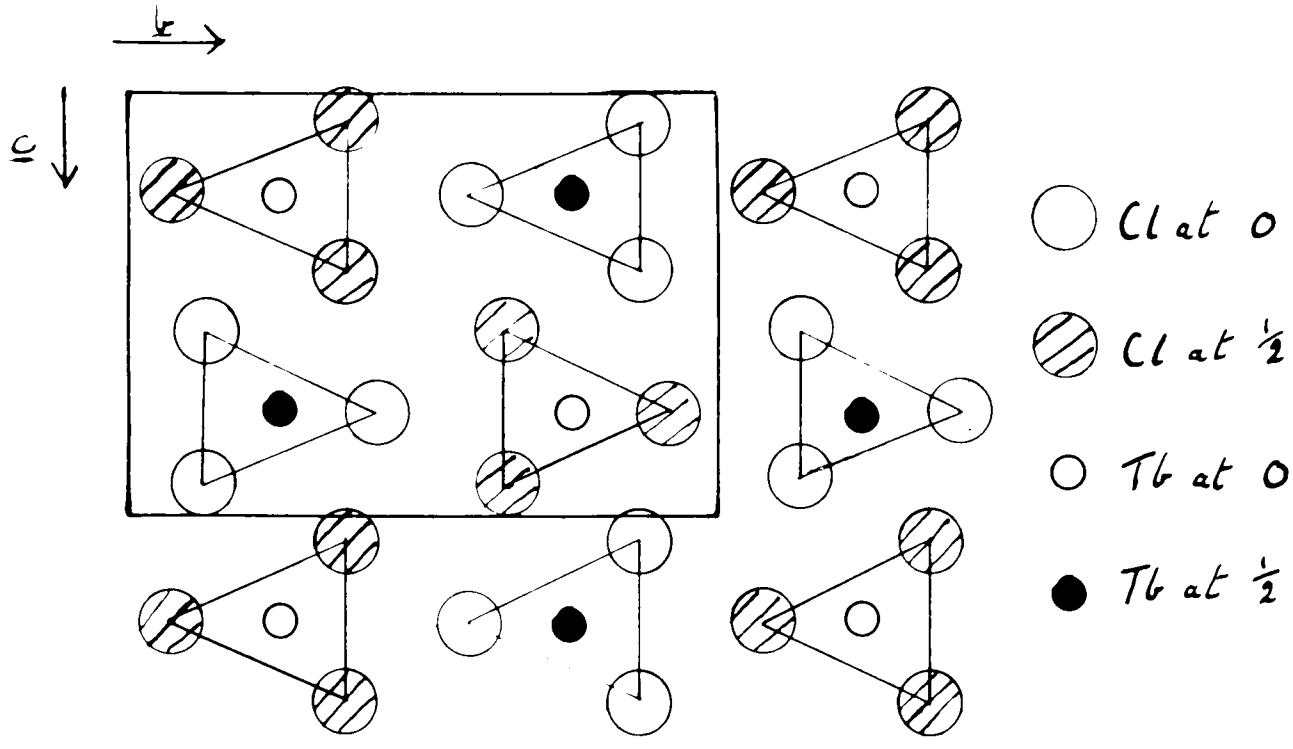
It has been known for some time that $TbCl_3$, $DyCl_3$ and $HoCl_3$ are dimorphic (5), but until recently only the high-temperature monoclinic crystalline form has been characterised (5,20). There have been no reports of any attempts to grow large single crystals of these compounds until the present work. While the work described in Chapter 6 on the structure of the low temperature form of $TbCl_3$ was being completed, independent work on this structure was published (24) in complete agreement with the author's results. However, there has been no information published on the structures of the low temperature forms of $DyCl_3$ and $HoCl_3$, and their existence has only been inferred from heats of solution (5).

Before discussing the author's observations on these chlorides, it is appropriate to compare the crystal structures of $GdCl_3$, $TbCl_3$ and $DyCl_3$, which have been described in detail elsewhere.

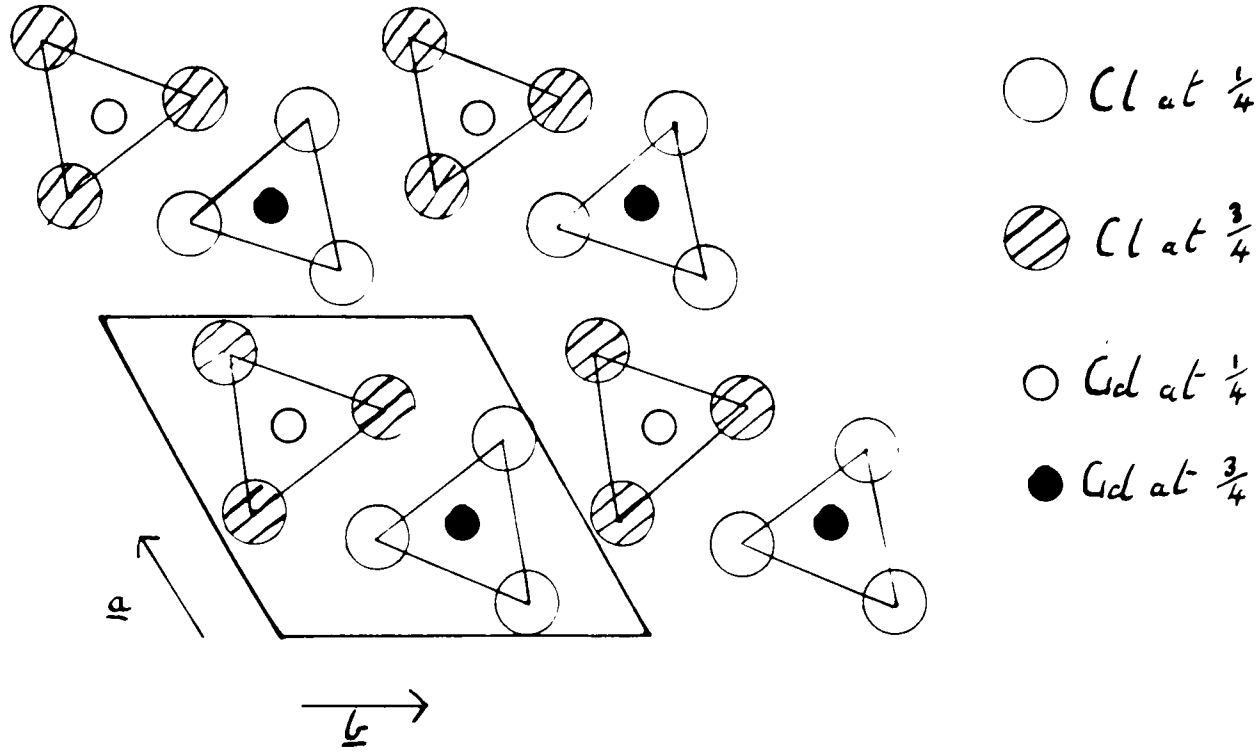
$GdCl_3$ crystallizes with the hexagonal $LaCl_3$ structure, in which the rare-earth ion is symmetrically 9-coordinated. This is only possible by considerable distortion of the supposedly spherical ions. The ionic radius of Tb is apparently too small for stable 9-coordination, and $TbCl_3$ crystallizes, in its low temperature form, in the $PuBr_3$ structure, where the terbium is 8-coordinated. The relationship between the two structures may be described in two ways.

The 9-coordination can change to 8-coordination by "pushing" one chlorine ion out of the symmetrical coordination polyhedron, and rotating the coordination prisms through 60° relative to one another (Fig. 9.1).

Another way of relating the two structures is to consider the way in which the coordination prisms are packed together. Both structures consist of parallel columns of triangular prisms of chloride ions with the rare-earth ions along the centres of the prisms.



$TbCl_3$



$GdCl_3$

Fig 9.1

In the $GdCl_3$ structure neighbouring columns are arranged so that each Gd^{3+} ion has three chloride neighbours adjacent to the prism faces. In the $TbCl_3$ structure each column has four neighbouring columns, but only two of these provide a close chloride ion neighbour to each Tb^{3+} ion.

The high temperature forms of $TbCl_3$, $DyCl_3$ and $HoCl_3$ crystallize in a monoclinic structure in which the rare-earth ion is unsymmetrically 6-coordinated. The chloride ions are approximately cubic close-packed.

These changes in the coordination number of the rare-earth ions are broadly what one would expect from the application of radius ratio rules, making some allowance for the distortion caused by the triply charged cations. A measure of the stability of the crystalline forms is shown by the variation of the melting-points and transition temperatures for a number of rare-earth chlorides (Fig. 8.2).

The orthorhombic $PuBr_3$ structure is stable over a greater range of radius ratios in the bromides than in the chlorides (Table 8.1)

One factor which may affect the stability of the orthorhombic structure type, is the closeness of one pair of anions (Cl-Cl $\simeq$ 3.07 Å) relative to the sum of the

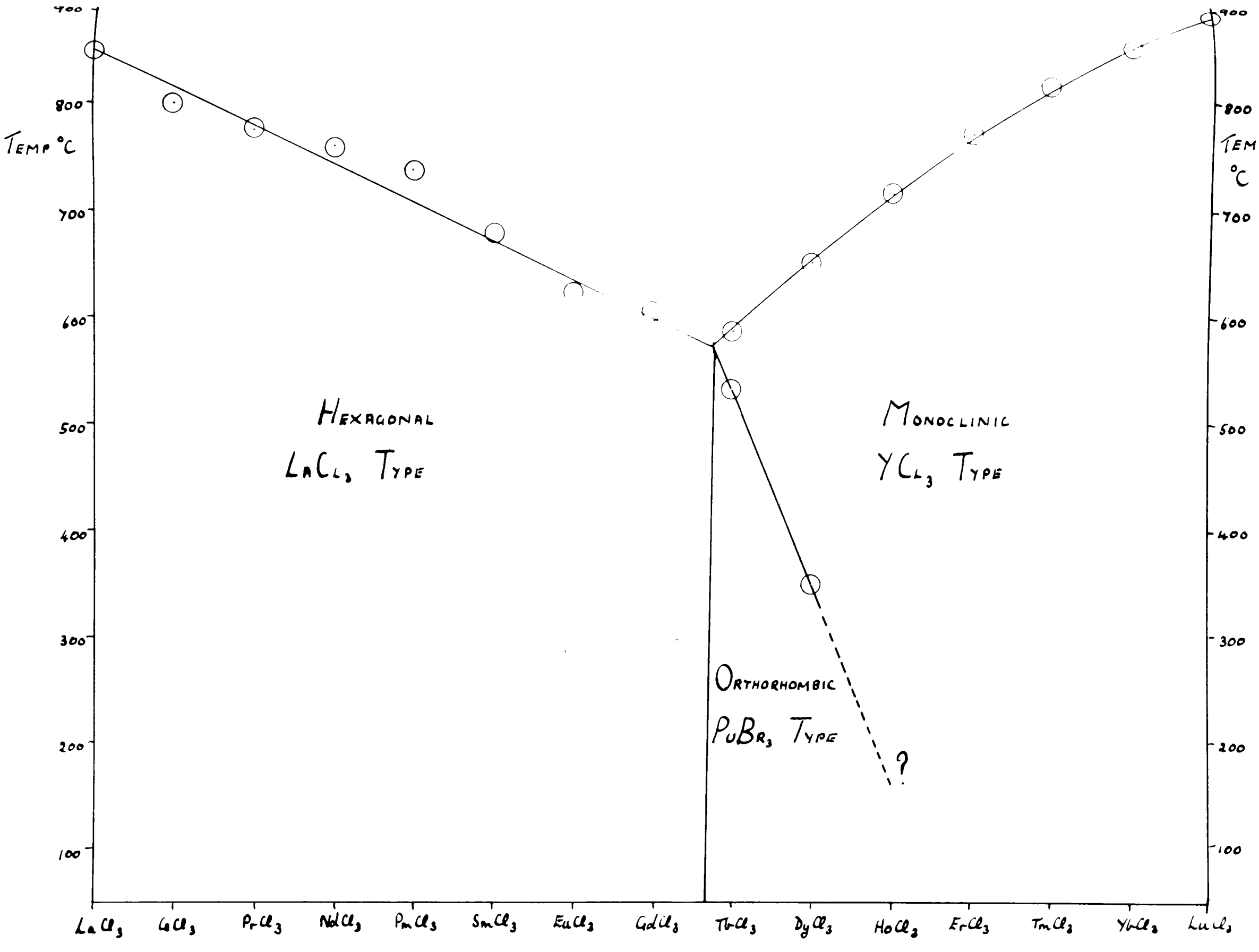

TEMP °C
900
800
700
600
500
400
300
200
100
HEXAGONAL
LaCl3 TYPE
MONOCLINIC
YCl3 TYPE
ORTHORHOMBIC
PuBr3 TYPE
?
TEM
°C
LaCl3
CeCl3
PrCl3
NdCl3
PmCl3
SmCl3
EuCl2
GdCl3
TbCl3
DyCl3
HoCl2
ErCl3
TmCl3
YbCl2
LuCl3

Fig 9.2

Van der Waal's radii ($3.6\mathring{A}$). This close distance of approach is only possible by considerable distortion of the anions, which is easier for the more polarisable bromide ion. The triangular columns of anions in the orthorhombic structure are held together by Van der Waal's forces to a greater extent than in the $LaCl_3$ structure, and these forces are greater for Br-Br interactions than for Cl-Cl interactions.

The existence of different structures at different temperatures for $TbCl_3$, $DyCl_3$ and $HoCl_3$ is also understandable from consideration of ionic radius ratios. The effective radius of the chloride ion increases more rapidly than that of the rare-earth ion, due to increasingly greater amplitude of thermal vibration, as the temperature increases. The radius ratio therefore decreases until a point is reached when 8-coordination is no longer stable with respect to 6-coordination of the rare-earth ions, and the low temperature $PuBr_3$ structure type changes to the high temperature YCl_3 structure type. The transition temperature would be expected to fall with decreasing relative size of rare-earth ion.

$TbCl_3$ reverts readily to the $PuBr_3$ structure at 535°C when cooled from the melt. Pure $DyCl_3$ (usually) remains in the high temperature form even when cooled slowly to room temperature, but its transition temperature has been

established as 351°C. The rate of transformation is certain to fall with decreasing temperature, and it would appear that at 351°C and below the activation energy of the transformation high $DyCl_3$ ⟶ low $DyCl_3$ is too high for the available thermal energy. The presence of small amounts of impurity lowers the activation energy sufficiently for the transition to be observed.

By extrapolation from measurements on mixtures, $HoCl_3$ should have a transition from the Pu Br_3 structure to the YCl_3 structure at about 160°C, but this has not been observed directly.

Both $DyCl_3$ and $HoCl_3$ have been grown as good single crystals in the monoclinic form, which is metastable at room temperature. Deliberate efforts to induce the transition such as very slow cooling and cooling in liquid nitrogen were unsuccessful, but measurements of specific heats and magnetic moments of $DyCl_3$ and $HoCl_3$ at liquid helium temperatures gave inconsistent results. X-ray powder photographs of $DyCl_3$ which had been cooled to liquid helium temperatures showed that some change in structure had taken place, but its nature could not be ascertained from the diffuse diffraction patterns, and none of the samples gave exactly the same pattern.

Crystals of $DyCl_3$ became opaque on cooling to liquid helium temperatures, preventing any measurement of the optical absorption spectra. Crystals of $HoCl_3$ remained clear, and the absorption spectra were measured but the relative intensities of some of the absorption peaks varied from one specimen to another. It must be concluded that part of the crystals of $DyCl_3$ and $HoCl_3$ change structure when they are cooled to very low temperatures. At such temperatures the energy of the metastable monoclinic form must be very much greater than the energy of the orthorhombic form, and once the change is initiated it might well be continued by the heat of transition, but the chance of acquiring sufficient activation energy to start the process is even less than at room temperature. How the activation energy is acquired is a matter for conjecture. It may arise from fracturing of the crystal on cooling.

The effects which have been observed at low temperature cannot be explained until an X-ray camera for liquid helium temperatures has been made because at the moment X-ray photographs of the compounds are not taken when they are in the same state as when the physical measurements are being made.

A recent paper (32) has details of similar phenomena in rare-earth tungstates. Crystals of $Dy_2(WO_4)_3$ remained in a

metastable form at room temperature when in a dessicator, but exposure to moisture, X-rays or grinding accelerated this change. No mention is made of the effect of impurities on this phase-change.

A large part of the work described in this thesis has been directed towards finding new compounds of the rare-earths which could be used for detailed study of the properties of magnetic ions. Wolf (33) has listed the desirable properties for compounds suitable for such research:-

(i) Strong antiferromagnetic coupling between neighbouring inequivalent magnetic ions.

(ii) Well-defined, regular and preferably simple crystal structure.

(iii) One-to-one relationship between the different crystal sites and types of constituent ions.

(iv) Unique valency for each type of ion present, with accurate control of valency in the method of preparation.

(v) A simple method for growing large and perfect single crystals.

(vi) A wide range of compositions possible for the same structure in order to vary the magnetic properties.

In the present investigations the important criteria were (ii), (iii), (iv) and (v). The types of compounds which

were investigated can be divided into three classes:-

(i) Compounds of tetravalent rare-earths, i.e. Ce^{IV}, Pr^{IV} and Tb^{IV}.

(ii) Compounds formed between rare-earth chlorides of different structure.

(iii) Compounds formed between rare-earth chlorides and alkali metal chlorides.

The experiments were described in Chapter 4, but here we can summarize the properties of the compounds which were discovered. The compounds in class (i) were so thermally unotable that it was not possible to make them as single crystals. In addition, it was not possible to make the compounds absolutely pure, since there was always some trivalent rare-earth metal present.

The phase systems of the second category produced no new compounds, although the phase diagrams gave much interesting information on the relative stabilities of the three structures in which the rare-earth chlorides crystallize, as discussed above.

Several compounds are formed between rare-earth chlorides and alkali metal chlorides, of which the most promising is Li_3YCl_6. This compound crystallizes in a hexagonal structure

and a series of similar compounds are formed by Tb, Dy, Ho, Er, Tm, Yb and La. A similar series of compounds is formed by sodium chloride (34) and potassium chloride (7 and Chapter 4) but Na_3YCl_6 melts incongruently, and would be difficult to grow as a single crystal. K_3YCl_6 is not stable at room temperature. It would appear that the only compounds of this type which are of potential interest to physicists are the compounds formed with lithium chloride.

Of the miscellaneous compounds of Gp III metals, the only ones of potential interest appear to be the tricyanides and trithiocyanates. Both the compounds are deliquescent, similar to the trihalides, and are consequently difficult to handle. The tricyanide is difficult to synthesize in quantities sufficient to grow large single crystals. However, while $Y(CN)_3$ crystallizes in an orthorhombic structure, $In(SCN)_3$ is cubic. The trithiocyanates would therefore appear to be a better proposition for physical studies, but it has not been possible as yet to make the rare-earth analogues.

The cubic elpasolite type compounds $Cs_2K\,LnCl_6$ have been briefly investigated. No cooperative phenomena have been observed in the magnetically concentrated materials Cs_2KGdCl_6 and Cs_2KDyCl_6. although $Cs_2K\,LaCl_6$ may prove to be an interesting host lattice.

Table 6.1.

Metal Ion.	Ionic o Radius A.	rc ra	Structure.	rc ra	Struc- ture	rc ra	Struct- ure.
La	1.061	.586	$LaCl_3$	.545	$LaCl_3$	.492	$Pu\ Br_3$
Ce	1.034	.571	"	.531	"		
Pr	1.013	.560	"	.521	"		
Nd	.995	.549	"	.511	$PuBr_3$		
Sm	.964	.532	"	.494	"		
Er	.950	.524	"	.488	"		
Gd	.938	.518	"	.482	YCl_3		
Tb	.923	.509(5)	$Pu\ Br_3$				
Dy	.908	.501	YCl_3				
La	.848	.469	"				
Y	.881	.486	"				
Pu	1.00	.552	$LaCl_3$				

REFERENCES.

(1) C. Hutchison and E. Wong. J.Chem.Phys, 29 754 (1958).

(2) G. Garton, M.Hutchings, R.Shore and W.Wolf. J.Chem. Phys 41 1970 (1964)

(3) A. Wyatt, D.Phil Thesis. Oxford 1963.

(4) D. Hukin, D.Phil Thesis. Oxford 1966.

(5) H. Bommer and E.Hohmann. Z.Anorg.Allgern.Chem. 248 373 (1941)

(6) A. French, Chem.Pt.II Thesis. Oxford 1962.

(7) J. Reed, B.Hopkins and L.Audrieth. J.A.C.S. 57 1159 (1935)

(8) F. Block and T.Campbell. "The Rare Earths." Ed. Spedding and Daane John Wiley and Sons 1961.

(9) D. Williams. Private Communication.

(10) D. Williams. Chem.Pt.II. Thesis Oxford 1964.

(11) B. Korshunov and D.Drobot. Zh.Neorg.Chim. 9 222 (1964).

(12) Cunningham, Feay and Rollier. J.A.C.S. 76 3361 (1954).

(13) W. Smothers and Y. Chiang. "Differential Thermal Analysis: Theory and Practise" Chemical Publishing Co. New York. 1958.

(14) T. Cooke. Chemistry Pt.II Thesis. Oxford 1964.

(15) L. Asprey and T. Keenan. J.Inorg. Nucl.Chem. 16 260.

(16) W. Zachariasen. J.A.C.S. 70 2147.

(17) J. Phillips. Chem.Pt.II. Thesis, Oxford 1965.

(18) G. Engel. Z. Krist. 90 341 (1935).

(19) J. Baker, J.Riley and R.Shore. Phys. Rev. 150 198 (1966).

(20) Templeton and Carter. J.Phys. Chem. 53 940 (1954).

(21) W. Zachariasen. Acta Cryst. 1 266 (1948).

(22) R. Shore Chemistry Pt.II Thesis. Oxford 1963.

(23) F. McKim and W. Wolf. J.Sci.Inst. 1956

(24) Forrester, Zalkin, Templeton and Wallman. Inorganic Chem.3 185 (1964)

(25) J. Baker. Private Communcation.

(26) G. Weber, G. Weitz. Private Communication.

(27) B. Cullity "Elements of X-ray Diffraction" Addison-Wesley Publishing Coy. Inc. (1959).

(28) G. Reddy. D.Phil. Thesis. Oxford 1964.

(29) H. Forsberg. Acta Chem. Scand. 10 1287 (1956).

(30) I. McColm. D.Phil. Thesis Oxford 1964.

(31) R. Wyckhoff. Crystal Structures. John Wiley 1963.

(32) K. Nassau, H. Levenstein and G. Loiacomo. J.Amer.Ceram.Soc. 47, 363 (1964).

(33) W. Wolf. Rep. Prog.Phys. 24 220 (1961).

(34) B. Korshunov and D. Drobot. Zh. Neorg.Chim. 9 22 (1964).

(35) G. Menzer Fortschr. Min. 17 61 (1932).

(36) C. Frandel Amer. Min. 33 84 (1948).

(37) L. Helmholz J.Chem.Phys. 31 172 (1959).

(38) K. Knox, D. Mitchell J.Inorg. Nucl.Chem. 21 253 (1961).

(39) D. Hukin D.Phil. Thesis Oxford 1966.

(40) D.Cox. Chem.Pt.II Thesis. Oxford 1967.

(41) See Refs in D.Smith, D.Phil. Thesis. Oxford 1967

ABSTRACT.

The work described in this thesis falls into four major divisions. Firstly, it is concerned with the preparation of large, single crystals of rare-earth halides and mixed halides of rare-earth and alkali metals. Secondly, it describes the discovery of new magnetic materials, which incorporate rare earth ions, by means of thermal and X-ray analysis of a number of mixed halide systems. Thirdly, the results of the measurements of A.C. magnetic susceptibility and specific heat of some rare-earth trichlorides are presented. Finally, crystallographic studies of some rare-earth and Group III B compounds are described.

In the first part, the preparation and purification of rare-earth chloride and bromides, and the method used to grow both pure and doped single crystals for various physical measurements are discussed in detail. A very large number of crystals have been grown by the Bridgman-Stockbarger method, and have been used for physical measurements of various types, not only in the laboratory, but also in France and the U.S.A. It has been found that, to prepare optically clear crystals of mixed rare-earth chloride-alkali metal chloride compounds, the starting materials must be of very high purity. The methods of purification used were either distillation or zone refining.

An investigation of phase systems containing sodium fluoride and praseodymium or terbium tetrafluorides showed that compounds of the formula $NaMF_5$, Na_2MF_6 and Na_3MF_7 were formed, but none of these were thermally stable, and therefore could not be grown as single crystals from the melt. The phase diagram of the system $LiCl/YCl_3$ showed the presence of a congruently melting compound Li_3YCl_6, which has since been grown as a single crystal, both pure and doped with 10% Er^{3+}.

An extension of previous work on materials similar to elpasolite, K_2NaAlF_6, revealed the existence of isomorphous compounds Cs_2KMCl_6, where M is any trivalent rare earth or yttrium. In these compounds the rare earth ion occupies a site of cubic symmetry. A single crystal of Cs_2KYCl_6 has been grown from zone-refined materials.

Several phase diagrams of systems containing two rare-earth chlorides of different crystallographic structures have been constructed. The mutual solubilities of several rare-earth chlorides were determined.

The dimorphism of $TbCl_3$, $DyCl_3$ and $HoCl_3$ was investigated by differential thermal analysis. The transition temperature of $TbCl_3$ was found to be 535°C, and that of $DyCl_3$ to be 350°C. The latter transition was never observed directly, but could

be inferred from other data. $DyCl_3$ in the purely low temperature form could not be made, but the transformation was found to be aided by high pressure. The transition temperature of $HoCl_3$ was estimated to be about 160°C, but was never observed.

Techniques for handling the hygroscopic rare earth halides were evolved, and methods of shaping and orienting single crystal fragments for various types of physical experiments are described. In addition various forms of container used to transfer the sample from a drybox to a cryostat are shown.

Measurements of the A.C. susceptibility of $DyCl_3$ and $HoCl_3$ at low temperatures are described, but a full interpretation of the phenomena was not possible. The specific heats of $DyCl_3$. $HoCl_3$ and $ErCl_3$ were measured at temperatures in the liquid He^3 temperature range.

At the start of this work, the low temperature crystallographic form of $TbCl_3$ had not been fully characterised. The crystal structure was published while work on the structure was still in progress, and the author's results agree with the published results within experimental error.

The positions of the rare-earth ions in Li_3YCl_6 and $CeCl_3.7H_2O$ were determined from Patterson syntheses. The unit cell size and symmetry of $GdBr_3$ was also determined.

Several Group III B. compounds were studied by X-ray powder diffraction, in order to determine their unit cell size and symmetry. The only compound of possible interest as a host lattice for rare-earths, appears to be $In(SCN)_3$ which possesses cubic symmetry.